DESIGNING A FAST FOURIER TRANSFORM BASED ISLANDING DETECTION METHOD FOR DC MICROGRIDS

Korawege Nimesh Chathuranga Jayasena

188070B

Degree of Master of Science by Research

Department of Electrical Engineering

University of Moratuwa

Sri Lanka

April 2020

DESIGNING A FAST FOURIER TRANSFORM BASED ISLANDING DETECTION METHOD FOR DC MICROGRIDS

Korawege Nimesh Chathuranga Jayasena

188070B

Thesis submitted in fulfillment of the requirements for the degree of Master of Science by Research

Department of Electrical Engineering

University of Moratuwa

Sri Lanka

April 2020

DECLARATION

I declare that this is my own work and this thesis does not incorporate without acknowledgment any material previously submitted for a Degree or Diploma in any other University or institute of higher learning and to the best of my knowledge and belief it does not contain any material previously published or written by another person except where the acknowledgment is made in the text.

Also, I hereby grant to the University of Moratuwa the non-exclusive right to reproduce and distribute my thesis, in whole or in part in print, electronic or another medium. I retain the right to use this content in whole or part in future works (such as articles or books).

Signature: Date: 11-05-2020

The above candidate has carried out research for the Masters/~~MPhil/PhD~~ thesis~~/ Dissertation~~ under my supervision.

Signature of the supervisor: Date:11-05-2020

Dr. Lidula N. Widanagama Arachchige

Signature of the supervisor: Date: 11-05-2020

Prof. Athula D. Rajapakse

ABSTRACT

The scarcity of the natural resources, environmental issues and rising population in the world, demands for innovative concepts, such as microgrids to the modern power system. Nowadays, microgrids are becoming very popular and the most appropriate options to enrich the power system with renewable generation. In addition to that, rapid growth in the DC nature of the loads within the power system is apparent due to the popularity of power electronic devices and recent trends in electrified transportation systems. Hence, researchers are introducing direct current microgrid concepts to the power system, and it has become a highly emerging and trending research area at present. DC microgrids can operate under two main operating modes: grid-connected and islanded operation. The main difficulties of implementing the concept in this concept are the lack of proper international standards, safety features, and protection issues within the systems. Islanding detection is the most challenging and vital requirement in microgrid protection to ensure the safety of the personnel and microgrid equipment and to maintain a smooth and reliable operation of the DCMG. Islanding detection is used to detect the disconnection of the DC microgrid from the utility and switch to proper controls to serve critical loads in the power island.

This thesis presents a novel method of islanding detection for DC microgrids by using Fast Fourier Transform based analysis of DC-link voltage. Further, testing was carried out adopting a 10-kW low voltage DC microgrid with a single-phase bidirectional inverter interface. In addition, a DC microgrid consisting of photovoltaic model with maximum power point tracking, DC loads, AC loads and a battery module with state-of-charge based multi-mode battery management system was modeled. All the modeling and simulations were carried out considering several network configurations and network conditions with the EMTDC/PSCAD v4.2 environment. Simulations were evaluated according to the IEEE 1547-2018 standard. The probabilistic approach was applied to show the robustness of the experimental results of the proposed method.

Keywords: *Battery Management System, DC microgrid, Islanding Detection, Maximum Power Point Tracking.*

ACKNOWLEDGMENTS

I want to acknowledge my supervisors, Dr.N.W.A Lidula, Senior Lecturer, Department of Electrical Engineering, University of Moratuwa, Sri Lanka and Prof. A.D. Rajapakse, Department of Electrical and Computer Engineering, the University of Manitoba gratefully for their insights and tremendous support, guidance and encouragement given to this research from the beginning to the end. Their constructive comments and guidance gave me solid strength to complete my research successfully.

I would especially like to acknowledge the University of Moratuwa for the financial support given under the senate research grant scheme (SRC/CAP/2018/01), and the academic staff in the Department of Electrical Engineering, the University of Moratuwa for their valuable comments, feedback and suggestion for the continuous progress of my research.

Moreover, I would like to extend my heartiest gratitude to my family for their encouragement and motivation and giving me constructive ideas towards the research. I want to thank my colleagues who always helped and motivated me during the research.

TABLE OF CONTENTS

TABLE OF FIGURES

LIST OF TABLES

ACRONYMS

BEMS-Battery Energy Management System

DCMG-DC microgrid

DES-Distributed Energy Storages

DQ-Direct and Quadrature axis

EMS-Energy Management System

EPS-Electrical Power System

FFT-Fast Fourier Transform

GWN-Gaussian White Noise

IDM-Islanding Detection Method

IEEE- Institute of Electrical and Electronics Engineers

IoT-Internet of Things

LPF-Low Pass Filter

MPPT-Maximum Power Point Tracking

NDZ-Non-Detection Zone

OSG-Orthogonal Signal Generator

PCC-Point of Common Coupling

PFC-Power Factor Correction

PLCC-Power Line Carrier Communication Method

PLL-Phase Lock Loop

PV-Photo Voltaic

PWM-Pulse Width Modulation

P&O-Perturb & Observe

ROCC-Rate of Change in Current

ROCV-Rate of Change in Voltage

SCADA- supervisory control and data acquisition method

SNR-Signal to Noise Ratio

SoC-Stata of Charge

SPD-Signal Produce by Disconnection

SPWM -Sinusoidal Pulse Width Modulation

TT-Transfer Trip Method

VSC-Voltage Source Converters

1. INTRODUCTION

1.1 Overview

In the world scenario, over 70% of the power generation is governed by fossil fuel generation, as shown in Figure 1-1[1]. However, high fossil fuel consumption is responsible for the emission of greenhouse gases, such as CO_2, which ultimately contributes to global warming and air pollution. It also causes various environmental issues, adverse economic and social effects that directly impact the living beings. Moreover, due to the rapid growth of the population and global economic development, such as new market trends, global energy demand is continually rising. Therefore, the requirement of clean and affordable energy sources has become one of the foremost topics over the world, leading to the integration of more renewable energy sources into the power system.

The concept of implementation of DC microgrid technologies with the integration of renewable resources is considered a novel solution to the aforementioned issues. As a subsystem of the primary grid, DC microgrids are capable of self-sustained for a specific limit incorporating renewable generation and energy storage systems. Hence, the power system reliability will be improved while reducing the burden on the existing primary grid.

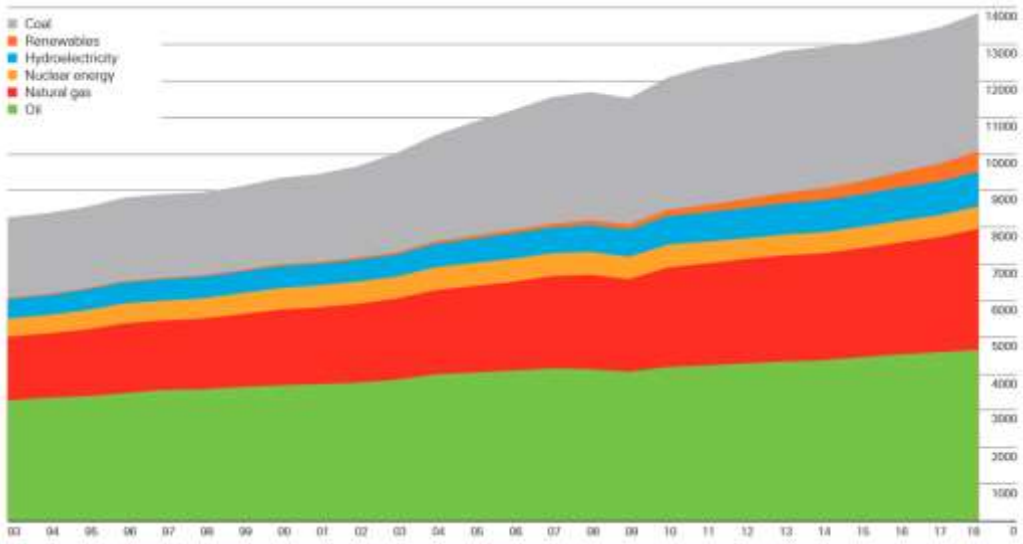

Figure 1-1 **Electricity demand in the world (1990-2018)**[1]

Furthermore, due to the high penetration of renewable generation compared to conventional technologies, the sustainability of the power sector will be preserved.

The microgrid can be defined as a localized grid system that contains the distributed energy resources (DER) and distributed loads while operating with the primary utility grid synchronously. The microgrid concept can be classified into two main types naming AC microgrids and DC microgrids. AC microgrids can be considered as the most deployed microgrid system in the world because those can be integrated with the existing power system easily without any major changes. They are more popular in some regions where most of the loads are AC. However, DC microgrids have become a trending concept over the AC microgrids at present due to their efficiency, stability, and reliability perspectives.

Despite the advantages of DC microgrids, they inherit some challenges in devising the system protection due to the connection of DER, different operating modes of the microgrids, various configuration methods of the DC microgrids with reference to its DC-link polarities and link configurations and mostly due to unavailability of frequency and phasor information. Considering the above critical aspects of the DC microgrid operation, islanding detection has taken as one of the most challenging issues, which needs a firm solution. There are several proposed islanding detection techniques for some microgrid configurations, and most of the proposed islanding detection methods (IDM) in recent researches concentrate on the AC microgrid systems. Therefore, further research is required to develop fast, reliable islanding detection for DC microgrid systems.

1.2 Electrical power system

An electrical Power system (EPS) is a network of electrical components that includes the transmission/distribution lines, DER, and power consumers as end-users. Its main objective is to maintain the uninterrupted power supply to its customers with the support of internal power generation and control functions of the system. Energy resources can be divided into renewable and nonrenewable generations. The transmission lines connect the power generators and distribution substations through long-distance and transfer the power from one point to another. In addition to that, the

distribution lines transmit the power to the end customers using a distribution feeder. In the same manner, it connects the distribution substation and end customers to transfer the energy in a short distance. When the overall view of the EPS is considered, the microgrid acts as a proactive localized subsystem to the primary grid, which can be recognized as an independently controllable entity.

1.3 DC microgrid concept

DC microgrid has become an emerging concept in the power sector throughout the last decades because of the rapid growth of DC-based renewable technologies such as solar power due to the dramatic price reduction of solar photovoltaic (PV) equipment, as indicated in Figure 1-2 [2].In addition to that, it is influenced by the substantial growth of the DC-based loads in the power system, such as electric vehicles, as shown in Figure 1-3[3].

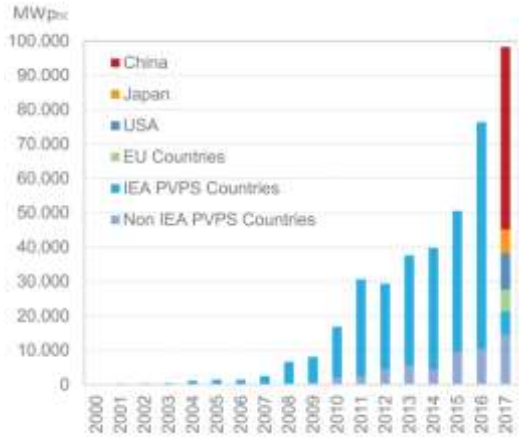

Figure 1-2 Solar power generation in the world [2]

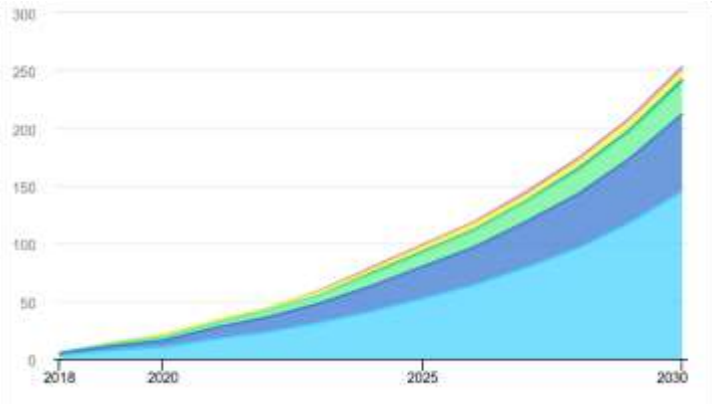

Figure 1-3 World electric vehicle demand (2015-2040)[3]

Table 1-1 DC Loads[4]

Equipment	Rated Current	Operating Voltage
Telephone	20mA	10VDC
Laptop	5A	15.6VDC
Wi-Fi Routers	2A	12VDC
LED TV	750mA	12VDC
LED Bulb	350mA	3.6VDC

The same pattern in electrical transportation also applies to DC loads in commercial and domestic applications and other power electronic technologies in the primary grid. Application of power electronic-based technologies can be recognized in domestic appliances such as laptops, cellphones, TVs, lighting equipment as illustrated in Table 1-2. They are energized through AC-DC power adapters with the rectification process; however, this equipment can also be operated directly through DC power very efficiently. Furthermore, some resistive loads in the general application of heating and lighting including incandescent bulbs and universal motor-related applications such as mixers and other kitchen equipment can be operated with both AC and DC power supply.

In addition to that, telecommunication-based concepts like the internet of things (IoT), smart grid technologies are more reliant on the DC-based equipment. Furthermore, space technology also has used solar as its primary power source. Hence DC microgrid is more reliable in such conditions.

1.4 Advantages of DC microgrid concept

The DC microgrids have more advantages over AC microgrids. It does not contain frequency and phase components. Therefore, the internal control structure of the DC microgrids is less complicated than the other conventional approaches. The DER renewable generation can be easily integrated into the system in the higher margin without any synchronizing techniques like in AC microgrid systems. Furthermore, it

is highly immune to electromagnetic interferences, harmonic distortions, and skin effect, which are incurred in the AC systems. As a result, it reduces the wire size along the copper volume required for the DC system. Hence, the construction cost for the line commissioning of DC microgrid is comparatively lower than the conventional power systems.

1.5 The popularity of DC microgrid concept

DC microgrids are available in different countries as indicated in Figure 1-4, and it is not only established in the research stage, but also implemented as commercial projects concentrated on the telecommunication sector, as shown in Table 1-3.

DC microgrids are very popular in many countries like German and Sweden etc. The countries, including Sweden and Japan, have widely utilized 5 MW capacity of DC microgrid systems to its primary grid. Most of the established projects are designed at high voltage levels, such as 360 VDC in Sweden and 400 VDC in Japan. Another DC microgrid found at a data center in New Zealand operates at 220 VDC. However, low voltage level DC microgrids can be applied at the domestic level. Some other countries including the US, Taiwan, France, Chine, and Korea have also implemented the new grid-connected DC microgrid projects.

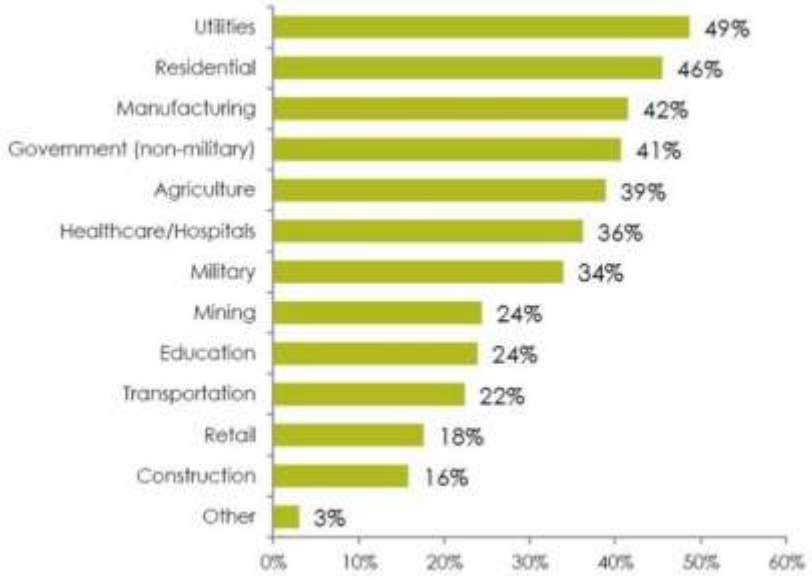

Figure 1-4 Global DC microgrid projects[5]

Table 1-4 DC Microgrids over the world [4]

Country	Institution	Voltage Level
Japan	NTT Group	380/400 VDC
Norway	UPN AB	350/380 VDC
Sweden	Net power Lab AB	350/380 VDC
Korea		300/380 VDC
China	China Telecom	240/380 VDC
United States	Clustered Systems	380VDC
New Zealand	Validus ABB	550VDC
New Zealand	University of California	380VDC
New Zealand	Telecom NZ	220VDC

1.6 Basic components in DC microgrid

DC microgrid (shown in Figure 1-5) consists of DER, distributed energy storage (DES), distributed loads, power electronic converters including grid interfaced converter and other required control modules that ensures the proper operation of DC microgrids,.

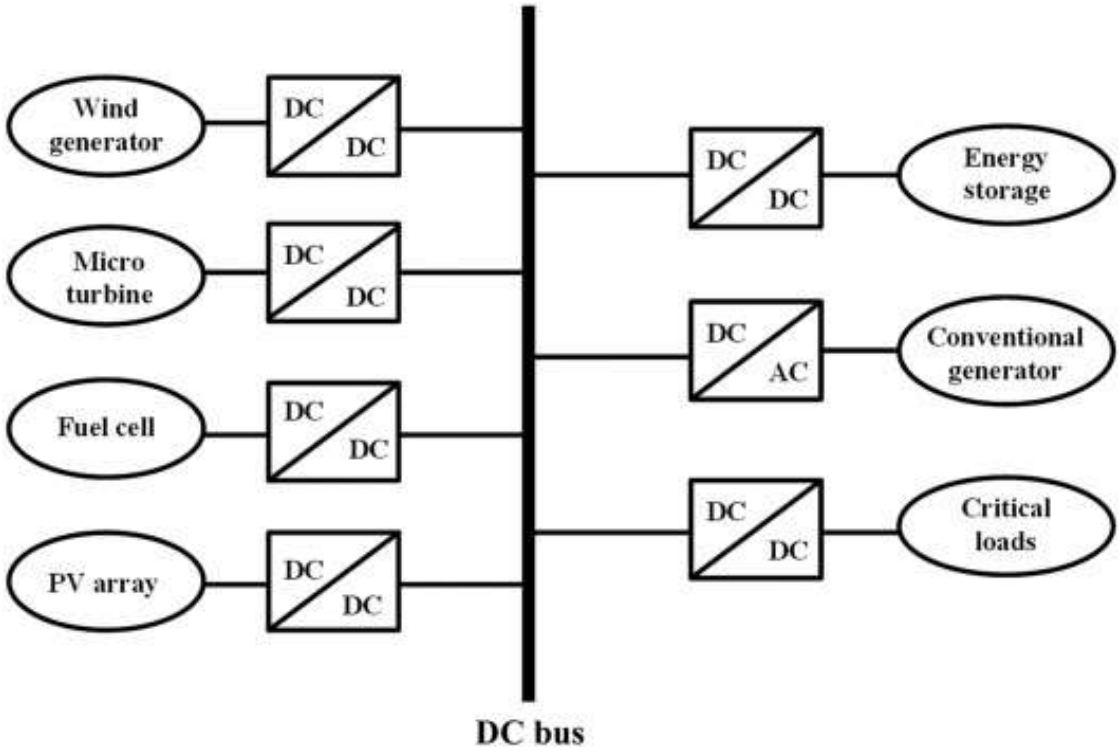

Figure 1-**5 Components of the DC Microgrid**[6]

1.6.1 Distributed energy generation

DER can be classified as renewable energy resources and nonrenewable energy resources. DC microgrids have higher penetration levels of renewable generation to preserve sustainability. Solar power generations play a significant role among the DER in both configurations, single module and multiple solar PV generation. In addition to that, other renewable generation types such as wind can be integrated using an AC-DC converter.

1.6.2 Distributed energy storage

DES is the most important asset in the DC microgrid system concerning the protection and reliable operation of the system. It ensures smooth operation in the different transient situations and operating modes in the DC microgrid system. The DES is fully responsible for regulating the system voltage under the islanded mode of operation of the DC microgrid. DES can be broadly classified in terms of technology, capacity, response time, and capital cost. Among the DC microgrid systems, super-capacitors, hydrogen Energy storage, and electrochemical capacitors are more prevalent in both commercial and domestic projects. However, Lithium-Iron is the most widely spread technologies within the DC microgrids due to its large capacity and availability. It is very costly when compared with the other available battery types.

1.6.3 Distributed loads

The prime objective of any power system is to deliver the power to end users any interruptions and maintain the power quality. The end users typically are modeled as AC or DC loads in the simulation environment. Therefore, it plays a significant role in DC microgrid designing, controlling, and operating functions of the system. Typically, those loads can be categorized as commercial, residential and domestic, etc. In the present power system, more than 90% of the loads are in DC nature due to the various reasons and trends. Specially, the DC microgrids are modeled only for DC loads; but AC loads are acceptable in a small range. If the AC loads are growing high in a DC microgrid, it will proportionally decrease the overall efficiency of the system as a result of the losses in the conversion stages.

1.6.4 Power converter and control

Power electronic devices are more familiar in the DC microgrid systems. The AC-DC converters and DC-DC converters (unidirectional/bidirectional) are highly utilized and serve the function of transformers in the AC networks.

Variable Source Converter (VSC) is a power electronic device that contains the bi-directional AC-DC converter to connect the DC microgrid system with the primary grid. It controls the power exchange between the network and DC microgrid system while regulating the internal voltage by using the complex internal control system in the grid-connected operation of the DC microgrid. Furthermore, DER is connected typically through the DC-DC converters to match the different voltage levels in the energy resources and microgrid voltage. In some rare cases, the AC loads are connected to the system via DC-AC inverters in small percentages to the grid.

1.7 Operating modes of DC microgrids

The DC microgrid has two major operating modes: islanded and grid connected. The transition in between above-mentioned operating modes needs seamless transitions to ensure the power quality as shown in Figure 1-6. In addition to that, the following essential functions need to be concerned when designing the internal control system as mentioned below,

1. To regulate the voltage of DC link at an acceptable range
2. To obtain the maximum power output from renewable energy sources.
3. To manage the internal battery module with proper battery energy management system to operate under both grid-connected and islanding mode effectively.

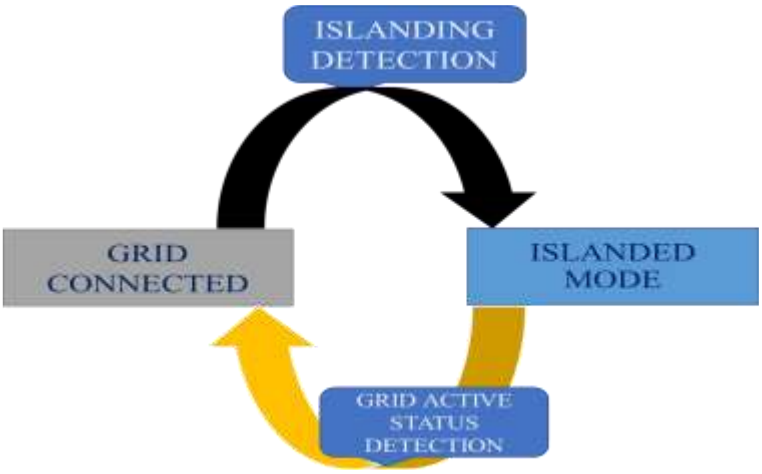

Figure 1-6 Operating modes of the DC microgrids

1.7.1 Islanded mode:

The internal control of the DC microgrid in islanded condition is sophisticated as the microgrid operation is independent from the primary grid. In the islanded conditions, the microgrid internal voltage is regulated by using the battery module.

DC microgrid can be islanded when the primary grid operates under faulty conditions, at system blackouts, due to intentional tripping conditions in the protection schemes and unintentional VSC failure situations. Under any condition, the islanding must be detected using proper mechanism under the supervisory control scheme and direct the appropriate signals to the primary controller of the DC microgrid. The primary controller immediately isolates the system from the primary grid with a switchgear system located near to the point of common coupling. Thus, the DER operates as the main power supply to DC microgrid during the islanded mode of operation while regulating the internal voltage and the DES compensates the power mismatch between the generation and load requirement with the help of battery energy management system (BEMS).

In most cases, the generation of the DER is insufficient to meet the internal demand in islanded mode. In such a situation, BEMS enables the discharging mode of the battery and regulates the internal DC voltage. Furthermore, the situation in which the battery module cannot cater the power mismatch in microgrid due to the power limitation of the DER, the load shedding scheme is carried out to supply uninterrupted power to critical loads.

1.7.2 Grid connected mode:

The DC microgrid connects to the primary grid via a VSC and switchgear system at the point of common coupling (PCC). In the grid-connected operation, the switchgear system is in closed status and DC microgrid is synchronized with the AC system with the internal control system. There are various types of grid synchronizing strategies used in the DC microgrid system. In all the strategies, the variables such as grid voltage and frequency in the upper stream are fed into microgrid to ensure the better working of internal controls. The DER fully contributes to the internal demand of the DC microgrid system and the power mismatch is accomplished with direct power-sharing with the primary grid.

The VSC is responsible for managing the power exchange with the primary grid and the DC microgrid system. The DC microgrid system imports power from the primary grid in a power deficit condition, where the internal generation is lower than the power demand. The VSC exports power to the primary grid in power surplus situations where the system has more internal generation than the demand. Therefore, The VSC has fully controlled the energy exchange between the DC microgrid and the primary grid while regulating the system parameters. Sometimes, due to the internal limitations, the VSC cannot handle transient situations including fault conditions, significant load switching, and large capacitors switching. Under such situations, BES compensates for the sudden variations in the DC microgrid system.

1.8 Challenges and motivation

Despite many advantages, implementation of DC microgrids are limited due to significant disadvantages like, lack of proper standards, compliance and testing procedures. However, some international bodies such as the Institute of Electrical and Electronics Engineers (IEEE) have published some relevant standards, including IEEE 1547 relevant to these areas. IEEE 1547 states that the main requirement need to be satisfied in detection of islanding in an electrical power system, is to detect the islanding situation in less than two seconds.Any islanding detection method needs to have fast and accurate detection to secure the proper functioning of the DC microgrid system. The following are some other challenges associated with islanding detection,

- ❖ Voltage is the unique parameter, which can be measured at any point in the system irrespective of the operating mode of the system.
- ❖ Available islanding detection methods are mostly explored for AC microgrids, but the heavily used parameters like frequency, phase angle in AC systems are not existing in DC systems.
- ❖ Transient conditions like islanding, in the primary grid are slightly reflected in the measurable parameters in DCMG system.
- ❖ Under the critical power condition in DC microgrid: where the power generation and load are matching, islanding transients are hardly visible on the locally measured parameters.
- ❖ Active methods have low power quality.
- ❖ Passive methods have generally larger non detection zones (NDZ) and longer detection times.

In any microgrid system, detection of islanding under critical power condition is challenging as there is near zero power flow through the point of common coupling (PCC). As a result, any measurable changes cannot be observed in the DC microgrid system. Therefore, it appeals for some sophisticated methods to detect the islanding. This condition is infrequent due to the real-time load fluctuations and the intermittent nature of the distributed generators.

However, any islanding detection method needs to have fast, accurate and robust detection even under rare cases including critical power condition. An illustration of critical power condition is given in shown in Figure 1-7[7]. The NDZ needs to be maintained at a minimum range to ensure the accurate operation under the different operating conditions of the DC microgrid system.

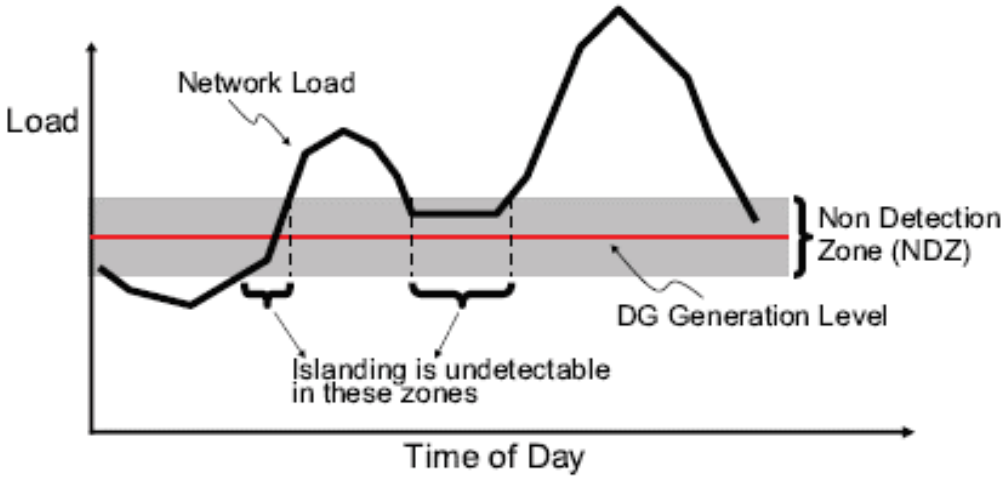

Figure 1-7 Non-Detection Zone at Critical Operating Mode[7]

1.9 Objectives

The main objective of this research to, design a fast, accurate, reliable, and unsophisticated Islanding Detection Method (IDM) for DC Microgrids. This main objective is accompanied by the following sub-objectives:

- To design and model the DC microgrid (DCMG) and validate using a transient simulation software
- To analyze the transient behavior of the DCMG during islanding operation
- To design a suitable IDM for reliable detection of islanding in a DCMG
- To evaluate the performance of the designed method in terms of detection accuracy and time under different network configurations

1.10 Thesis Outline

This thesis workflow has eight chapters.

Chapter one contains the introduction to the microgrids and islanding detection of these systems and research problem and objectives.

Chapter two contains a literature review on the modeling of the single-phase DC microgrid system while introducing its significant components with possible modeling techniques of it.

Chapter three extends the literature review on islanding detection of DC microgrid systems.

Chapter four provides the details of the modeling and simulation of the designed DC microgrid system.

Chapters five gives the details of the proposed islanding detection method and the selection of the important parameters of the algorithm.

Chapter six contains the performance evaluation of the proposed islanding techniques with simulations and case study under different scenarios.

Chapter seven contains the sensitivity analysis on proposed islanding detection method based on accuracy and detection time.

Chapter eight extends with conclusion and recommendation for the islanding detection in DC microgrid system.

2. LITREGER REVIEW ON DC MICROGRIDS

2.1 DC microgrids architectures

DC microgrid (DCMG) concept is opening the new era for the higher penetration levels of renewable resources like solar PV technologies which are naturally producing DC but, highly intermittent in nature[8][9]. Interfacing the DC microgrids with a primary grid is highly essential for improving system reliability and stability.

There are many DC microgrid architectures and each type has its own advantages and disadvantages[9][10][11]. The radial type is considered as the mostly used type in DC microgrid systems, which includes some advantages like simplicity, ease of commissioning, and low initial cost involved.

2.1.1 Radial configuration

The radial network is the most deployed architecture in the distribution phase. In this configuration, DC microgrid is connected to the primary grid from the one end, and the loads are consuming power from one direction. The single line diagram of this type is shown in Figure 2-1[10][12]. It is mostly useful in residential buildings, where low voltage system preferred.

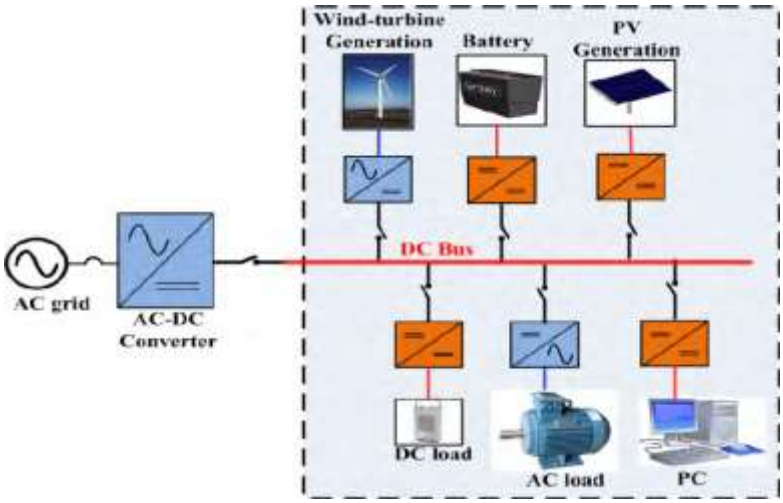

Figure 2-1 Radial Configuration[10]

This concept is not only applicable for small scale projects, but also, they can be extended to complex systems such as multi-storied buildings and locally distributed systems, where the system has many energy storage systems, renewable energy sources, and AC loads and DC loads. In such network, every building is acting as a cluster to the DC microgrid, which accepts the power exchange with the neighboring clusters. The main disadvantage of this architecture is that it has low reliability than the other available systems because the radial system powers its loads in a single direction[10]. If there is any breakdown in the DCMG, it causes a blackout in the whole system. Radial DCMGs are interconnected to the AC grid from one point.

2.1.2 Ring configurations

This microgrid approach was introduced as an alternative to the radial networks to improve the reliability. This architecture is named as a loop configuration as well[10]. The main characteristic of these networks is they have more power flow paths from the AC grid interface to the loads as shown in Figure 2-2[10][12].

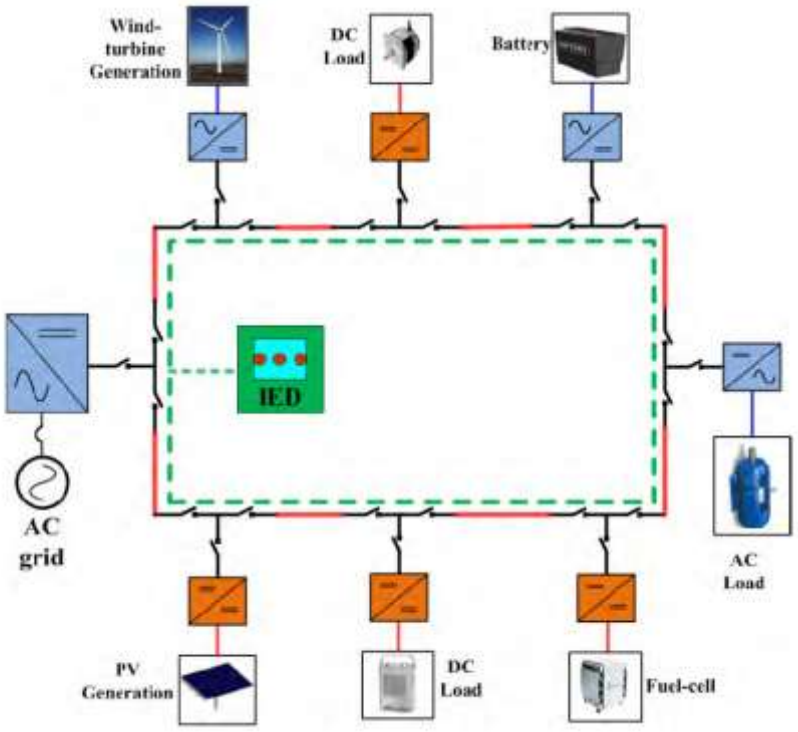

Figure 2-2 Ring Configuration[10]

Each grid subsections of the grid contain a DC switchgear system in both directions to isolate the system when there is any faulty situation in the grid. This system has some additional electronics called intelligent electronic devices to detect and isolate faulty buses from the system. It ensures secured the uninterrupted power flow to the end-users by isolating the faulty feeders in the microgrid. Therefore, it enhances the reliability of the system. Moreover, these systems are much expensive compared to the radial systems as this need additional devices, including switches, breakers, and conductors in construction[10][12].

2.1.3 Interconnected configuration

The interconnected configuration increases the reliability of the system by the integrating of multiple AC grid interfaces to the microgrid. This approach ensures the power to its end users even the situations that have failures occurred in multiple feeders in the distribution system. These architectures are quickly adopted in Zonal and Mesh type of DC microgrid systems as shown in Figure 2-3[10].

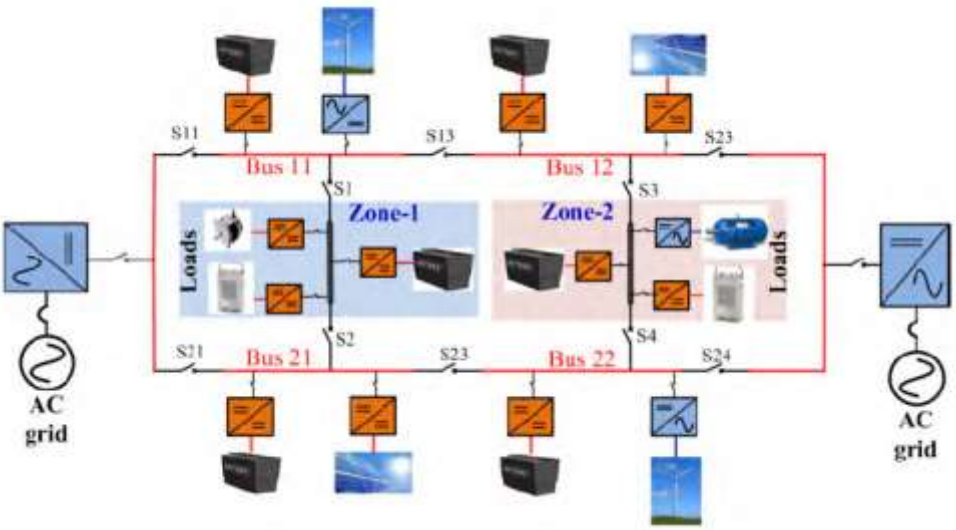

Figure 2-3 Interconnected Configuration (Zonal Type)[10]

2.2 AC interface of DC microgrid

The modern DC microgrids are integrated with the primary grid to enhance the reliability of the system. However, there are some microgrids, which are implemented for the rural electrification, as isolated microgrid systems without any connection to the primary grid.

Integration of microgrid to the primary grid attracts more importance as it enhances the power quality, reliability of the system and availability of RES. Hence, most of the newly commissioned microgrid projects are proposed with grid interface converters to harness those benefits.

There are many types of grid interfacing converter topologies[10]. These converters must be capable of handling bi-directional power flow to ensure proper power exchange with internal power resources and utility. grid interfacing converters can be categorized as:

1. Diode Controlled Converter
2. Active Front End Converter
3. Other special technologies

2.2.1 Diode and controlled rectifiers

This technology is considered as a unidirectional power converter and currents consists of some low order harmonics less than 2 kHz. The passive filters connected to the DC link or front end of the diode rectifier is used to eliminate the harmonics and improve the quality of the line current of the system. This topology can be applied into the single-phase and three-phase system as shown in Figure 2-4[10]

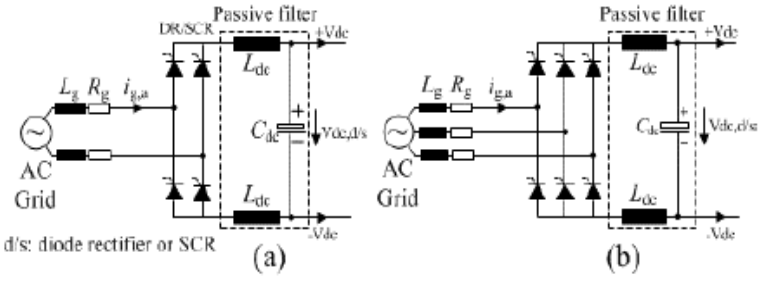

Figure 2-4 Diode Controlled Rectifier (a) Single Phase (b)Three phase[10]

2.2.2 Active front end converter

Active front end converter is the mostly used converter topology for interfacing DC microgrids to the AC systems. The design system has a bi-directional converter and pure sinusoidal waveforms capability and shows significant advantages over other available techniques. These converters are constructed with switching devices like IGBT or MOSFETS as relevant for applications. Those switching devices are controlled through pulse width modulation (PWM) signals generated with an internal control module[10]. The filters such as L, LC, LCL arrangements are deployed in the system to control the frequency ripple in a front end as shown in Figure 2-5 . It removes the high-frequency components from the line current in the primary grid. For that, it needs some additional damping method to ensure the stability of the system as mentioned below,

1. Passive Damping Methods

   A resistor in series with the capacitor is used in the design, and it may affect the total efficiency of the system [10].

2. Active Damping methods

   This design overcomes the issues in passive damping method. It is creating a virtual resistance with help of one of the state variables within the system such as capacitor current [10]. This method requires some additional sensors for measuring internal parameters and it will boost the system efficiency than previous method.

3. Proper Control Design

   This method is mainly focused on the proper selection of the L and C parameters in the filter to avoid the unwanted oscillations of the system [10]. However, it is an advanced and challenging technique due to the system poles close to the origin and complexity of the initial implementation

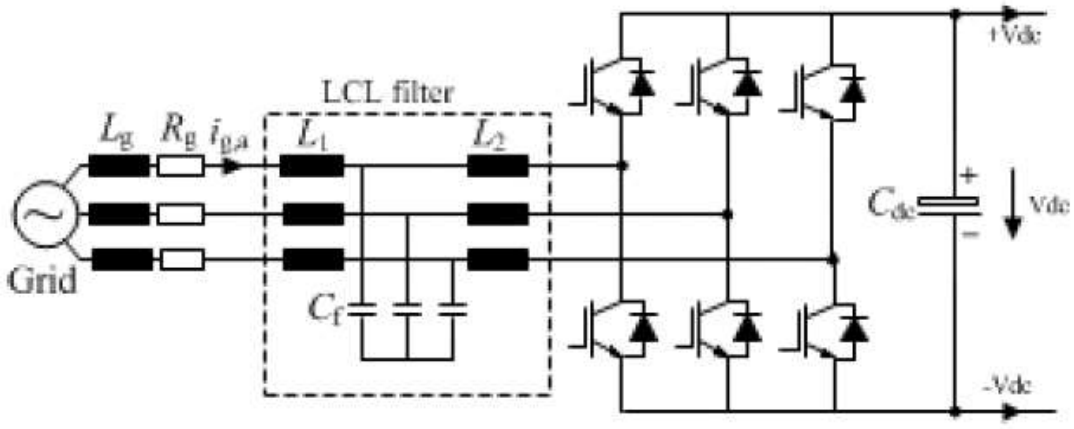

Figure 2-5 Active front end with integrated LCL filter[10]

2.2.3 Other special technologies

Some additional topologies have been featured in addition to the technologies mentioned above with additional features to improve the power quality of the systems.

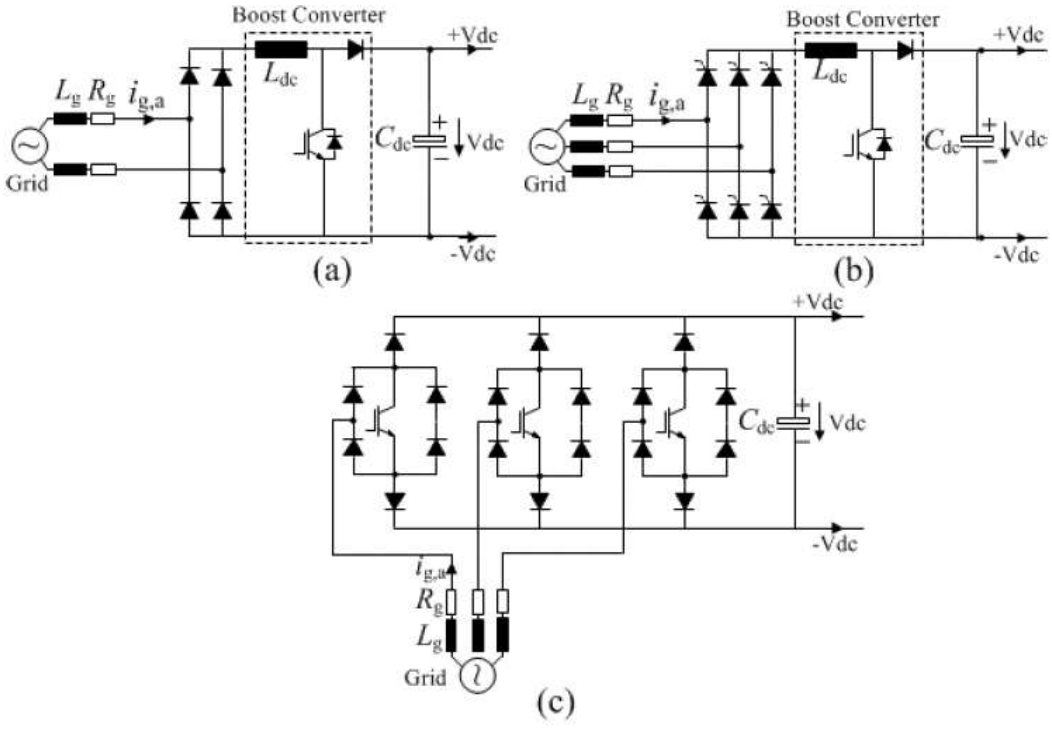

Figure 2**-6 Different AC-DC topologies (a) Single-Phase PFC (b) Three phase electronic inductor (c) Three Phase Vienna rectifier**[10]

Figure 2-6(a)[10] illustrates one of the technologies where there is a diode rectifier with a parallel-connected boost converter. The main advantage of this system is that it improves the current quality of the system with an additional feature called power factor correction (PFC) in a single-phase system. The same approach can be used in a three-phase system, as shown in Figure 2-6(b)[10]. The main advantage of this technique is the function of regulating the current and voltage in variable load conditions in the grid. The Vienna rectifier, which is shown in Figure 2-6(c)[10] has the unidirectional capability with sinusoidal line current. The main advantage of this topology is the application of lower power switches compared to the active frontend converter, and it enhances the reliability and lowers the cost of the system.

2.3 DC microgrid link configurations

DC-based applications in the power system are intensively popular among the power system due to the compact devices with power electronic applications and modern transportation trends in the industry. Although, the major voltage levels can be categorized as 12 VDC, 24 VDC, and 48 VDC[13], the most popular among commercial projects, such as data center and telecommunication related microgrid projects is 48 VDC[10][13].

The DC microgrid system with a 48 VDC range motivates the direct connection of these devices by reducing the redundant power conversion stages. DC microgrid concepts improve the system efficiency as well as reliability.

The isolated DC microgrid projects mostly use 12 VDC as the base voltage. It is used for rural electrification, where general power transmission lines cannot reach terrain areas with mountain ranges. The 12 VDC voltage is used for general lighting applications. However, these low voltage DC microgrids have some limitations of power carrying capacity and power transmission over the long-distance, which needs large conductors for supplying the power to the end-users. It may cause massive system losses due to the large currents and drastically reduce system efficiency. Therefore, 380VDC voltage level is used at most of the commercial projects with higher capacities[10][13][14], which allows maintaining the system losses below 5% - 8% range to improve the system efficiency. In this research, 48 VDC low voltage DC

microgrid is modeled considering small scale residential type applications for the smart house with IoT based technologies.

In the typical AC systems, the power is transmitted through two-wire (single-phase) or four-wire (three-phase) systems[10]. In the same way, DC microgrid has different power transmitting scenarios based on the number of voltage levels and polarities in the DC-link as indicated below[10],

1) Unipolar DC microgrid systems
2) Bipolar DC microgrid systems
3) Homo polar DC microgrid systems

2.3.1 Unipolar DC microgrid systems

Unipolar DC microgrid systems have a single voltage level. Then the loads are connected to the positive and negative poles as shown in Figure 2-7[10]. In any DC microgrid, the selection of the appropriate voltage level is a crucial factor. In this type of system, high voltage levels improve power transmission over long distances. However, it reduces the safety of the personals in the microgrid. In addition to that, it needs some additional power electronic converters such as DC-DC converter to supply loads of end-users, which requires the lower voltage level other than the DC-link voltage level. The low voltage level is suitable for short power transmission. The selection of proper lower voltage level reduces the redundant power conversion stages. It improves system efficiency.

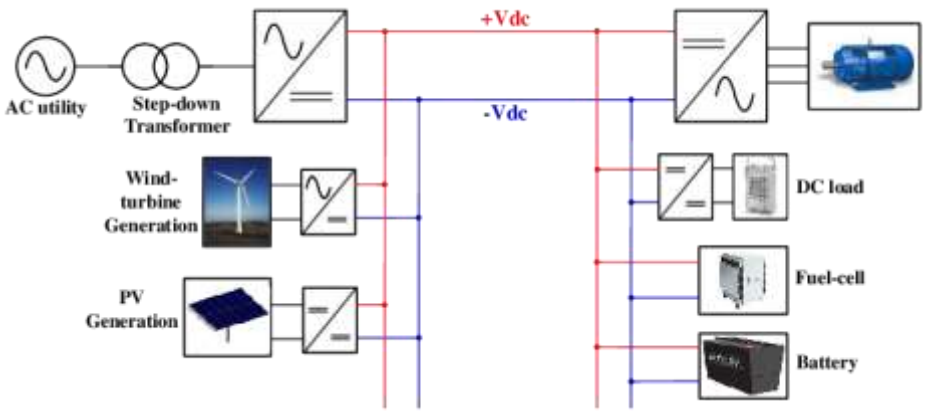

Figure 2-7 Unipolar DC Microgrid[10]

The unipolar system does not create an asymmetry between the DC poles. However, this system does not provide any redundancy, or any backup in the fault situation, whereas it can lead the overall system into the complete shutdown. Also, this does not offer any multi-voltage level capability to its customers.

2.3.2 Bipolar DC microgrid systems

Bipolar DC microgrid system is introduced as a solution to the issues with unipolar DC microgrids. It is known as the three-wire system too. This system consists of +V, -V and neutral wires as shown in Figure 2-8[8][10][15], where it enhances the options in voltage levels: +V, -V and 2V for the customers and improves the flexibility. Furthermore, when the system is undergoing a fault situation in one pole, the rest of the system can be operated by isolating the faulted feeder. It improves the reliability, power quality, and availability system of the system even in fault situations. Sometimes, bipolar DC microgrid causes asymmetry in the DC link due to the unbalance loading in different voltage levels. Therefore, proper control system for the front-end converter or advance voltage controller to the DC microgrid is highly recommended in the implementation.

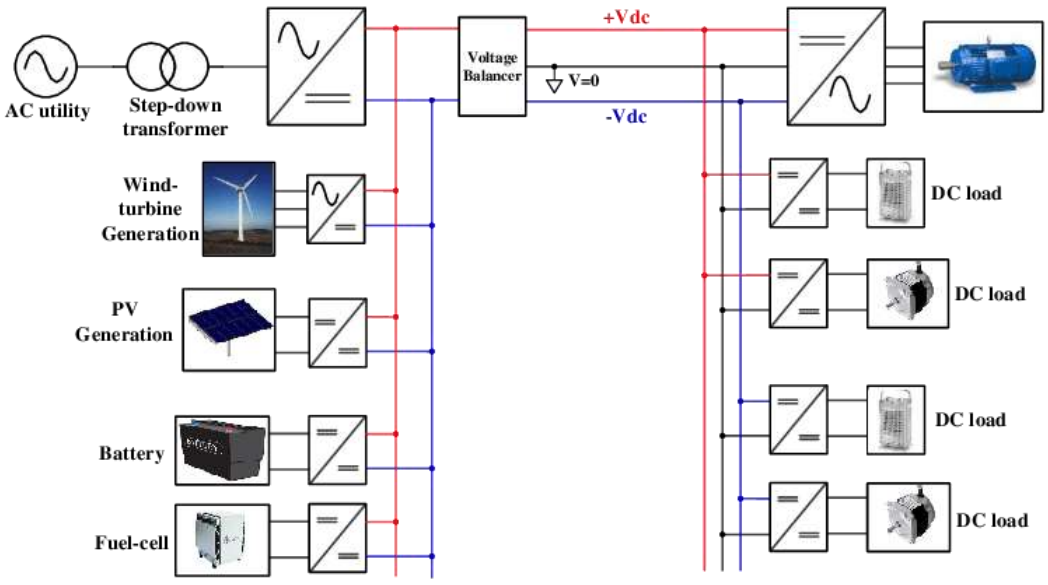

Figure 2-8 Bipolar DC Microgrid system[10]

2.3.3 Homo polar DC microgrid systems

Homo polar DC-link configuration is another type of DC microgrid system. It consists of two or more DC links with the same polarity, as illustrated in Figure 2-9[4]. These systems mostly consist of multiple negative polarities at low voltage levels with the ground return or metallic return. However, it creates undesirability in the controlling of the microgrid compared with the other available types mentioned above. Typically, those systems this has low insulation cost as the main advantage of this configuration.

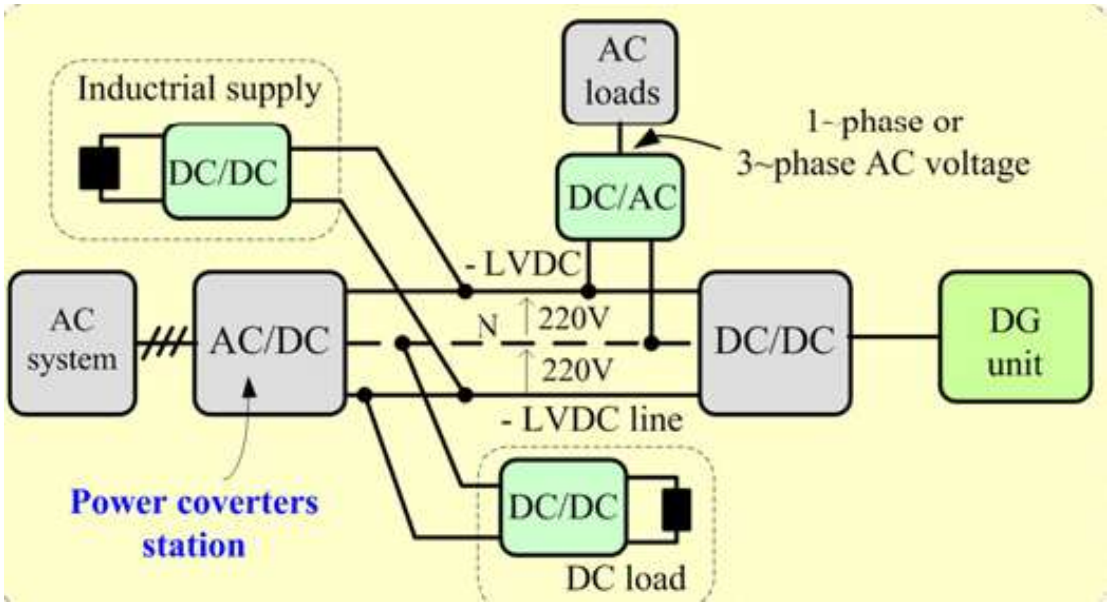

Figure 2-9 Homopolar DC Microgrids System[4]

The figure mentioned below consists of three wires, two of them have the same polarity level and another one is the neutral wire. In this configuration, the voltage is divided into two or more wires. It is mainly useful in the distribution level power transfer. If the 400VDC homo polar network, domestic customers can be supplied with 220VDC by voltage difference in between the one set. furthermore, if anyone needs 400VDC for the industrial purpose that can be catered with the neutral and outer wire together in higher voltage.

2.4 Hierarchical control architecture

The hierarchical control system consists of three major categories: primary, secondary, and tertiary control topologies [6]. This control architecture is mainly responsible for sensing, processing, monitoring, supervising, optimization, etc. The hierarchical control system for the DC microgrid is illustrated in Figure 2-10[16]. The sequence of the hierarchy is based on the response time of control function of each category. In the bottom contains the primary control section with quick response and the top contains tertiary control section with large response. The secondary control system is positioned as intermediate section in between aforementioned sections. The primary section relates to the tertiary control and secondary control with hierarchical bidirectional data path to ensure the continuous monitoring and control functions in the system.

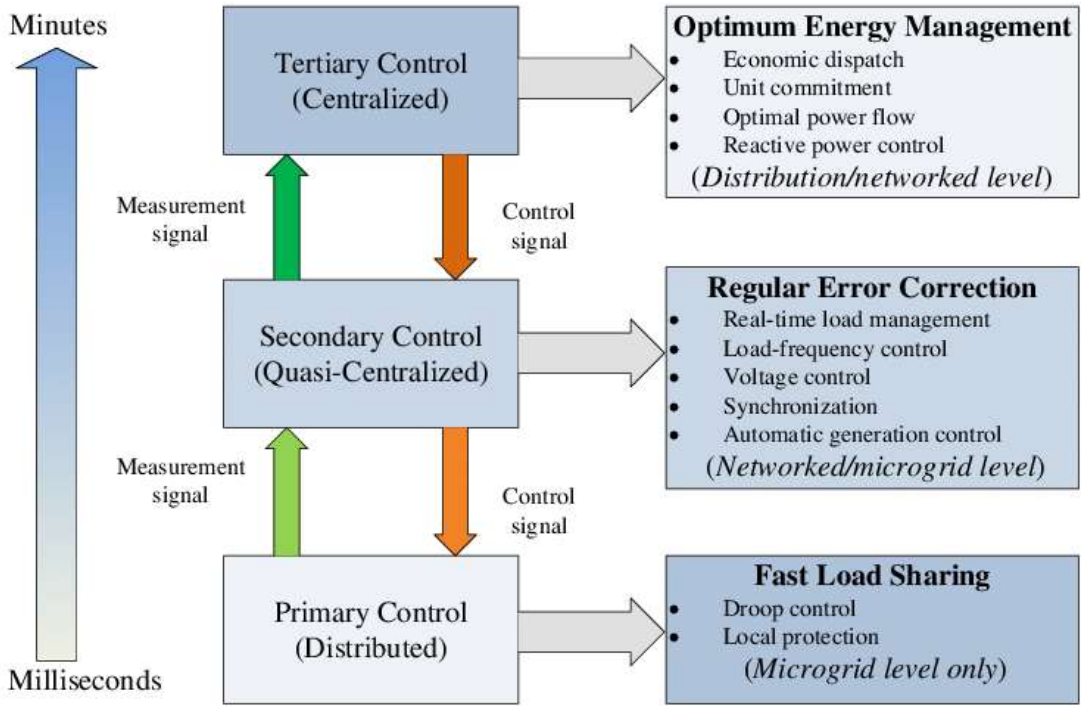

Figure 2-10 Control Architecture of Microgrids[16]

2.4.1 Primary control

Primary control stage has a faster response and higher bandwidth compared to secondary and tertiary control stages. It has a higher priority level in the control hierarchy which mainly responsible to the power-sharing, protection and reliability of the system[14]. The primary control is mainly responsible for regulating the voltage of the system even in the islanded situations. It provides the proper control reference to DER and maintains power-sharing between the utility and DC microgrid. Those control functions are mainly located in elements such as power electronic converters (AC-DC converter and DC-DC converter), which creates the controllable platform between the loads and the power resources. The outer control loop of the cascade control system mainly consists with the primary control. These cascade control systems mainly available in the current and droop control system in the dc microgrid environment.

2.4.2 Secondary control

The, power flow, power quality, and frequency synchronization are performed at the secondary control section. The secondary controls ensure that the essential parameters within the microgrid are maintained within the predefined value. As an example, when the system has higher droop gain in power-sharing control, it ensures the precise control of the power exchange between the microgrid and utility[14] [16]. However, the main problem is that the voltage shows some voltage variations while operating with the higher droop gains. At such situations, to maintain the voltages at its nominal value, the system needs to have a secondary control system to maintain the control parameters within the acceptable range. Figure 2-11[16] illustrates the function of the secondary control. The system is incorporated with the primary control as indicated in the figure; the no-load operating point is the V_0 point, it will shift to the PT_1 (operating point 1) under the I_{dc1}(Current 1) load condition and, it will shift to PT_2 under the I_{dc2} condition. After that the secondary control system is coming to the action, and it will shift the OP1 to OP1_new and OP2 to OP2_new and control the voltage level at the nominal voltage. Likewise, it always maintains the control parameters at its nominal values with the help of the secondary control system.

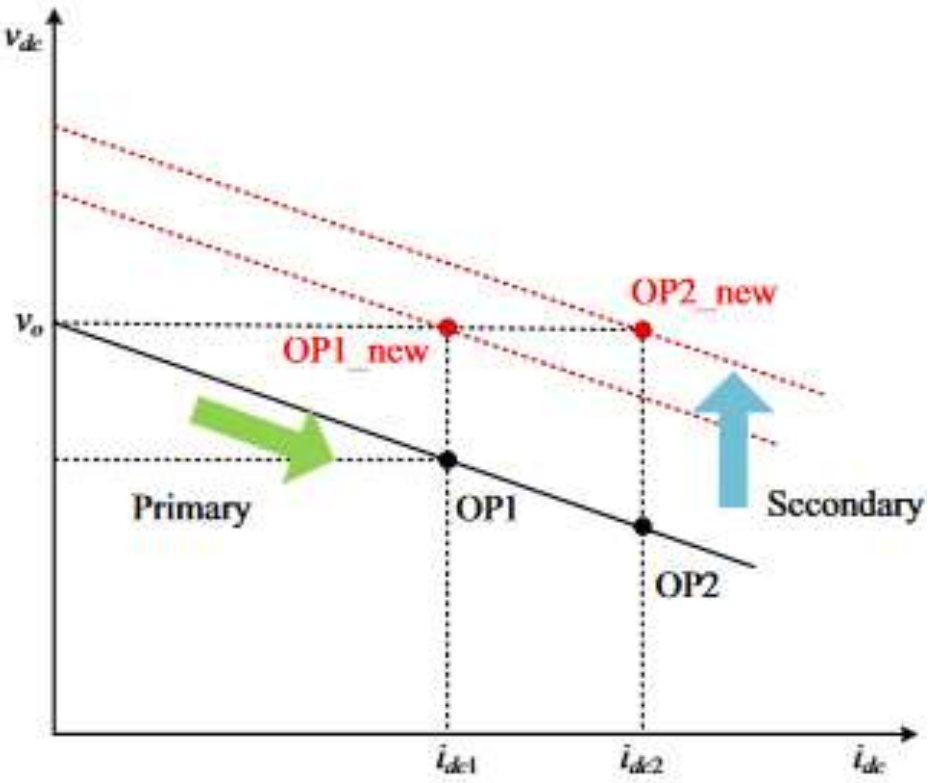

Figure 2-11 Secondary Control of the DC microgrid[16]

2.4.3 Tertiary control

It is the highest control level in the DC microgrid control hierarchy. Tertiary control is responsible for the power and energy management, system optimization, load forecasting and economic dispatch of the distributed energy resources at the distribution grid [4][14][16].Compared to the secondary control, tertiary control has a lower control bandwidth concerning the higher response time.

3. LITERATURE REVIEW ON ISLANDING DETECTION OF DC MICROGRID SYSTEM

A microgrid can be defined as an electrical network that compromises of distributed generation, storages, and loads at the distribution level, which can operate either connected to the utility grid following it or as an island in autonomous operation [17][18]. A typical DC microgrid is shown in Figure 3-1. DC microgrids are using DC power transmission lines to transfer the power to its loads. The renewable generation is increasingly popular among those DC microgrid systems.

The microgrid systems need to have greater control over the operations related to distributed generation, handling system disturbances, such as islanding situations including blackout, brownouts and voltage fluctuations due to the power quality issues. In most of the microgrid systems, the primary grid is used as the main power source. Hence, the probability of loss of the primary grid connection is a severe issue and detection of the microgrid islanding has been recognized as an emerging research area over the past decades. Most of the reported research are focused on islanding detection techniques in AC microgrids.

Each islanding detection technique has its pros and cons specific to its application. Most of the available islanding detection techniques cannot be used in DC microgrids due to the unavailability of the core parameters in the AC networks such as, phase shift and frequency [19]. Therefore, further research on fast and reliable islanding detection methods for the DC microgrid systems is highly recommended [15][20]. DC microgrids eventually have a limited number of measurable parameters compare to the AC networks[19]. Hence this is the most challenging protection design issue in the DC microgrid concept. Most of the explored islanding detection techniques in the DC microgrid systems have referred to the IEEE 1547 standard [19][21][22]. IEEE 1547 standard is mainly focused on distributed energy resources, and it has discussed about the interconnection of the distributed generators to the electrical power system. The detection of the islanding has recognized as more influential in areas such as worker

safety, equipment safety, power quality, and distributed energy resource management [22][23].

The available islanding detection techniques in AC microgrid system are also investigated as they are highly influential and mapping of those techniques into the DC microgrid systems would lead to achieve a reliable detection method. Moreover, the concerns about the lack of standards in this area yet filling this gap to develop and demonstrate the more reliable method with theoretical and technical approaches [14].

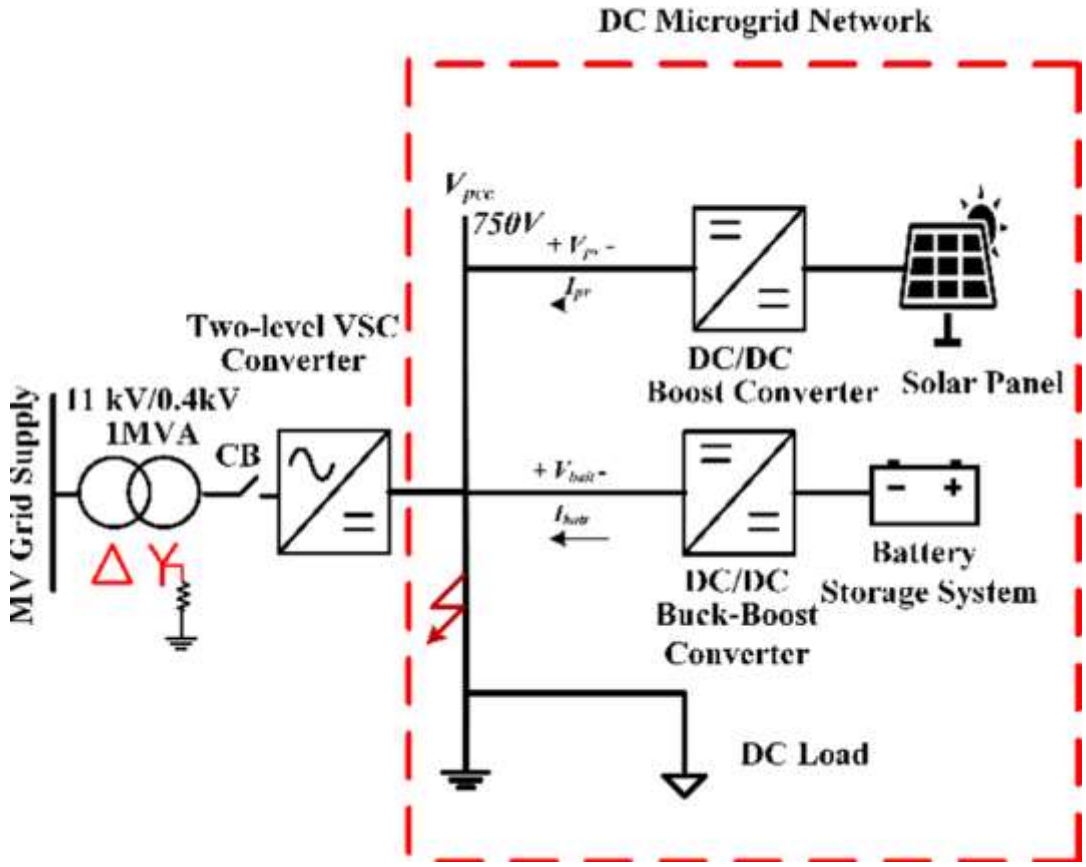

Figure 3-1 Islanding of Microgrid system[17]

3.1 Classification of islanding methods in microgrids

The detection of islanding can be broadly divided into the two main categories known as remote and local based techniques [23][24].

3.2 Remote islanding detection techniques

In remote islanding detection techniques, which is known as grid resident detection techniques as well, islanding detection is related to some change(s) in parameter(s), which is then informed among the resources of the microgrid through a communication method [19][23][25]. Hence, the reliable data transfer [6][8][19] between the utility and the distributed generators becomes the vital requirement in this approach. There are some available detection methods such as transfer trip method (TT) [25], power line carrier communication method (PLCC)[25][26], Signal produce by disconnect method (SPD), supervisory control and data acquisition method (SCADA) [8][16][23][25]. Almost all the methods are highly acceptable for the detection of the islanding because remote islanding detection techniques do not encompass any NDZ compared to the other available detection methods found in recent publications. Hence, remote islanding detection techniques ensure reliable and accurate detection. In addition, it is allowing single and multiple inverter operation. It does not rely on the power flow in

between the grid and microgrid or effect to the regular operation in the typical microgrid operation. The complexity of the design and the high implementation cost are recognized as the major disadvantages of this method [24]. Hence, this system is highly adaptable for the microgrid networks with high penetration levels of distributed generation.

3.3 Local islanding detection

Local islanding detection techniques, which is also known as the inverter resident detection techniques operate based on the local monitoring of the system parameters in the microgrid, like the voltage, frequency, etc. It does not need any external equipment as in remote techniques for the detection process. The local techniques can be further classified as active, passive and hybrid as shown in Figure 3-2.

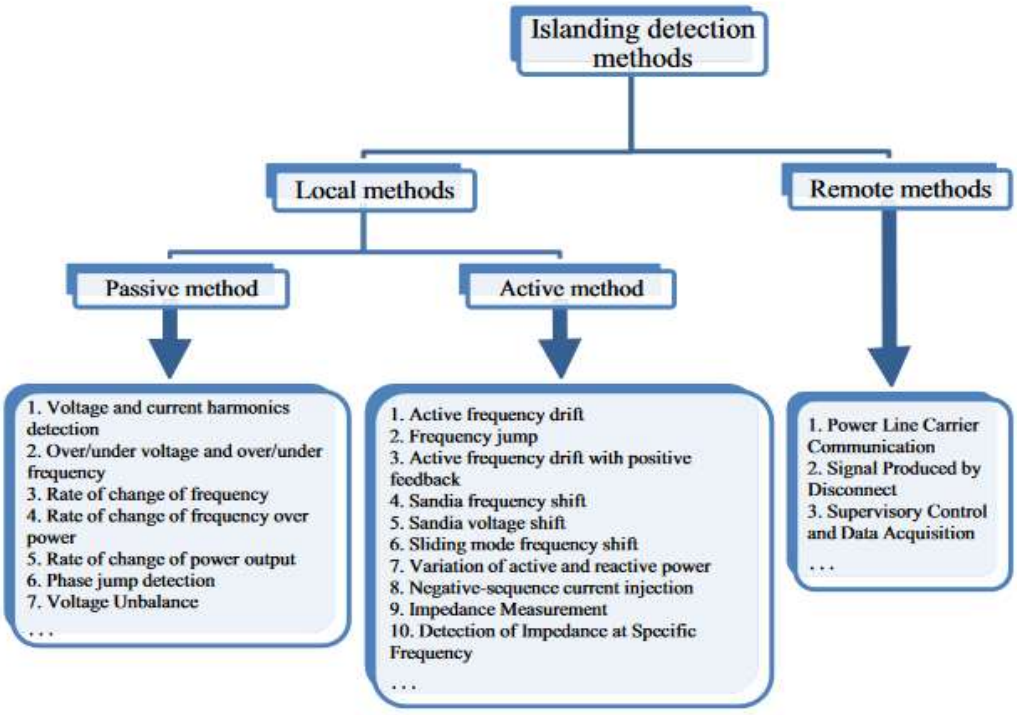

Figure 3**-2 Available Islanding Techniques**[27]

3.3.1 Active islanding detection techniques

The active islanding detection method is based on injecting a pre-defined perturbation level for selected parameters in the microgrid to enhance the measurement of the local parameter variations [28]. Detection of the islanding is based on monitoring the real-time variations of the grid parameters by comparing the predefined threshold values. The injected perturbations do not introduce any measurable variations in the measured parameters during the grid-connected status. However, measurable variations are observed during the islanded condition. Among some active islanding detection techniques, single injection [15], positive feedback [28] or controlled distortion [29] can be identified.

Active islanding technique typically has low NDZ [25] as well as a high accuracy level. The level of perturbation injected would increase the harmonic level of the inverter and reduce the power quality of the system by creating unnecessary transients in the grid. The implementation of active techniques is hard due to its complexity of the control system integration. The basic working procedure is shown in Figure 3-3[30].

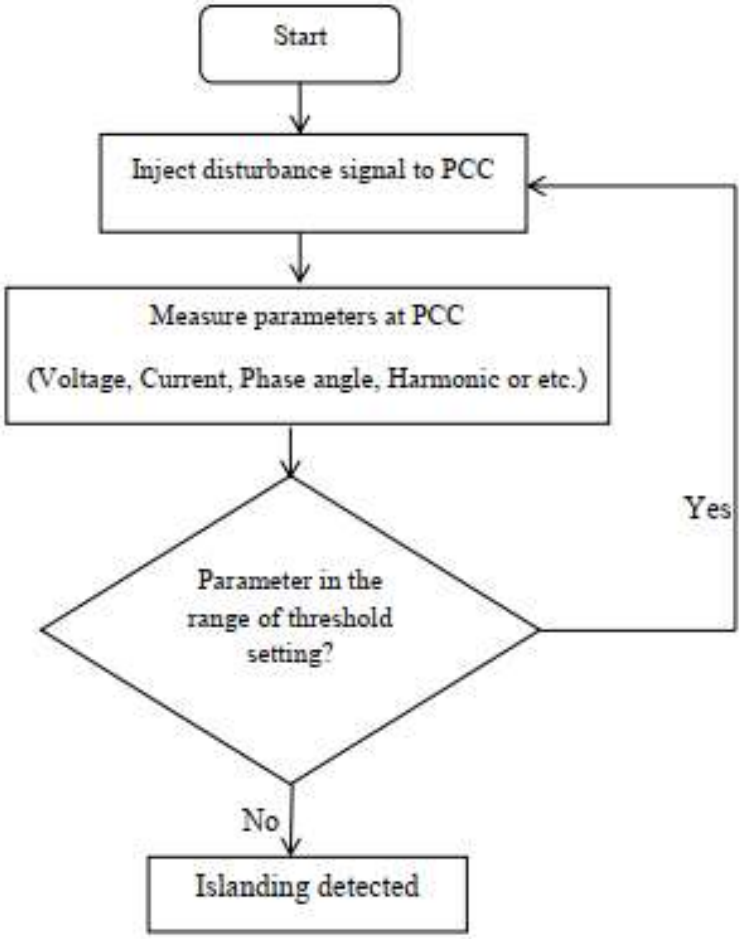

Figure 3-3 working principle of Active islanding detection[30]

3.3.2 Passive detection techniques

Passive detection techniques can be used when there is a significant power mismatch in the islanded system. These techniques detect the islanding condition through the measuring of the local parameters such as voltage, current, frequency and comparing with the predefined threshold values, as shown in Figure 3-4. These techniques have not created any disturbances to the regular operation of the microgrid but encompass higher NDZ. The basic operation of these techniques is illustrated in Figure 3-4 [30]. Many passive islanding techniques are already introduced for the AC microgrid related applications.

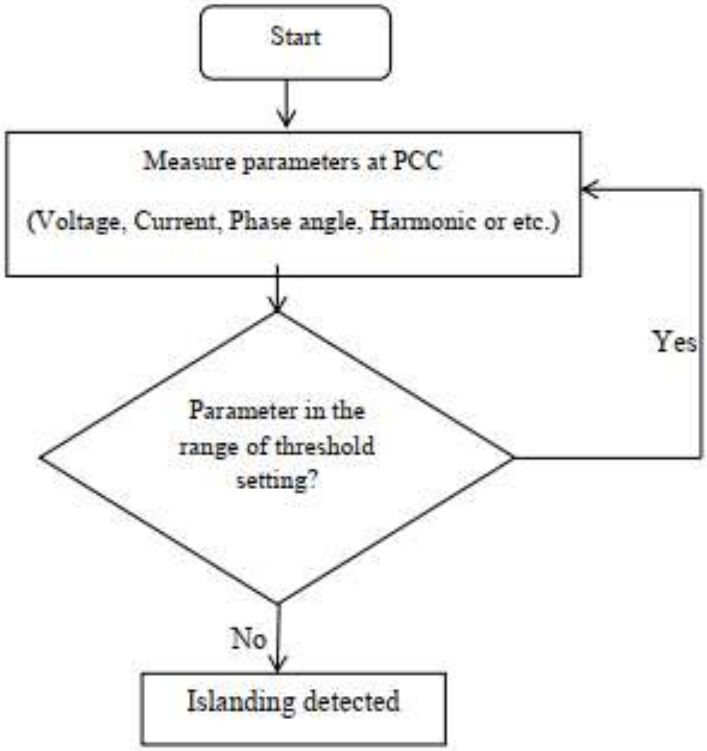

Figure 3-4 working principle of passive islanding technique[30]

3.4 Comparison of the islanding detection techniques

Pros and cons of existing islanding detection techniques discussed in the previous section is summarized in Table 3-1[31].

Table 3-1 Comparison of the islanding detection techniques[31]

Islanding Detection Techniques		**Advantages**	**Disadvantages**
Remote Techniques		Highly Reliable	High initial cost
Local Techniques	Passive	• Small detection time. • Doesn't perturb the system.	• Large NDZ • Difficult to detect islanding in critical condition. • Selection of the threshold values in comparatively difficult.
	Active	Smaller NDZ	• Apply perturb to the system. • Low efficiency in system.
	Hybrid	• Smaller NDZ. • Perturb the system when the system is triggered islanding condition	The design is complexed with both active and passive techniques. High detection time

3.5 Standards related to islanding detection

The main reason why the microgrids are still not widely popular among the power system developments is due to the lack of standards and related testing procedures in this area. Specifically, Islanding detection is an essential area in the microgrid concept because of the difficulties of islanding detection under critical operation conditions such as when the power generation and consumption slightly match each other. Inaccurate islanding detection creates a higher danger to the maintenance people as well as the safety of the equipment in islanding conditions and creates unwanted hazards in the microgrid systems. There IEEE 1547[22][32] is being extended to incorporate microgrid concepts. In addition, there are several standards related to specific utilities and standard bodies specific to the limited regions with their own recommendations, standards, practices, and guidelines as per their requirements. Some of the related standards for the DC microgrid systems are as mentioned below,

- IEEE C37.95-2014: IEEE Guide for Protective Relaying of Utility-Consumer Interconnections[33].
- IEEE 929-2000: IEEE Recommended Practice for Utility Interface of PV Systems[22].
- IEEE 242-2001: Recommended Practices for Protection and Coordination of Industrial and Commercial Power Systems[34].
- IEEE 1547-2018: IEEE Standard for Interconnection and Interoperability of Distributed Energy Resources with Associated Electric Power Systems Interfaces[32].

From those, the IEEE 1547-2018 is the latest and the most adaptive standard, which is most relevant for the islanding detection of the microgrids and yet to be extended this for the DC microgrid system. The IEEE 1547-2018 defines unintentional islanding as situations in which distributed energy resources are energizing the portion of the area in the electrical power system that is disconnected from the point of common coupling.

Then the islanding should need to be detected, cease the energy supply of DER, and avoid the forming of the electrical power island in less than 2 s [22]. The present standard is to avoid unintentional power islanding. The IEEE 1547-2018) [32] brings down the technological barrier to some extent towards intentional islanding or microgrids. This thesis has also given some inspiration for the extension of IEEE1547 standards to the microgrid area.

3.6 Active islanding techniques for DC microgrid systems

Active islanding techniques are mainly integrated with the system's distributed generators, which are interfaced with the DC-DC converters. The basic concept of these systems is the injection of disturbances into the controls of the converters. However, these perturbations have not affected the system in grid-connected status because the voltage source converter (VSC) controls compensate those variations with the help of the primary grid. In the islanded condition, the disturbances are expanded with the perturbation method due to the loss of the VSC controls without the primary grid connection. It creates some measurable variations to the system, and it may use to detect the islanding of the system very easily. The active method related approaches are more economical compared to the other available islanding techniques because these techniques do not need any major changes to the existing system other than updating of the control algorithm of the system. Also, these techniques have shown a small NDZ due to its feedback control approach along with perturbation. It shows measurable variation in parameters such as voltages/ current near the distributed resources even under the power mismatch within the system stays close to zero levels [15]. However, repetitive injection of the perturbation to the DC microgrid causes significant loss of power while reducing the power quality in the system. That is recognized as the major disadvantage of these active techniques. These techniques contain some complex control algorithms and it may slow down the detection of the islanding. The mostly used active islanding detection methods in DC microgrids are positive feedback, harmonic injection and insertion of the controllable load into the DC microgrid [15][30].

3.6.1 Positive feedback-based method

Positive feedback-based method of islanding detection techniques are tested under various scenarios, including multi DGs operation, different load conditions, and load quality factors and under load switching [27]. In Positive feedback-based method of islanding detection, the parameters in the primary grid side is measured at the PCC and transferred to the microgrid for creating the perturbation in the DER to detect the islanding [15][35]. It needs some additional information exchange form the primary grid system that reduces the reliability of the system [27].

3.6.2 Current perturbation-based techniques

In current perturbation-based islanding detection techniques, current perturbation has been introduced to create the current imbalance [29]in the DC microgrid with a specific frequency. The current perturbation is implemented with the solar PV MPPT tracking algorithm. It does not show any measurable variations of measured parameters in the grid-connected operation but shows significant variation in islanded operation. In this technique, the injected perturbation amount is continuously increasing with variations of the parameters thus, reducing the detection time. This method is also tested in different network configuration and it has fast detection of less than 0.2s [32]. The MPPT efficiency of the PV modules is near 99.7% [15]. However, this was not tested for the multi distributed generators and variable load conditions. In addition to that, this technique needs to optimize further to improve the power quality of the system.

3.6.3 Controllable load base method

Controllable load base islanding detection method is designed based on adding real-time variation to the controllable loads connected parallel to the DC link [14]. The MPPT of the distributed generators is not discussed in [14] and islanding detection is tested only for the worst-case scenario in which power generation is closely matched with loads within the system. In addition, the system is tested for the different irradiance levels but still, this islanding detection method needs to be optimized by further testing under different scenarios. The perturbation introduced by the insertion of real-time variation of the loads is normally compensated by the VSC and it does not

show any measurable voltage variations in the DC microgrid in normal operation. However, in the unstable condition of the system under the islanded condition has created measurable variations to its parameters and it is used to detect the islanding of the system with pre-defined threshold values. The major disadvantage of this technique is the degradation of system efficiency over time due to continuous perturbation activity in the system and, this technique is only applicable in the fixed load conditions, which is practically scarce.

3.7 Passive islanding techniques available for the DC microgrids

Passive islanding techniques are designed with continuous monitoring of the predefined system parameters such as voltages and current. The system creates some abnormal variations in the system parameters in the islanded condition and it is detected as islanding with pre-defined threshold values. After the detection of islanding, it initiates signals to the appropriate control modules in the microgrid system. These techniques are straightforward and productive when there is a high-power mismatch in the DC microgrid system, but these techniques have a higher NDZ than other available techniques. There are important passive islanding techniques such as the rate of change of voltage and under/over voltage methods.

3.7.1 Rate of change of voltage and current based method

Rate of change of voltage and current based islanding detection methods are mainly based on the voltage and current signatures captured locally near the distributed generators. The rate of change in voltage and current in the system is observed to detect the islanding status of the microgrid [29]. Proposed techniques are tested with different scenarios. The rate of change in voltage and current are measured at the local terminal of the battery and PV. The major disadvantage of this system is the higher NDZ and limitations on the differentiation of islanding status and the high impedance fault situations in the microgrid. In [7], it is stated that the passive islanding techniques like rate of change in voltage (ROCV), rate of change in current (ROCC) types are not suitable for the reliable detection of islanding in DC microgrids due to their limitations in the typical operation.

3.8 Remote islanding techniques for the DC microgrid systems

Remote islanding detection methods are based on the information exchange between the various systems through the communication links [24][31]. Mainly these techniques are based on the basic relay operation and other abnormal changes in the parameters such as voltages and currents. Remote islanding detection methods have higher reliability and better performance compared with other available techniques. These systems have zero NDZ as well as the high immunity to the system disturbances. However, these systems typically have a sophisticated design and high initial cost as disadvantages over the others [36]. In addition, these telecommunication technologies create new challenges such as cyber-security issues in power system protection. Transfer trip method and power line carrier-based methods are the common methods of remote islanding detection.

3.8.1 Transfer trip method

This method is based on the monitoring of the circuit breakers and re-closers in the system in the DC microgrid and analyzes this information to detect the islanding of the microgrid [37]. For the successful operation of this method, islanding detection is incorporated with SCADA to build up proper communication between the utility and distributed generators. When disconnection from the utility is detected at the substation level, it sends the appropriate control signals to the distributed generators and the main controller of the microgrid that may needed to be changed for islanded operation.

Transfer trip has very accurate detection with recent machine learning concepts. The DC microgrid with limited distributed generators in a radial network can be easily equipped with this method. This method can be used in microgrids with multiple grid interfaces and ring architectures as well but, the decision making becomes complex.

The major weaknesses of these techniques are the complex control approach and high implementation cost[23]. The reliability issues with data transferring over the distance are the common challenges of these systems[23][30]. However, it has not existed in any non-detection zone in the DC microgrid systems.

3.8.2 Power line carrier-based communication methods

The power line carrier-based communication method for islanding detection is designed as to transfer the information through distribution feeders to the distributed generators as a signal carrier [30][23]. In these systems, receivers are placed close to the distributed generators and continue monitoring signals from the transmitters. When the system has detected an interruption of the signal while system transition from grid-connected status to islanded status, it will trigger the islanding of the system quickly. Not like previous cases, this can be used with the multiple distributed generators as well as future expansions without any effect on the detection of islanding in the system. The frequency of the signal transmitting through the network needs to be determined as close or below to the fundamental frequency of the utility but, with minimum inference to the detection of the islanding.

This method has advantages, such as high accuracy and fast detection. The radial network can be operated with a single transmitter, which improves the design simplicity compared to the transfer trip method. There are some situations including faulty and interconnecting breaker open situations where the transmitting signal can be interrupted other than the islanding situation. Therefore, these methods need to have further optimized with the recent machine learning concepts to avoid unrealistic detections. Requirement of additional electronics to connect with high voltage system and requirement of proper isolation and higher cost in the multi inverter operation are some of the disadvantages of this technique.

4. MODELING AND SIMULATION OF THE DC MICROGRID

4.1 Proposed DC microgrid system

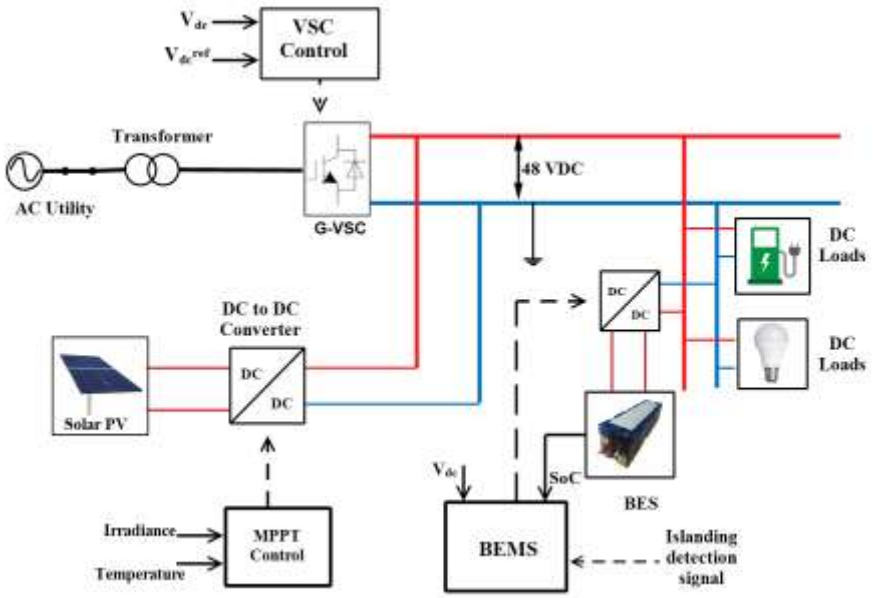

Figure 4-1 Proposed DC Microgrid system

The proposed DC microgrid system was designed for a residential application. The basic structure of this design is illustrated in Figure 4-1. A simple radial DC microgrid system was designed and it was configured as a mono-polar DC-link system. This microgrid consists of a 3-kW solar PV system, a 4-kW battery system, and several DC loads. The grid interfaced AC-DC converter regulates the DC voltage at 48 VDC. It enables the reliable power exchange between the primary grid and DC microgrid. The solar PV system operates with maximum power point tracking (MPPT) algorithm made to harness the maximum power output form the PV modules. A Lithium-Ion based battery model is used and the battery system rated at the 240 VDC is interfaced through the DC-DC bi-directional buck-boost converter. All the modeling and simulation was done in the PSCAD EMTDC V4.6. The main characteristics of the system are shown in Table 4-1.

Table 4-1 Characteristics of the DC Microgrid

DC nominal bus voltage	48 VDC
Utility nominal voltage L-N (single phase)	230 VAC
AC side voltage L-N	14 VAC
G-VSC nominal power	7 kW
Battery nominal power	4 kW
Battery terminal voltage	24 VDC
Battery Capacity	250 Ahr
Battery internal resistance	0.1 ohm
PV maximum power	3 kW
PV short circuit current	15 A
PV array Open circuit voltage	260 VDC
MPPT algorithm	P&O

4.2 Modeling and simulations of DC microgrid system

4.2.1 Voltage source inverter design

Grid interfaced converter design consists of a bi-directional AC-DC converter. This proposed system has a voltage source converter with the active and reactive power control method with PI-based direct and quadrature axis current control design (DQ control) [38]. In this proposed method IGBTs are controlled with sinusoidal pulse width modulation (SPWM) signals.

The reference of the quadrature current referred to the reactive power was taken as zero due to the nonexistence of the reactive power in the DC microgrid systems. Then, the reference of direct current is referred to the active power and was given by the DC voltage PI loop. Accordingly, the phase lock loop (PLL) was used to synchronize the AC side of the VSC with the primary grid [39]. The PLL control module takes the voltage of the primary grid as the reference signal. It creates the actual DQ components of the primary side into the PI-based control loops. It can regulate the DC microgrid voltage while exchanging power between the DC microgrid and the utility.

In the PI-based DQ control strategy, first it compares the actual DQ axis current components with the reference DQ components. The error between the actual value and reference value is fed into PI control loops and output signals are injected into the SPWM generator. The SPWM generator controls the IGBT bridge with the appropriate control signals.

4.2.1.1 Mathematical modeling and design of grid interfaced controller

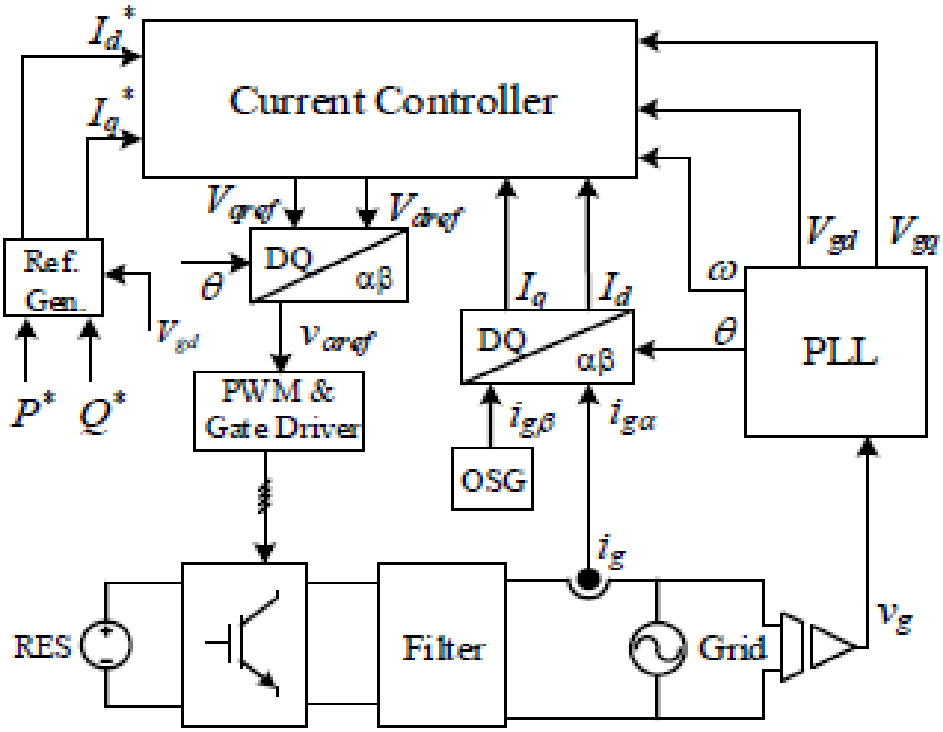

Figure 4-2 block diagram of the DQ controlled single phase grid connected inverter [40]

The single line schematic diagram of the single-phase PI-based DQ current-controlled grid interfaced converter is shown in Figure 4-2 [40]. This VSC topology consists of a single-phase H bridge, which is interfaced with the grid through the line reactor filter and grid-connected transformer as illustrated in Figure 4-2. The system filter is consisted of an inductor and leakage reactance due to the transformer-coupled with the grid. Also, it adds some internal resistance to each phase.

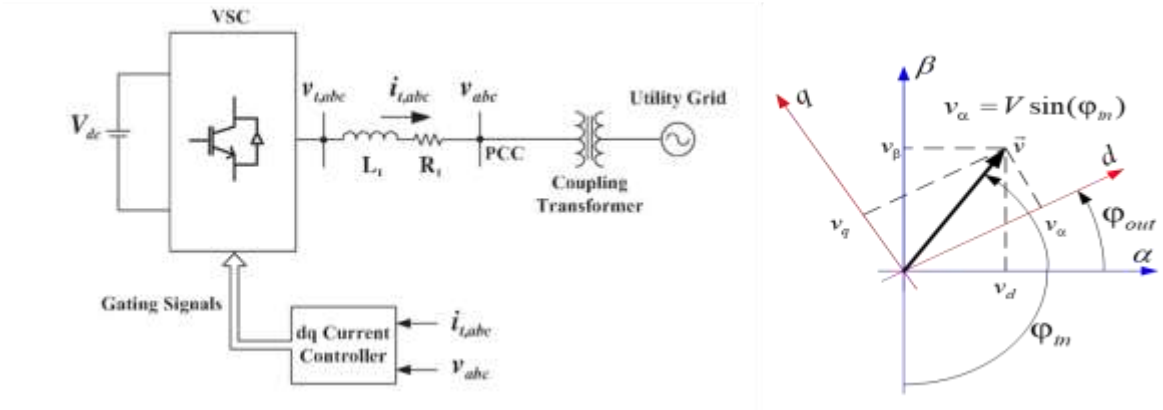

Figure 4-3 relationship in between rotating reference frame and fixed reference frame[38]

This section discusses the mathematical model of the VSC controller. When the switching losses are ignored, the transient equation for voltage in the rotating reference frame of VSC can be written as referred with Figure 4-3 [38]. As the first step, we need to derive the basic electrical equation with instantaneous parameters for the VSC in abc reference frame as shown in Equation 4.1.

$$\boldsymbol{V_{t,a} = R_t \times I_{t,a} + L_t \times \left(\frac{d(I_{t,a})}{dt}\right) + V_a} \quad (4.1)$$

In which, VSCs' primary grid side terminal voltage is denoted as $\boldsymbol{V_{t,a}}$ and, $\boldsymbol{L_t}$ and $\boldsymbol{R_t}$ are represent the parameters of the line filter. The line current, $\boldsymbol{I_{t,a}}$ is measured between the utility and VSC.

$$\boldsymbol{V_{t,\alpha\beta 0} = R_t \times I_{t,\alpha\beta 0} + L_t \times \left(\frac{d(I_{t,\alpha\beta 0})}{dt}\right) + V_{\alpha\beta 0}} \quad (4.2)$$

Equation 4-2 can be obtained by transforming Equation 4-1 (abc reference frame) into the $\boldsymbol{\alpha\beta}$ reference frame. It consists of the two orthogonal parameters known as $\boldsymbol{\alpha\beta}$, and it can be treated as complex numbers such as ($\boldsymbol{P_{\alpha\beta} = P_\alpha + P_\beta j}$). This static reference frame equations can be transformed into the rotating reference frame ($\boldsymbol{\alpha\beta}$ *to* $\boldsymbol{dq}$) as shown in Equation 4-3 by using, $\boldsymbol{P_{dq} = P_{\alpha\beta} * e^{-j\omega t}}$.

$$\boldsymbol{V_{t,dq} = R_t \times I_{t,dq} + L_t \times \left(\frac{d(I_{t,dq})}{dt}\right)} + j\omega \times \boldsymbol{L_t \times I_{t,dq} + V_{dq}} \quad (4.3)$$

After simplification of Equation 4-3, the real and imaginary terms in the above dynamic equation can be separated as given in Equation 4.4 and Equation 4.5,

$$\boldsymbol{R_t \times I_{t,q}} + \boldsymbol{L_t} \times \left(\frac{\boldsymbol{d(I_{t,q})}}{\boldsymbol{dt}}\right) = \boldsymbol{V_{t,q}} - \omega \times \boldsymbol{L_t} \times \boldsymbol{I_{t,d}} - \boldsymbol{V_q} \quad (4.4)$$

$$\boldsymbol{R_t \times I_{t,d}} + \boldsymbol{L_t} \times \left(\frac{\boldsymbol{d(I_{t,d})}}{\boldsymbol{dt}}\right) = \boldsymbol{V_{t,d}} + \omega \times \boldsymbol{L_t} \times \boldsymbol{I_{t,q}} - \boldsymbol{V_d} \quad (4.5)$$

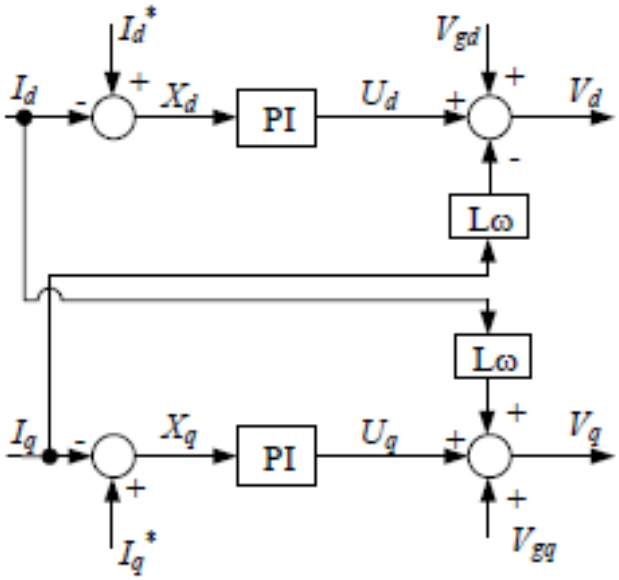

Figure 4-4 **Current Control Diagram**[40]

The current control diagram of the system refers to Equation 4.4 and Equation 4.5 is illustrated in Figure 4-4 [40]. It contains the coupling terms ($\boldsymbol{\omega \times L_t}$) to generate the $\boldsymbol{V_d}$ and $\boldsymbol{V_q}$ components. Besides that, this control approach needs DQ current reference from the primary grid named $\mathbf{I_d}$ and $\mathbf{I_q}$ in Figure 4-2 The output of the current control module, which is fed through the ***dq*** to $\boldsymbol{\alpha\beta}$ block, is used to create the reference signal to the SPWM generator. This method is preliminary discussed with the three-phase grid connection. However, this control method can be extended to the single-phase system by using additional control module: an orthogonal signal generator (OSG) module, to generate the virtual orthogonal signal ($\boldsymbol{\beta}$ components of the signals) because, single-phase systems have only a single voltage [41]. Furthermore, the PLL is an important requirement in the system to synchronize with the utility grid.

4.2.1.2 Mathematical modeling of phase look loop controller

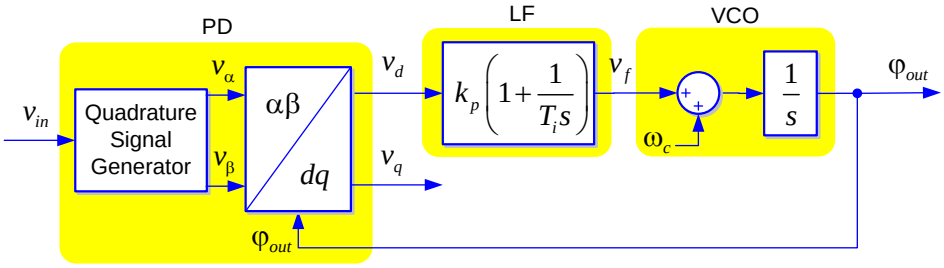

Figure 4-5 PLL control system[39]

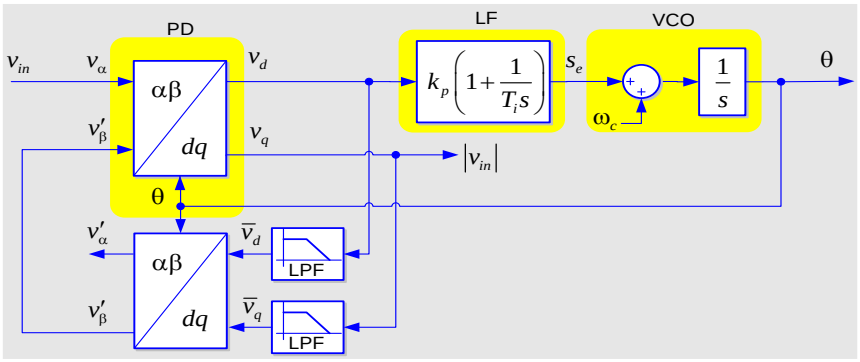

Figure 4-6 Quadrature Signal Generator[39]

The designed system contains the single-phase grid interfaced converter, as illustrated in Figure 4-5 [39]. The VSC needs to be synchronized with the primary grid to ensure the power exchange between the primary grid and DC microgrid. The control modules of the phase lock loop design have taken the responsibility of the grid synchronization while doing the power exchange. In every islanded to grid-connected transition situation, the PLL handles the synchronizing with the grid.

PLL controller is a feedback-controlled system, which adjusts the phase angle of the locally produced signal to match the phase of the grid reference. The primary function of this PLL design is to synchronize the voltage angle of the inverter, $\boldsymbol{\theta_{inv}}$ with the angle of the voltage of the utility, $\boldsymbol{\theta_{grid}}$ accordingly to obtain the unity power factor. The working principle of this PLL is to control the error between the frequency of the inverter output, $\boldsymbol{\omega_{inv}}$ and the $\boldsymbol{\omega_{grid}}$ as shown in Figure 4-5 and Figure 4-6 [39]. In the situations where the inverter voltage signal lags the grid voltage signal, the PLL will decrease the frequency, $\boldsymbol{\omega_{inv}}$ until the voltage signal is in phase with each other. In the

same way, if the inverter voltage signal leads the voltage signal, $\boldsymbol{\omega_{inv}}$ will be increased until both signals are in phase with each other.

Many PLL topologies have been established in most of the grid-interfaced converters, which need synchronizing with the primary grid. In this proposed method, the creation of the virtual orthogonal voltage is the major challenge in the single-phase PLL design. Most of the grid interface converters are based on the three-phase supply due to some advantages like easy accessibility, availability and large capacity. Therefore, most simulation software like PSCAD contains three phase-related libraries other than the single-phase models but, inbuilt model of single phase PLL is not available in the libraries. Hence, a single-phase PLL was successfully designed as a requirement of this research.

The designed PLL module is based on the Park transform and inverse Park transform ($\boldsymbol{dq}$ to $\boldsymbol{\alpha\beta}$) method, as illustrated in Figure 4-6. The single-phase primary voltage ($\boldsymbol{V_{in}}$) and internally generated orthogonal signal $\boldsymbol{V_{\beta'}}$ are injected as inputs to the park transform block. One of the outputs from the inverse park transform block, $\boldsymbol{V_{\beta'}}$ is used as the input to the park transform block ($\boldsymbol{\alpha\beta}\ to\ \boldsymbol{dq}$). The DQ components of the Park transform block are fed into the inverse Park transform block through the low pass filter (LPF), which adequately needs for the proper operation of the PLL. Although the PLL topology can be implemented easily by using the Park transform, inverse Park transform, two low pass filters, and PI controller, of the PI controller is quite tricky due to the interdependent two nonlinear loops, and the selection of the proper time constant for the low pass filter is also complicated for the smooth operation of the PLL.

4.2.2 Solar PV with MPPT design

The solar power is the widely spread renewable technology in the world because of the recent price reduction and technological advancements in solar PV technologies gained in past decades. The solar PV modules with series and parallel arrangements are connected to the DC microgrid by considering the system requirements.

(a)

(b)

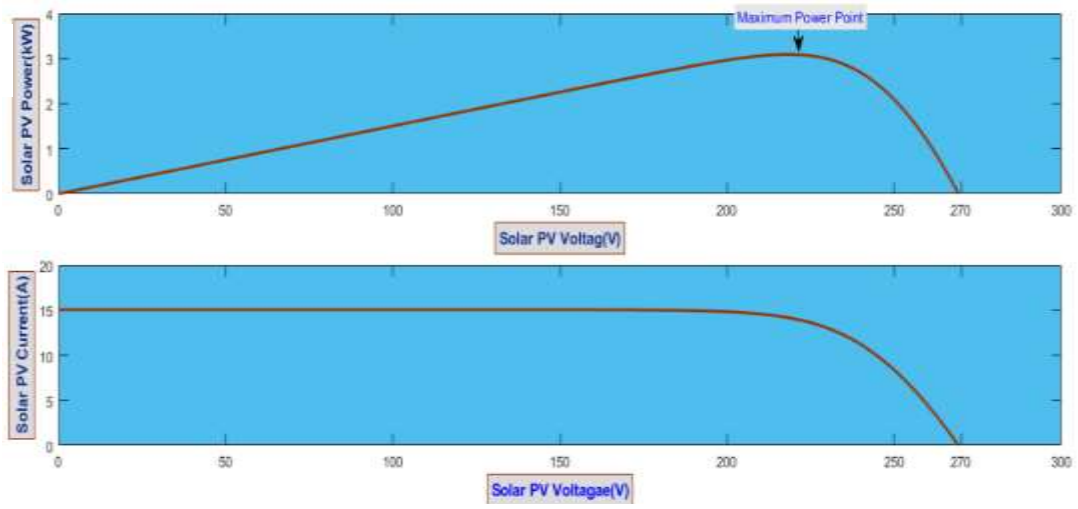

Figure 4-7 V-I characteristic curve of solar PV system (a) P-V characteristics (b)V-I characteristics

Every PV cell converts the energy of the sunlight into electrical energy as a result of the photovoltaic effect. Typically, PV systems generate DC power output. Thus, the solar PV modules are more popular in DC microgrid applications. The voltage of the no-load condition of the PV panel is equal to the sum of the voltages in series-connected solar cells. The designed solar PV module consists of a 3-kW rated capacity module. The P-V curve, and the voltage and current characteristics of the designed solar PV system is demonstrated in Figure 4-7.

4.2.3 Maximum power point tracking (MPPT)

The voltage of the PV cell terminals mainly depends on the amount of the energy received from the sun and current flowing through the solar cells. The P-V curve of the solar PV module is shown in Figure 4-7 (a) and it indicates the maximum power delivering point at a certain voltage level. That point can be recognized as the maximum power point, which can be delivered from the solar PV cell under the given conditions. Each maximum Power Point has the appropriate combination of the voltage and current, as indicated in Figure 4-7(b). Nowadays, most of the solar PV based power converters and inverters are operated with the maximum power point tracking mode to harness the maximum power from the solar PV module. There are many MPPT algorithms like perturb and observe (P&O) method, incremental

conductance, and fractional open-circuit voltage introduced in the previous literature [42][43]. The perturb and observe method was used in the solar PV model in the proposed microgrid model.

Perturb and observe method is one of the popular MPPT algorithms used in the solar industry. This method injects small perturbation to the operating voltage and measures the power generated from the solar PV array. If the controller detects any incremental power situation, it continues the perturbation process until no longer there is a power increase in the PV system. It adversely affects the system with continuous power oscillations and degrades the overall efficiency of the system. This technique was inspired by the "hill-climbing" technique, which monitors the rise of the power in the voltage vs. power curve below the maximum power point and falls after the above point. The significant advantage of this technique is the higher efficiency and ease of implementation than the other available techniques.

4.2.4 Bi-directional battery controller design

Battery systems deployed in the DC microgrid system ensure maintenance of power quality of the system even in the islanded mode of operation. Battery modules are typically consisted of series and parallel-connected battery cells to ensure the desired voltage level and current concerning their applications. The battery converts the chemical energy into electrical energy and vice versa in its basic operation. In the DC microgrid, the battery module is operating under both charging and discharging to ensure the reliable operation of the system. There are many battery types like lithium-ion, nickel-cadmium, and nickel-metal hydride available to use and the designed system considers a lithium-ion battery technology.

4.2.4.1 Lithium-ion battery technology

Having higher energy density, higher cycle life, lower self-discharge effect, and higher efficiency, Lithium-ion battery technology is widely accepted for DC microgrid projects. Lithium-ion battery modules are typically consisting of internally connected battery cells up to the rated voltage requirements in the system. These technologies have few drawbacks like rapid rising of cell temperature, and it will course thermal

runaway to further increase in cell temperature. The thermal runaway is defined as the triggering of the unstoppable chain reaction and rapidly releases a higher amount of stored energy in the millisecond range. There is also a higher risk of explosion happen in the battery.

Currently, the transportation sector is converting to the fully electric vehicle concept with recent technological advancements in battery technologies in the world. Typically, those batteries required to be replaced when it reaches 80% of its usable range of the original capacity. The disposal of those used batteries needs a highly complex recycling process. However, those batteries can be used for the DC microgrid projects at a low cost. These concepts will reduce environmental pollution, and it will improve the reliability of the system. Most of the time implementation of these projects face financial difficulties and low return on investment with the high-cost energy storage system.

4.3 Multi-mode energy management system

The battery module of the designed system is working with the multi-mode energy management system. The battery module used in the designed system has a capacity of 0.25 kAhr and terminal voltage of 0.024 kV. The selection of the proper battery chemistry and sizing of the battery is highly vulnerable in designing the DC microgrids. Mainly, these battery modules have the prime responsibility to cater to the power requirements of the DC microgrids in grid-disconnected mode and compensation of grid transient conditions in the grid-connected mode of operation. However, the cost and size of the battery module proportionally increase along with the capacity of the battery system.

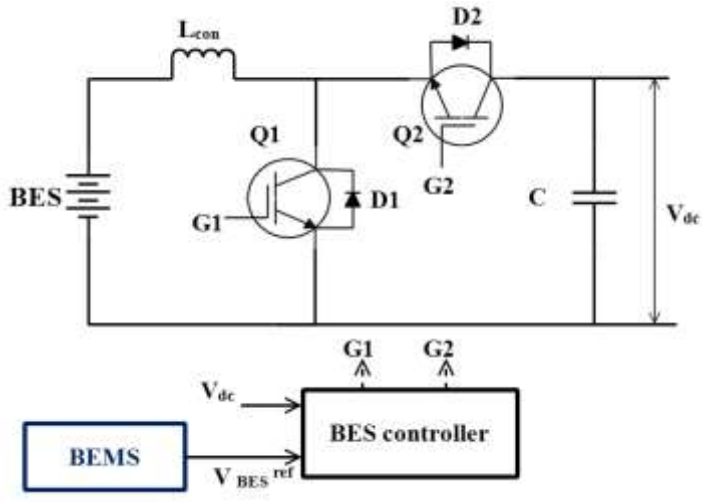

Figure 4-8 DC-DC battery control module

Hence optimizing the DC microgrid with an appropriate capacity of the battery module is highly recommended to reduce the cost burden of these new technologies.

The main control objectives in the usage of the energy storage systems are to regulate the DC-link within the acceptable limit and maintain the smooth functioning of the DC microgrid. This control function has become more challenging in the islanded mode of operation because, the energy storage device is the only responsible resource for managing the internal energy requirements in a microgrid at that time. In addition, if any voltage fluctuation happens in the grid-connected mode of the microgrid due to the intermittency nature of the distributed power generation or due to sudden load variations then also energy storage system can be used to compensate the energy imbalance. The battery module also has its limitations with its effective state of charge (SoC) range and SoC balancing method integrated with an energy management system (EMS) of the DC microgrid. Therefore, a proper energy management system is required to regulate the DC-link voltage by considering the variations in power generation, loads, SoC, and voltage requirements for the internal loads. This designed system is introduced to the reliable battery energy storage system for DC bus voltage regulation, SoC regulating under the different modes of operation. The proposed battery energy management system is introduced to stabilize the DC bus voltage even in extreme grid fluctuations such as fault conditions too.

4.3.1 Bidirectional DC-DC converter control method

Several types of grid-interfaced technologies have been introduced in recent works of literature for the connection of the energy storage systems to the DC microgrid systems. Figure 4-8 demonstrates the bi-directional DC-DC converter topology used in the microgrid model. The control algorithm for this converter consists of the dual-loop control structure with outer and inner control loop configuration, as shown in Figure 4-9. The battery energy management system works as the supervisory control system, which selects the appropriate reference voltage (V_{BES_Ref}) to the DC-DC converter considering the parameters like the SoC level of battery module / DC bus voltage (V_{dc}) and microgrid operating mode. The control block diagram of the DC-DC converter is illustrated in Figure 4-9. The V_{BES_Ref} values; V_{BES_Disref} and V_{BES_Chgref} set the discharging and charging control mode in the DC-DC converter. The reference current for the inner current loop, I_{BES}^{ref} is given by the outer DC-link voltage control loop. The outer loop solves the error between the V_{BES}^{ref} and Vdc and injects into the PI block for creating the I_{BES}^{ref}. The current error in the inner loop is fed through the PI controller and generates the PWM signals to drive the IGBT module. The appropriate output signals from the drivers: ***G1*** and ***G2***, are used to control the IGBTs in the DC-DC converter.

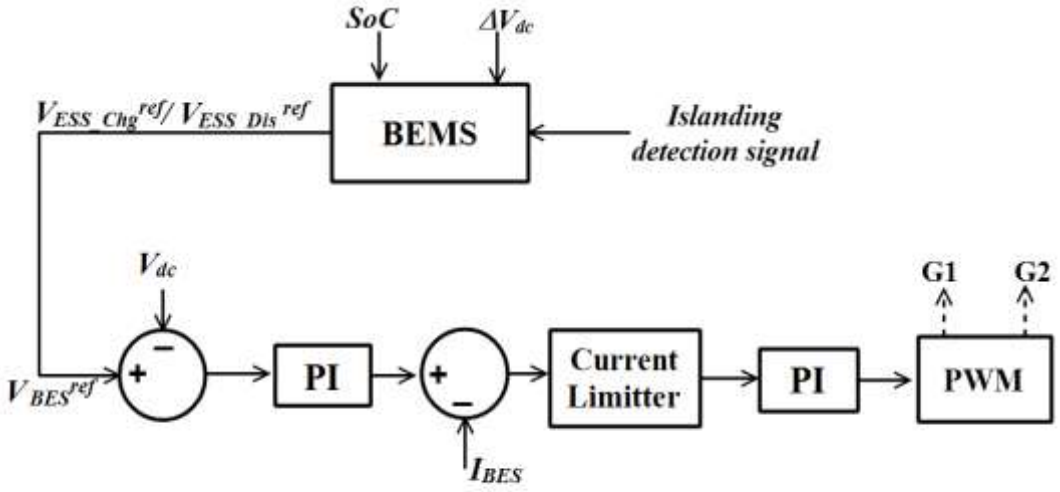

Figure 4-9 **dual loop PI based controller**

4.3.2 Control scheme and operating modes of the energy storage system

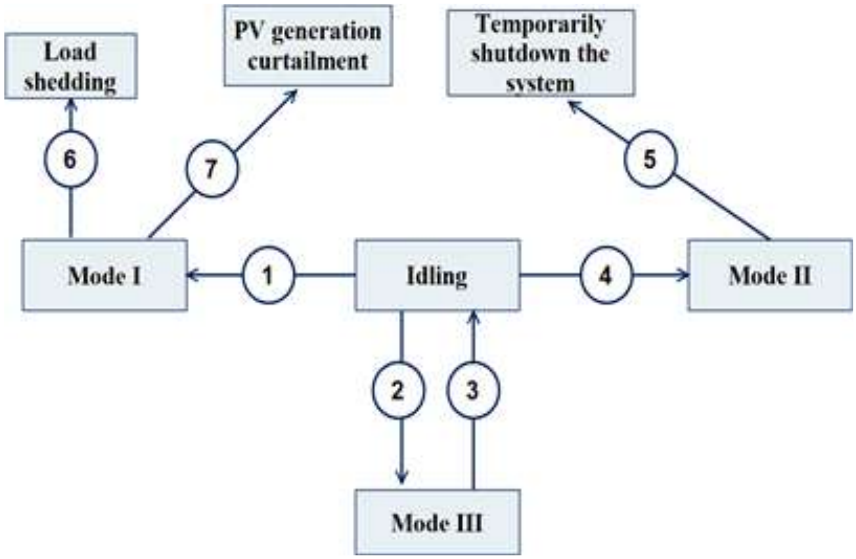

Figure 4-10 State Diagram of Control Operation

The battery energy management system is an essential feature for the smooth operation in DC microgrid as a supervisory control level. It has some main useful features: controlling the charge-discharge operation of the battery, regulating the proper SoC range in a battery, and regulating the DC-link voltage during the islanded operation of the DC microgrid. Also, it can be used as a backup power source to maintain the transient grid conditions, such as sag and swell situations in grid-connected situations. The proposed DC microgrid system is designed with a multimode supervisory battery energy management system (BEMS). The proposed systems consist of three modes of operation. The control operation will work in both grid-connected and islanded situations. All three operating modes are based on the SoC level of the battery, the real-time operating condition of the DC microgrid, and voltage fluctuations in the grid (ΔV_{dc}). The state diagram in Figure 4-10 illustrates the different operating conditions in the proposed algorithm. The conditions adequate for each transition are shown in Table 4-2. Each operating mode of this proposed system is discussed in the following sections.

Table 4-2 Conditions for the states

Transition	Conditions
1	***Islanded*** AND 30% < ***SoC*** < 90%
2	(***SoC*** < 50% OR SoC > 80%) AND ***Grid-connected*** AND $\|\Delta V_{dc}\|$ < 0.03 pu
3	***SoC*** = 70%
4	***Grid-connected*** AND (0.11 pu ≥ $\|\Delta V_{dc}\|$ ≥ 0.09 pu) AND 30% < ***SoC*** < 90%
5	$\|\Delta V_{dc}\|$ > 0.11 pu
6	Islanded AND ***SoC*** < 30%
7	Islanded AND SoC > 90%

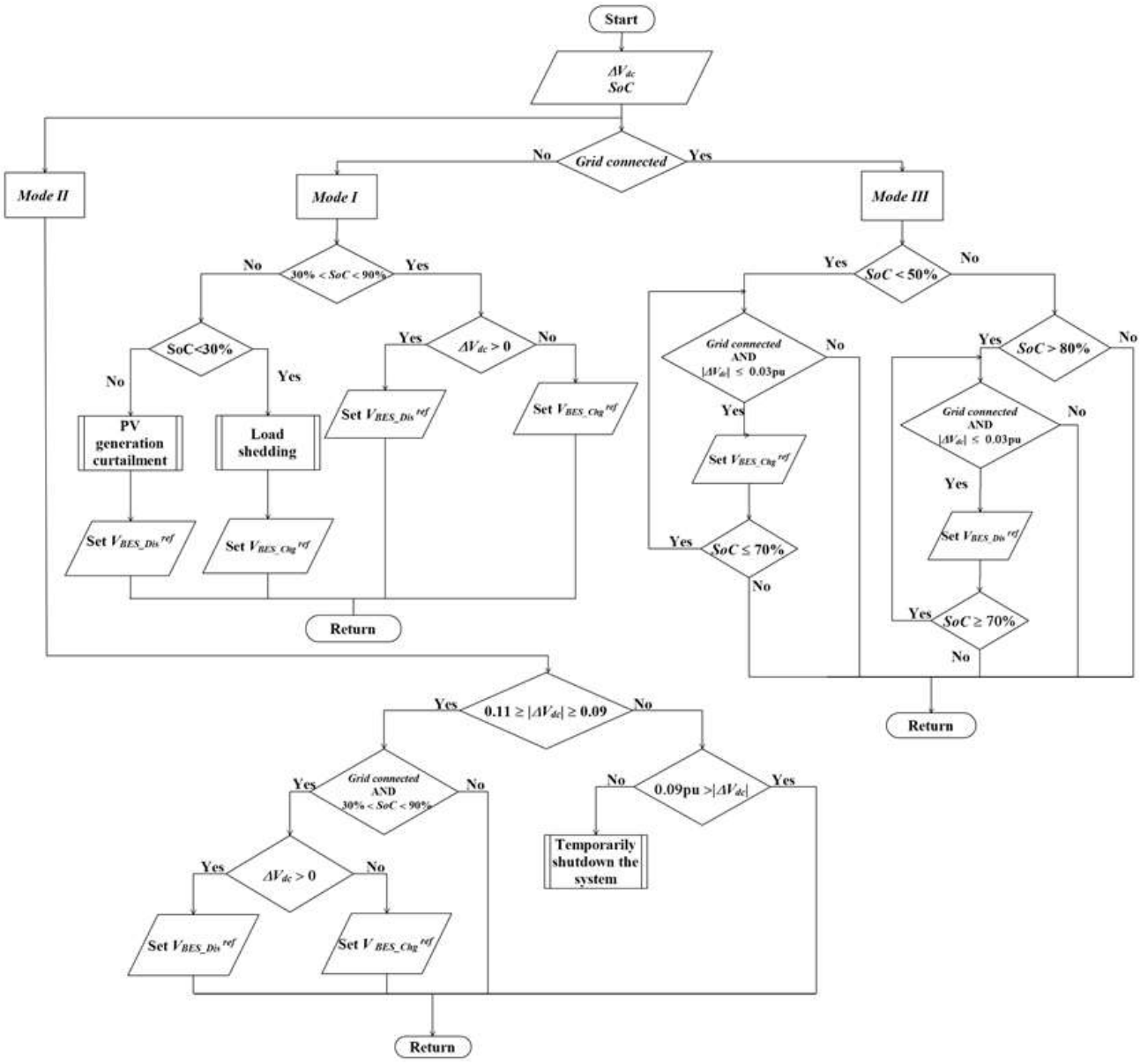

Figure 4-11 BEMS control algorithm

The selection of the operating mode of the BEMS operation is carried out by the supervisory control algorithm shown in Figure 4-11. Different reference voltage levels are defined in the BEMS algorithm for different modes of operation of the microgrid thus, operating mode can be identified without the requirement of any additional data transfer method.

4.3.2.1 Operation in mode I

This mode refers to the islanded operation of the DC microgrid, which needs to regulate the DC bus voltage using battery energy storage. In this system, BEMS manages the SoC level of Battery Energy Storage. Any Battery Energy Storage has its operating SoC range within maximum SoC level ($\boldsymbol{SoC_{max}}$) and minimum SoC level ($\boldsymbol{SoC_{min}}$). Based on the charge-discharge profile and safe operating temperature levels of the appropriate battery type, the typical operating range of the battery is maintained within 30%-90% range: $\boldsymbol{SoC_{max}}$=90% and $\boldsymbol{SoC_{min}}$=30%.

When the battery has acceptable SoC level as mentioned above, BEMS access the voltage variations ($\boldsymbol{\Delta V_{dc}}$) in the DC-link in real-time as given in Equation 4.6. If the $\boldsymbol{\Delta V_{dc}} > 0$, BEMS sets the reference voltage of DC-DC converter ($\boldsymbol{V_{BESref}}$) to $\boldsymbol{V_{BES\_Disref}}$ which enables the discharging mode of operation of the energy storage to regulate the DC voltage of the microgrid. If the system is undergoing with $\boldsymbol{\Delta V_{dc}} < 0$ conditions, BEMS sets the $\boldsymbol{V_{BES\_Chgref}}$ to the $\boldsymbol{V_{BESref}}$ and enables the charging mode of the BES. However, when the SoC level reaches its lower or upper bound ($\boldsymbol{SoC_{max}}$ and $\boldsymbol{SoC_{min}}$) levels, the BEMS cannot regulate the DC bus voltage. Hence, if the BES is undergoing $\boldsymbol{SoC} < \boldsymbol{SoC_{min}}$ condition, loads are shedded, and the battery is operating in charging mode to regulate the DC-link voltage. Moreover, if $\boldsymbol{SoC} > \boldsymbol{SoC_{max}}$ condition, solar PV is curtailed. The battery is operating in discharging mode to maintain the voltage within its acceptable limits. Mode-I operation of the BEMS algorithm is shown in Figure 4-11.

$$\boldsymbol{\Delta V_{dc} = V_{dc\_nom} - V_{dc}} \tag{4.6}$$

4.3.2.2 Operation in mode-II

The mode II operates under the grid-connected operation of the DC microgrid in which BES needs to compensate for the power variations in the network to support the VSC in the regulation of voltage at significant disturbance conditions of DC microgrid. The control algorithm relevant for the mode II operation is illustrated in Figure 4-11. In this operating mode, the BES is acting as a backup power source to the primary grid connection. When the system is operating under $\boldsymbol{SoC}$ < 90% and $\boldsymbol{\Delta V_{dc}}$ < -0.09 pu condition, BEMS enables the charging mode while setting up the $\boldsymbol{V_{BESref} = V_{BES\_Chgref}}$. In addition, if the $\boldsymbol{SoC}$ > 30% and $\boldsymbol{\Delta V_{dc}}$ > 0.09 pu, then BEMS enables the discharging mode while setting up the $\boldsymbol{V_{BESref} = V_{BES\_Disref}}$. However, if $|\boldsymbol{\Delta V_{dc}}|$ > 0.11pu, the microgrid is temporarily shut down and terminate the operation under this operating mode.

4.3.2.3 Operation in mode-III

This mode refers to the grid-connected operation of DC microgrid to maintain the acceptable SoC rage in the battery. This mode is essential to ensure the effective operation of the battery under other operating modes (Mode I/II) of proposed BEMS. The selection of the charge-discharge condition only relies on the SoC level of the BES. This model avoids the undesirable network interruptions due to the overcharging and deep discharging of the battery module.

The operation of the Model III in the BEMS is shown in Figure 4-11 This mode is activated only under the stable operation of the DC microgrid and based on the available SoC level it decides the charging and discharging operation. When the SoC level reaches the 50% margin with $\boldsymbol{\Delta V_{dc}}$ < 0.03pu, BEMS triggers the charge mode until the SoC reaches to the 70% margin. If the SoC level of BES goes beyond the 80% margin with $\boldsymbol{\Delta V_{dc}}$ < 0.03p condition, BEMS triggers the discharge mode until the SoC level of the BES reaches the 70% margin. Therefore, Mode III operation ensures the continuous stable operation of the DC microgrid in the islanded situation (Mode I) or during transient conditions within the grid (Mode II) to regulate the DC-link voltage.

4.3.3 Simulation of the proposed BEMS algorithm

The accurate operation of the proposed BEMS algorithm validated through simulations using PSCAD/EMTDC transient simulation software. The operating conditions appropriate for each mode are discussed under the selected case studies discussed in the following sections.

4.3.3.1 Case I: Mode I operation of the proposed BEMS

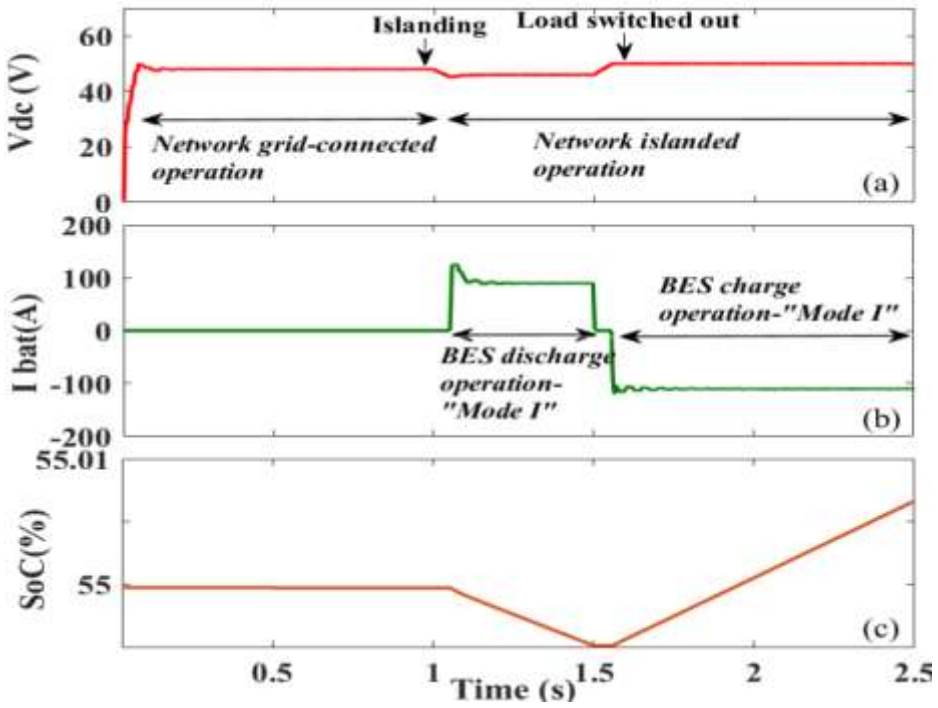

Figure 4-12 Case I simulations

Case I simulations correspond to the Mode I operation of the proposed BEMS and results are shown in Figure 4-12. The designed DC microgrid system is initially operating in the grid-connected mode, and the system is islanded at t = 1 s. At the islanded situation, solar PV generation (P_{pv}) is lower than the power consumption or power demand of the DC microgrid (P_{load}); ($P_{pv} < P_{load}$).In that instance, the system experiences energy deficit and BES enables the discharge mode to regulate the DC link voltage (V_{dc}). At t = 1.5 s, all the connected loads are switched off and it creates an energy surplus situation in the system ($P_{pv} > P_{load}$). Then BES starts to operate in charging mode to regulate the V_{dc} within its acceptable operating levels around nominal voltage. In this case study, the $V_{BES\_Dis}^{ref}$ and $V_{BES\_Chg}^{ref}$ parameters are set

0.96 pu and 1.04 pu accordingly to maintain the voltage within the stable limits of the designed system. When the system is operating in this operation, the current and SoC variation is shown in Figure 4-12(b) and (c) respectively. The battery current is varied smoothly with the help of the DC-DC converter controller and SoC of BES is changed with reference to the operating mode of the battery.

4.3.3.2 Case II: Mode II operation of the BES

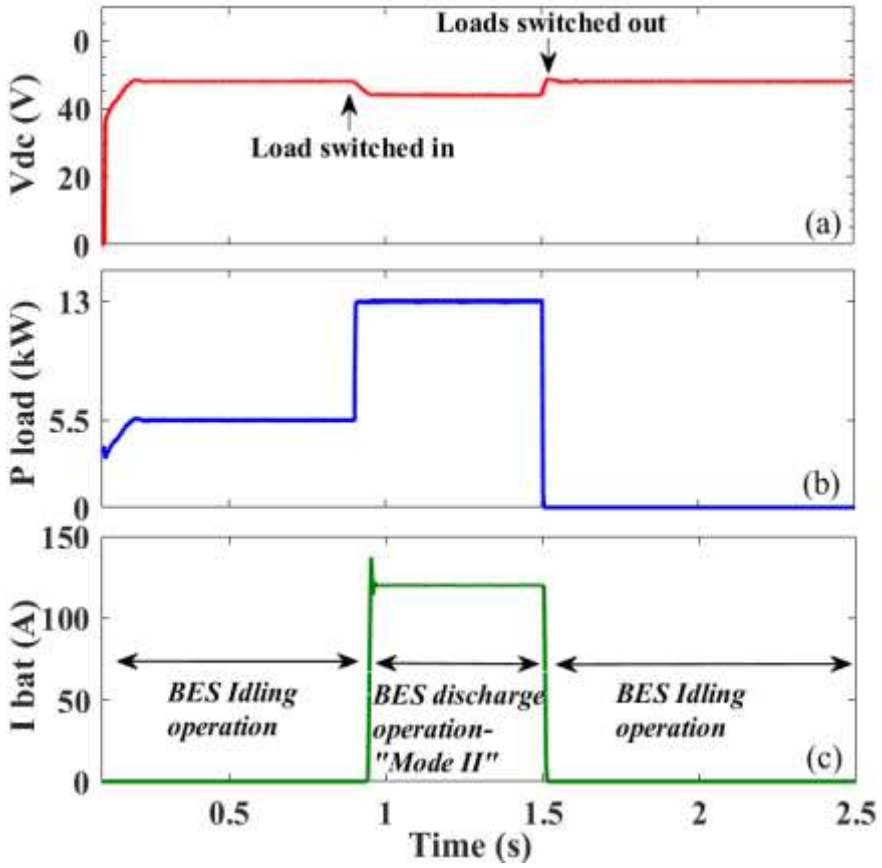

Figure 4-13 Case II simulations

Case II simulation corresponds to the Mode II operation of the BES as shown in Figure 4-13. This mainly corresponds to the grid-connected operation of the DC microgrid but, under transient situations, and that is the leading specialty of the proposed BEMS of this thesis. The grid connected VSC has maximum loading capacity of 10kW, which happens due to the control limits of the bi-directional converter. The system is initially operating in the grid-connected operation and at t = 0.9 s, the loads are connected to

the system. However, PV generation and grid connected VSC cannot handle total load power requirement at the instant of the load variation in the grid. Hence, the support of the BES to suppress such disturbances in the system is highly required for V_{dc} regulation of the system. As in the case II analysis, the BEMS system enables the discharging mode and regulates the V_{dc} at 0.95 pu. In this proposed algorithm, it distinguishes the different modes of operation based on the relevant reference voltages. That is convenient for the other controllers to detect the working mode of the battery without any additional communication method in the proposed decentralized control system. When all the connected loads are switched off from the system at t = 1.5 s the grid connected VSC takes over the DC link regulation. Mode II operation operates only when the SoC level of the BES are within the acceptable limits; if not, it operates in idle mode to avoid an unnecessary charge and discharge operation of the BES.

4.3.3.3 Case III: Mode I and Mode III operation of the BES

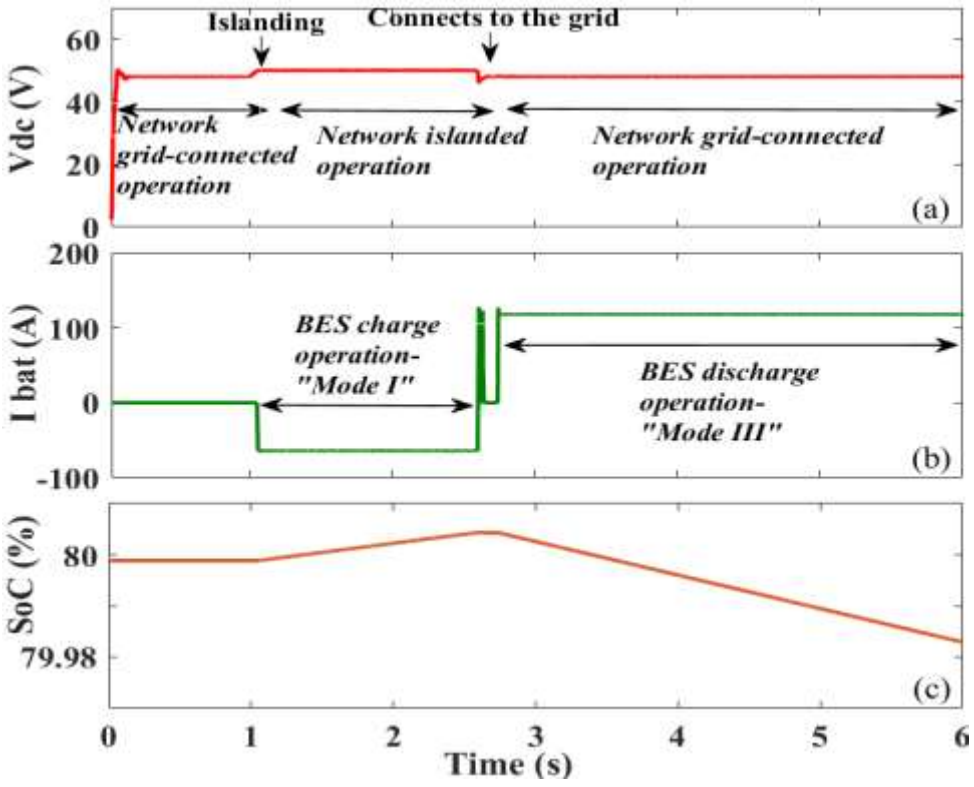

Figure 4-14 **Case III simulations**

Mode I and *Mode III* operation of the BES is evaluated in this scenario and simulation results for different events are shown in Fig. 4-14. The availability of an ideal islanding detection technique (which does not have any time lag for detection) was assumed throughout the study.

The DC microgrid system is islanded at $\boldsymbol{t}$ = 1 s. At the instant of receiving the islanding detection signal from the modules, the BEMS takes over the $\boldsymbol{V_{dc}}$ regulation of the system to maintain the DC-link voltage within acceptable limits. In this situation, the system is undergoing an energy surplus situation ($\boldsymbol{P_{pv} > P_{load}}$) as shown in Figure 4-14. It contains the SoC variation with the time, and the SoC level increases beyond the 80% limit during the BES charging in the islanded voltage regulatory mode. If the system experiences redundant charging or discharging situations, there might have a higher risk of maintaining the SoC level at the acceptable range. Therefore, the system requires a proper mechanism to control the SoC level of battery module at the desired level. Therefore, 70% SoC margin is considered as the effective range to ensure smooth, reliable operation. When the grid connects back with the DC microgrid at 2.5 s, the BES starts to discharge until the SoC level reaches the 70% margin.

5. PROPOSED ISLANDING DETECTION METHOD

5.1 Mathematical analysis for the frequency analysis of single-phase DC microgrid system

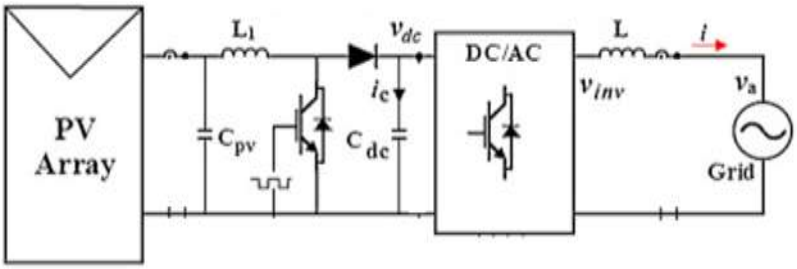

Figure 5-1 grid connected two stage solar PV Module with cascade inverter

In the figure 5.1 contains the simple microgrid designed with grid connected inverter which operates in unity power factor [44][45], the equation for the instantaneous output power of Inverter ($\boldsymbol{P_{out}}$) is derived as follows,

$$V_a = V_a \times \sin(\omega t) \quad 5.1$$

$$\mathrm{I} = I_a \times \sin(\omega t) \quad 5.2$$

$$P_{out} = V_a \times I_a \times \sin(\omega t)^2 \quad 5.3$$

The $\boldsymbol{V_a}$, $\boldsymbol{I}$ and $\boldsymbol{\omega}$ variables are known as Inverter output voltage/current and angular frequency in rad/s respectively.

$$P_{out} = V_a \times \frac{I_a}{2} \times (1 - \cos(2\omega t)) = V_a \times \frac{I_a}{2} - V_a \times \frac{I_a}{2} \times \cos(2\omega t) \quad 5.4$$

The average part of the inverter output power is equal to the solar PV output power. When the system losses are neglecting compared to the total power[45].

$$P_{pv} = I_{dc} \times V_{dc} \quad 5.5$$

The second term of the equation 5.4 represents the oscillations of the grid power with double frequency component[44][45]. The $\boldsymbol{P_{pv}}$, $\boldsymbol{I_{dc}}$ $\boldsymbol{and}$ $\boldsymbol{V_{dc}}$ represent instantaneous solar PV output power, dc link current and voltage, respectively.

The equation for the input power of the inverter can be derived as follow while neglecting the other losses in the dc microgrid side[44][45]. The instantaneous power consumption of the capacitor denotes as $\boldsymbol{P_{cap}}$.

$$P_{in} = P_{pv} - P_{cap} \tag{5.6}$$

Where the $\boldsymbol{I_{dc\_cap}(t)}$ and ($\boldsymbol{V_{dc\_cap}}$) illustrate the instantaneous current and voltage of the capacitor.

$$P_{cap} = V_{dc} \times I_{dc\_cap}(t) = V_{dc} \times C_{dc} \times \frac{d\,(V_{dc\_cap})}{dt} \tag{5.7}$$

While assuming the inverter input power equal to the output power[45],

$$P_{in} = P_{out} \tag{5.8}$$

$$I_{dc} \times V_{dc} = V_a \times \frac{I_a}{2} \tag{5.9}$$

In below represent the relationship between the DC link parameters with the grid parameters. Where the "m" denotes for the modulation index of inverter[44].

$$I = m \times I_{dc} \tag{5.10}$$

$$V_{dc} = \frac{m \times V_a}{2} \tag{5.11}$$

The AC power oscillations in the latter part of the equation 5.4 is reflected the DC side resulting oscillating power at the DC link capacitor as follows,

$$V_{dc} \times \mathrm{C}_{dc} \times \frac{\mathrm{d}\left(V_{dc\_cap}\right)}{\mathrm{dt}} = \frac{V_a \times I_a}{2} \times \cos(2\omega t) \tag{5.12}$$

$$V_{dc\_cap} = \frac{V_a \times I_a}{4\omega \times V_{dc} \times \mathrm{C}_{dc}} \times \sin(2\omega t) \tag{5.13}$$

Hence the double frequency term in the ripple frequency is sourced by the capacitor power oscillations as shown in equation 5.13.

$$I_{dc\_cap}(t) = \mathrm{C}_{dc} \times \frac{\mathrm{d}\left(V_{dc\_cap}\right)}{\mathrm{dt}} = \frac{V_a \times I_a}{2 \times V_{dc}} \times \cos(2\omega t) \tag{5.14}$$

$$I_{input} = I_{dc\_cap} + I_{dc} = \frac{I_a \cos(2\omega t)}{m} + \frac{2 \times P_{pv}}{m \times V_a} \tag{5.15}$$

The "$\boldsymbol{I_{dc\_cap}}$" term represents the instantaneous current in the capacitor .Where the input current to the inverter is known as the "$\boldsymbol{I_{input}}$" which contains the double frequency components .The inverter operation is carried out with the SPWM function "$\boldsymbol{m(t)}$" ,therefore instantaneous current can be derived as follows,

$$I_{out} = m(t) \times I_{input}(t) = m \times \sin \omega t \times \left(\frac{I_a \cos(2\omega t)}{m} + \frac{2 \times P_{pv}}{m \times V_a}\right) \quad 5.16$$

$$I_{out} = \frac{2 \times P_{pv}}{V_a} \times \sin \omega t + I_a \times \sin \omega t \times \cos 2\omega t \quad 5.17$$

$$I_{out} = \frac{2 \times P_{pv}}{V_a} \times \sin \omega t + \frac{I_a}{2} \times (\sin 3\omega t) - \frac{I_a}{2}(\sin \omega t) \quad 5.18$$

$$I_{out} = \left((\frac{2 \times P_{pv}}{V_a} - \frac{I_a}{2})\sin \omega t\right) + \frac{I_a}{2} \times (\sin 3\omega t) \quad 5.19$$

The output current term is consisted with $\boldsymbol{\omega}$ *and* $\boldsymbol{3\omega}$ angular velocities which is known as fundamental and third harmonics, respectively[46][47]. This series of odd harmonic components in output current of the DC link capacitor are enabled by the double frequency voltage ripple and repetitive iterations of the control system as shown in equation 5.19 [46].

5.2 Selection of proper threshold value for the islanding detection of single-phase grid interfaced DC microgrid

The proposed algorithm was designed based on the idea that the frequency signatures in voltages waveforms can be employed to obtain a reliable islanding detection in DC microgrids. Therefore, to analyze the frequency signatures in the DC-link voltage, Fast Fourier Transform (FFT) based model was adopted. The VSC module regulates the DC link voltage, but still it contains some frequency components as described in chapter 5.1 .But it contains in smaller magnitudes as shown in Figure 5-2(a) , which illustrates the variations of the frequency components up to seventh order in single-phase grid interfaced DC microgrid system. Figure 5-2(b) shows the variation of dominant frequencies (50Hz, 100Hz) and Figure 5-2(c) illustrates the real-time load variation during a selected time duration .The double frequency component of the

dominant frequencies (100Hz) has been sourced by the capacitor voltage ripple as represent in equation 5.13.The fundamental component(50Hz)in the dominant frequencies has been introduced by the series of odd harmonic components in output current of the DC link capacitor as shown in equation 5.19.

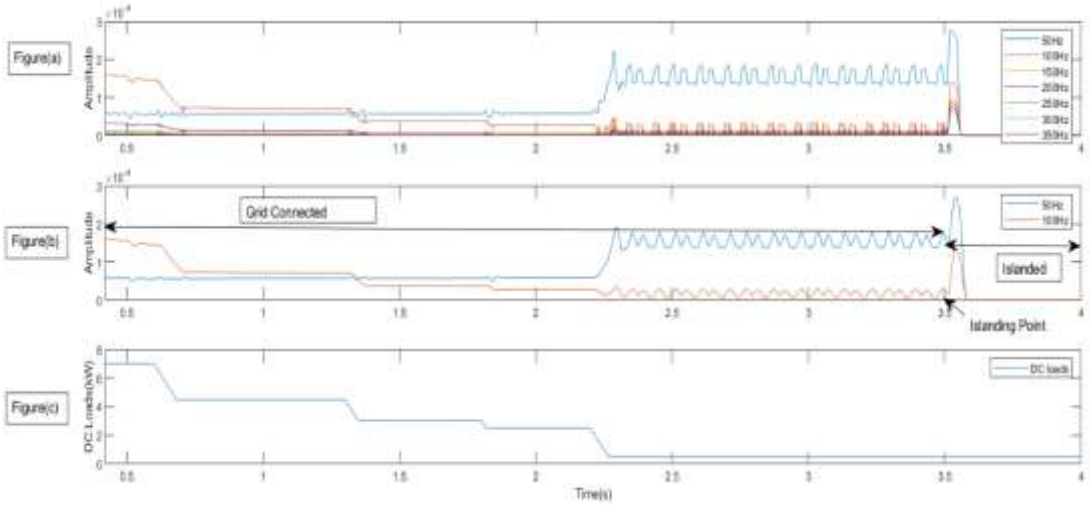

Figure 5-2 Variation of the Frequency components in different load conditions (a) frequency analysis up to seventh order (b)50Hz and 100Hz frequency variation (c)load variation

The system is initially operated in grid-connected condition and it is islanded at the 3.5 s. A considerable frequency variation can be seen during the load switching as well as at the instant of transition from the grid-connected operation to islanded operation. Compared to the grid-connected mode of operation, when the system is islanded at 3.5 s, the magnitudes of the dominant frequency components have decreased to lower values after the initial transient, and then they are maintained around minimum values as illustrating in Figure 5-2(b). Hence, this variation can be used to identify the islanded situation from other operating conditions in DC microgrids by setting up proper threshold values for the dominant frequency magnitudes.

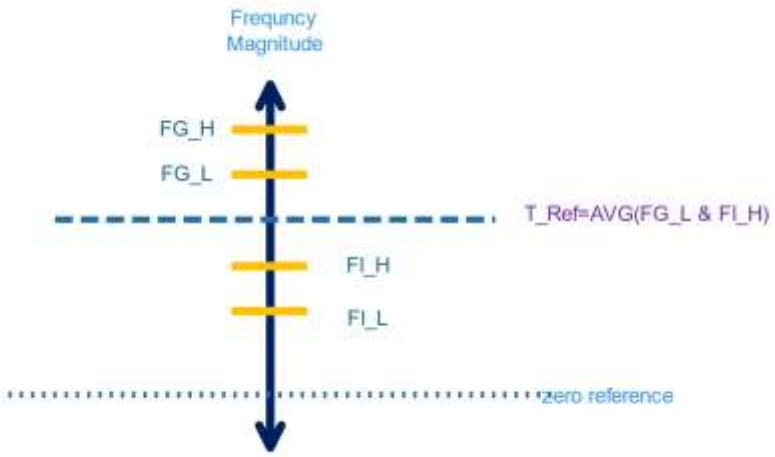

Figure 5-3 Operating ranges of frequency magnitudes

As the initial step, the maximum possible magnitude range of dominant frequencies (minimum and maximum) in the DC link voltage were identified in grid-connected mode (***FG_H*** and ***FG_L***) and islanded mode (***FI_H*** and ***FI_L***) considering possible load variations in the network. Then, the appropriate threshold values for each dominant frequency were selected to separate the islanded mode from grid-connected mode. As illustrated in Figure 5-3, threshold was selected by finding the midst value of the lowest value of grid-connected mode (***FG_L***) and the highest value of islanded mode (***FI_H***). The detailed procedure of threshold value selection is described in Table 5.1.

Table 5-1 Case study on selection of threshold value

Frequency (Hz)	**Level**	**Grid connected**	**Islanded**	**Threshold Range (*FG_L*-*FI_H*)**	**Threshold Value(*T_Ref*) Avg((*FG_L*-*FI_H*)**
100	Upper	***FG_H*** = 1.469× 10-4	***FI_H*** =5.38× 10^{-9}	(7.346×10^{-6}-5.38× 10^{-9})	3.5× 10^{-6}
	Lower	***FG_L***=7.346× 10-6	***FI_L***= 5.38× 10^{-9}		
50	Upper	***FG_H***=1.869× 10-4	***FI_H*** =1.169×10-8	(5.645×10^{-5}-1.169× 10^{-8})	3.0× 10^{-5}
	Lower	***FG_L*** =5.645× 10-5	***FI_L***=1.169× 10^{-8}		

5.3 Analysis of the factors that affect the selection of threshold

5.2.1 Effect of noise level

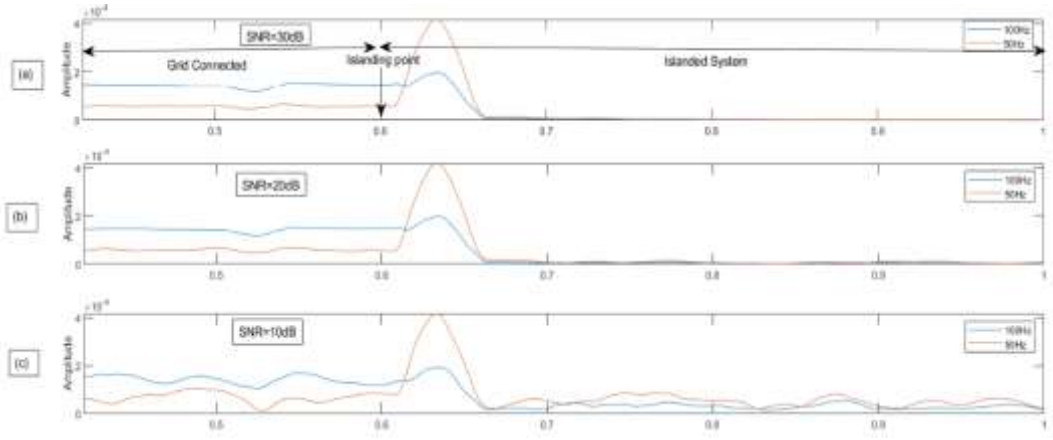

Figure 5-4 Effect of the Noise to the variations of frequency components. (a)SNR=30dB (b)20dB (c) 10dB

To analyze the effect of measurement noise on the selection of the threshold for islanding detection, Gaussian white noise (GWN), which is a random signal with zero means was introduced at the voltage measurements. In order to define the noise levels of the system, signal to noise ratio (SNR), which compares the actual signal with the background noise, (see Equation 5.20) is employed. Generally, the signal with SNR level of 30 dB or more is highly recommended for applications that can be interfered with the background noise [48][49]. In this research, noise level at 10 dB,20 dB and 30 dB with fixed load condition were used for the simulation.

$$\boldsymbol{SNR\ of\ signal = 20\ log \frac{S}{N}} \qquad 5.20$$

Figure 5-4 illustrates dominant frequency variations under different noise levels. The system was initially operating in the grid-connected mode and at time 0.6 s, system was islanded. The impact of noise levels on the pre-defined threshold values is not significant, at noise levels above 20 dB. When the SNR is 10 dB, some random variations can be observed (Figure 5-4 (c)) in the dominant frequencies. Therefore, agreeing with literature the SNR level require to be maintained at 30 dB or above[48][49]. Table 5-2 presents a summary of the operating ranges of the frequency magnitudes and comparison with the predefined threshold values (***T_Ref***).

Table 5-2 Case Study on effect of the noise to the frequency variations

	50 Hz (*T_Ref* =3.0× 10^{-5})		**100 Hz (*T_Ref* =3.5×10^{-6})**		
SNR	***FG_L***	***FI_H***	***FG_L***	***FI_H***	***FI_H < T_Ref< FG_L***
Noise=0	5.7× 10^{-5}	6.9×10^{-8}	0.000141	2.8× 10^{-8}	True
30dB	4.7×10^{-5}	1.37× 10^{-5}	0.000118	6.7× 10^{-6}	True
20dB	4.6×10^{-5}	1.6×10^{-5}	0.000116	9.0× 10^{-6}	True
10dB	1.3×10^{-5}	7.8× 10^{-5}	0.000106	3.1× 10^{-5}	False

5.2.2 Effect of AC loads

Mostly, DC microgrids consist of DC loads only. However, in some situations, the microgrid may contain some AC loads connected through DC-AC inverters. These inverters add some frequency components to the DC microgrid side that may affect the variation of the dominant frequencies and predefined threshold values (***T_Ref***).

In this analyze, the effect of AC loads on the variation of dominant frequencies was observed considering a hypothetical case of having 100% AC loads in a DC microgrid. It is known that the overall efficiency of the system decreases if the AC load margin increases. Figure 5-5 illustrates the dominant frequency variations and Table 5-3 compares the threshold margins with the pre-defined threshold values for the hypothetical case of having 100% (7 kW) AC loads. The designed AC loads are connected to the system via square wave inverters. Due to the higher harmonic content in the outputs of the inverters, slight variations in the magnitudes of the dominant frequencies can be observed. However, these variations have not affected the predefined threshold values.

Table 5-3 Case study on effect of AC loads on threshold value

	50 Hz (*T_Ref* = 3.0×10^{-5})		**100 Hz (*T_Ref* = 3.5×10^{-6})**	
Load	***FG_L***	***FI_H***	***FG_L***	***FI_H***
AC Load (AC full load)	5.47× 10^{-5}	1.45× 10^{-5}	0.0002117	7.14× 10^{-6}
FI_H* < *T_Ref*< *FG_L	True		True	

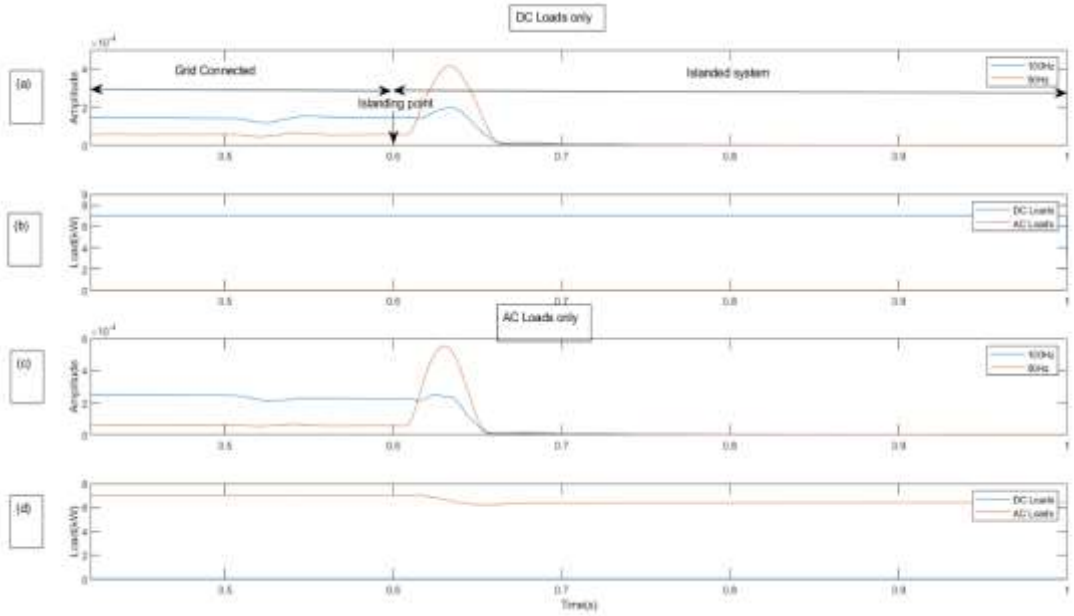

Figure 5-5 Effect of the types of the loads into the variations in frequency components. (a) Frequency variation (DC loads) (b) DC load (c) Frequency variations (three phase) (d) AC loads

5.4 The Islanding detection algorithm

The proposing islanding detection algorithm for DC microgrid systems is discussed in this section. The proposed algorithm is illustrated in Figure 5-6. The initial inputs to the proposed algorithm are dominant frequency components and relavent reference threshold values (***T_Ref*** (50 Hz), ***T_Ref*** (100 Hz), ***T_Ref*** (150 Hz), ***T_Ref*** (300 Hz)). Then, the magnitudes of dominant frequencies and their corresponding reference threshold values are compared. If the condition is satisfied, the algorithm detects the islading condition and sends the appropriate signals.

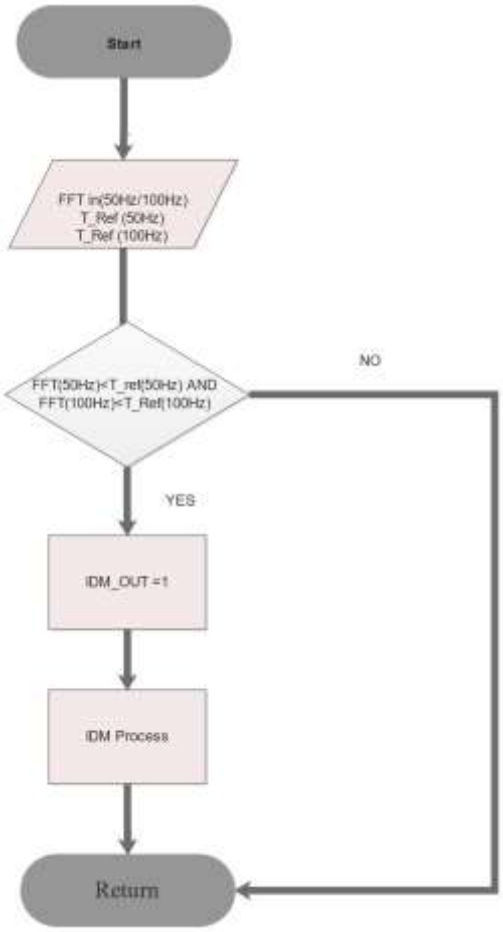

Figure 5-6 Proposed Islanding Detection Algorithm

5.5 Application of proposed islanding detection method for DC microgrid connected to three phase system

The proposed algorithm was applied to a DC microgrid connected to a three-phase system. In applying the technique, the dominant frequencies and thresholds have to be identified. Therefore, a frequency analysis was carried out for the DC microgrid connected to the three-phase system analyzing harmonics up to seventh order using a base frequency of 50 Hz as shown in Figure 5-7(a). In this analysis, 150 Hz and 300 Hz were identified as the dominant frequency components as shown in Figure 5-6(b). The real-time variations of the loads in the system are shown in Figure 5-7(c). The same method used to analyze the single phase system is employed for the three phase systm as well.

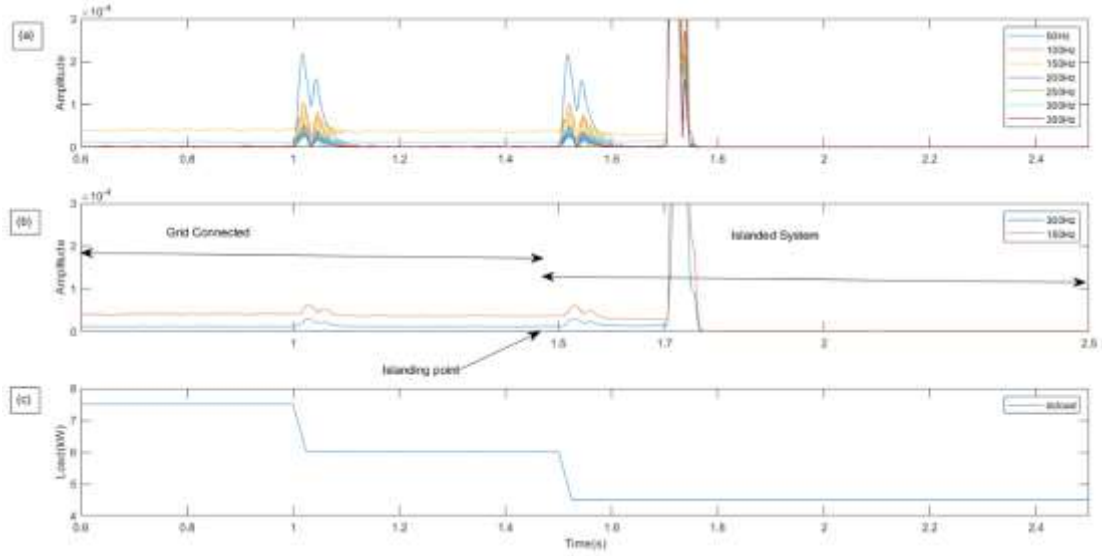

Figure 5-7 variations of the frequency components in different load conditions. (a)frequency components up to seventh order (b) 150Hz and 300Hz frequency variations (c)DC loads

The range of the threshold values were recognized by analyzing the maximum-minimum values of the frequency signatures in both grid-connected and islanded condition. The threshold values of the 150 Hz and 300 Hz frequency components are selected as 1.3×10^{-5} and 1.0×10^{-5} respectively. These values are also verified to be valid with high penetration of AC loads in the DC microgrid and with measurement noise (SNR ratio 30dB or above range) as in the previous analysis.

6. PERFORMANCE EVALUATION

The evaluation of the performance of proposed islanding detection algorithm under various system conditions is presented in this chapter.

6.1 Islanding detection with multiple solar PV generation

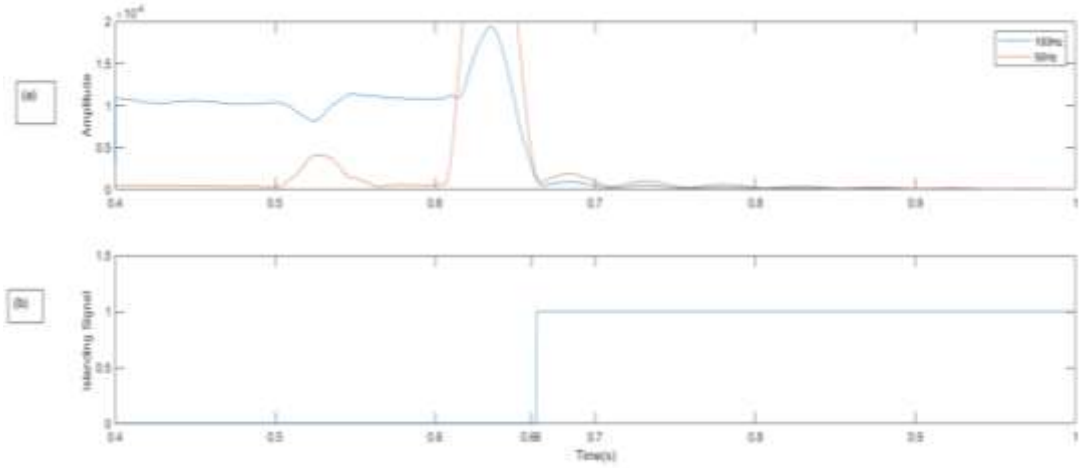

Figure 6-1 Multiple PV Generation (DC microgrid connected to Single Phase)

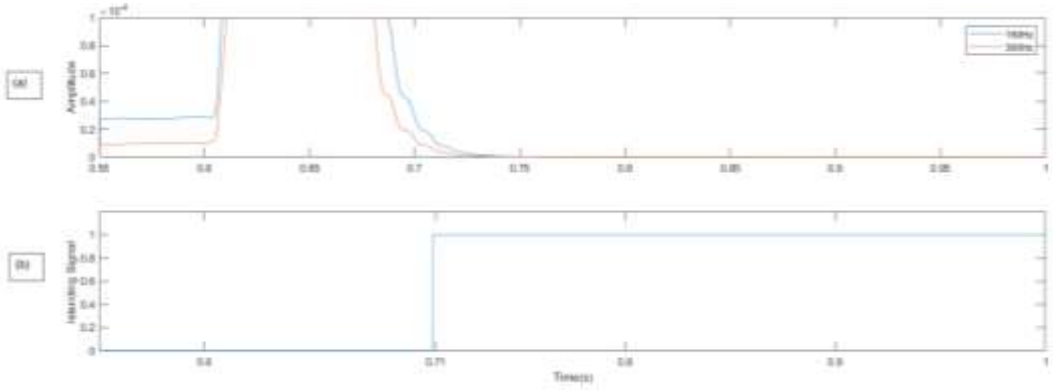

Figure 6-2 Multiple PV Generation (DC microgrid connected to Three Phase)

The analysis was carried out with different arrangements of DER including single PV and multiple PV. Figure 6-1 and Figure 6-2 present the variations of the dominant frequency components for an islanding of the DC microgrid. Initially, the system is operated in grid-connected conditions and it is islanded at the 0.6 s. At the islanding point, the dominant frequencies in both systems indicate some random variations and

then stabilizes at the lowest magnitude after some time. The islanding detection takes 0.06 s and 0.11 s respectively to identify the islanding of the DC microgrid from single phase system and three phase system. It can be stated that the detection time does not depend on the type of PV system (single PV system or multiple solar PV system), as in both cases, same power output is given to the system.

6.2 Islanding detection with noise

The analysis was conducted to evaluate the behavior of the proposed islanding detection with measurement noise. As shown in Figure 6-3, system response for an islanding of DC microgrid connected to the three phase and single-phase system under SNR level of 20 dB in measurements was observed. The system is islanded at 0.6 s and it is detected after 0.06 s and 0.07 s in DC microgrid connected to single phase and three phase systems respectively. Therefore, the detection time has not affected by noise.

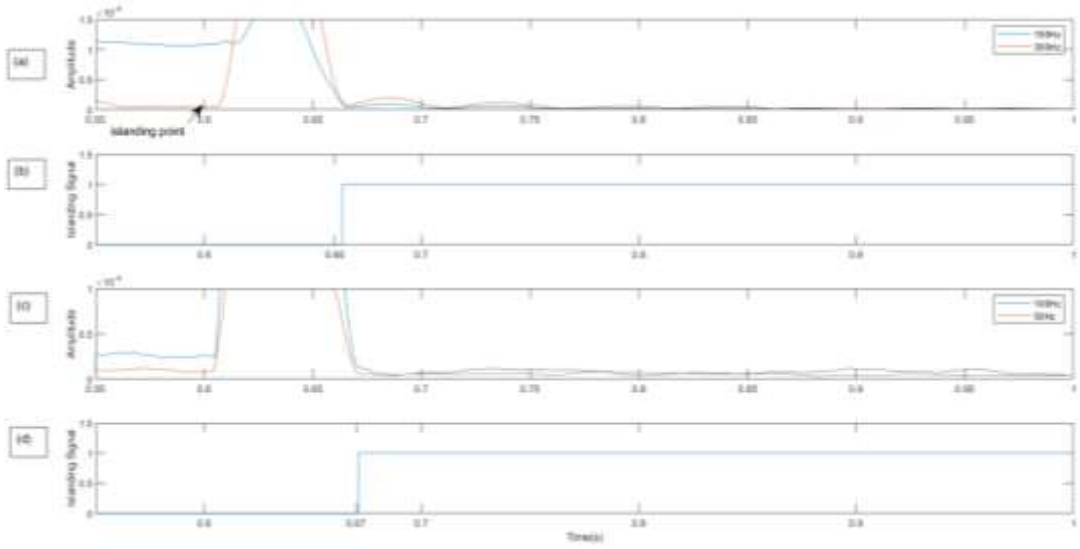

Figure 6-3 Islanding detection in the noise environment (a)150Hz and 300Hz frequency variation three phase(b) Islanding detection three phase (c)50Hz and 100Hz frequency variation in single phase (d) islanding detection in single phase

6.3 Islanding detection with different power generation and Load variation

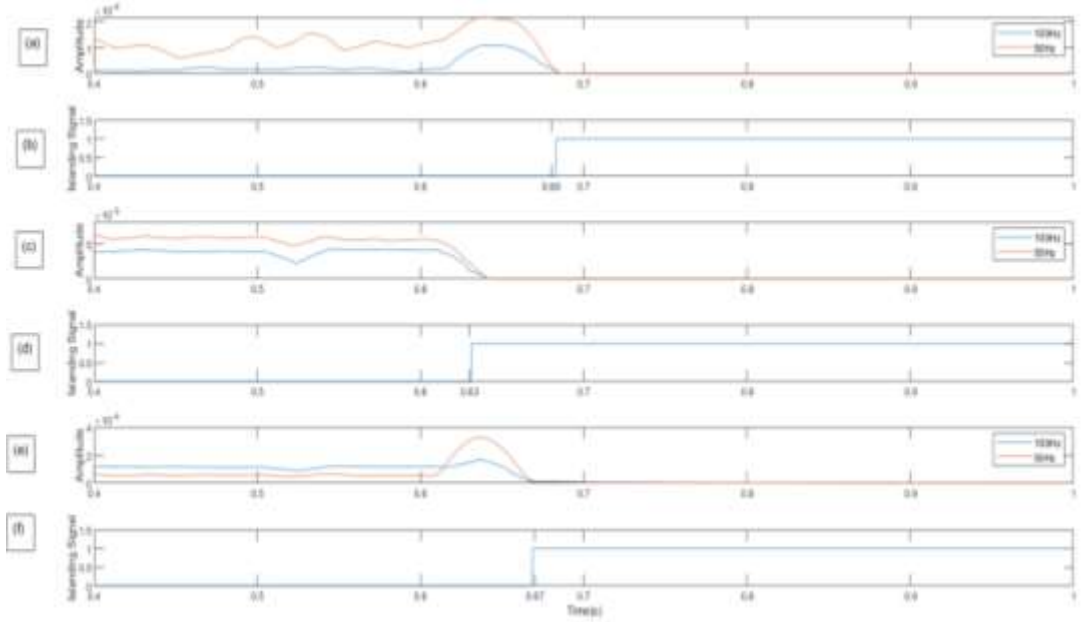

Figure 6-4 Islanding detection in the different loading condition in the system(single phase (a) $P_L<P_G$ (c) P_L and P_G slightly match (e) $P_L>P_G$ (b)(d)(f)islanding detection

To evaluate the impact of loading on the proposed islanding detection method, the system was analyzed under three different loading conditions as listed below:

Case 1: generation exceeds the demand ($\boldsymbol{P_L<P_G}$)

Case 2: generation slightly match with demand

Case 3: demand exceeds the generation ($\boldsymbol{P_L>P_G}$)

Figure 6-4(a),(c),(e) shows the dominant frequency variation for each conditions and the system are islanded at the 0.6s. The islanding detection time for the condition 1, the condition 2 and the condition 3 are 0.08s, 0.03s and 0.07s respectively.

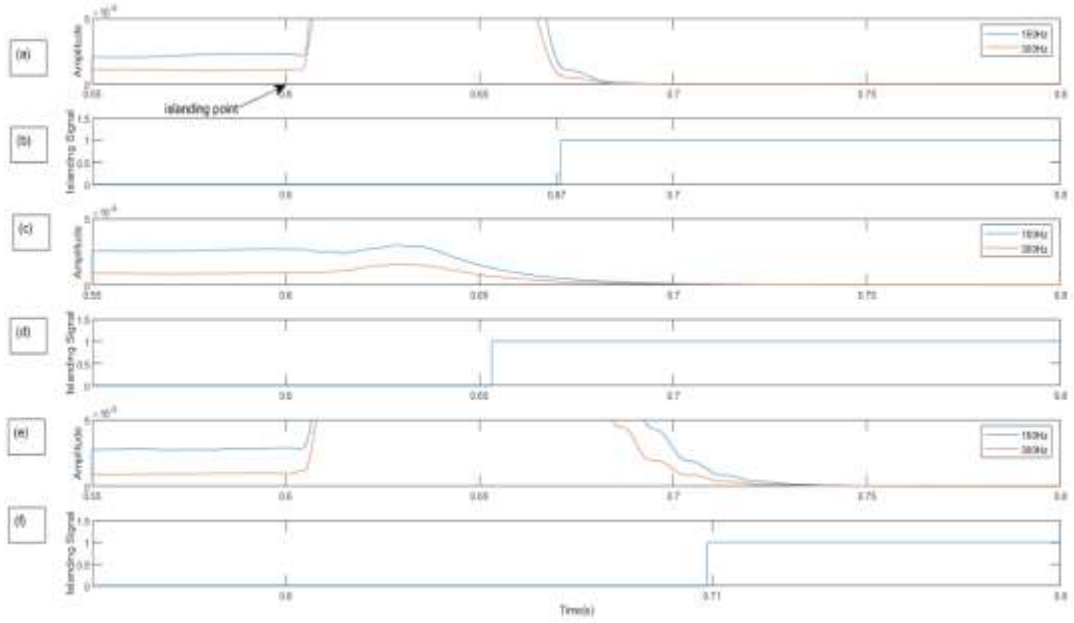

Figure 6-5 Islanding detection in the different loading condition in the system(three phase) (a) PL<PG (c) PL and PG slightly match (e) PL >PG (b)(d)(f)islanding detection

In the same manner, the detection time for for the condition 1, the condition 2 and the condition 3 are 0.07s, 0.05s and 0.11s respectively as shown Figure 6-5.

6.4 Islanding detection with AC loads

Figure 6-6 illustrates the islanding detection of DC microgrid under 10% of AC loads form rated power of the DC microrgrid for both single phase and three phase. Figure 6-6 (a) and (c) shows the variation of the dominant frequency components of the single-phase and three system when DC microgrid is islanded at the 0.6 s. The islanding detection time for DC microgrid being dicsonnected from single phase and three phase systems are 0.09 s and 0.07 s respectively. It shows that having few AC loads connected to the DC microgrid does not affect the response time of the proposed islanding detection method.

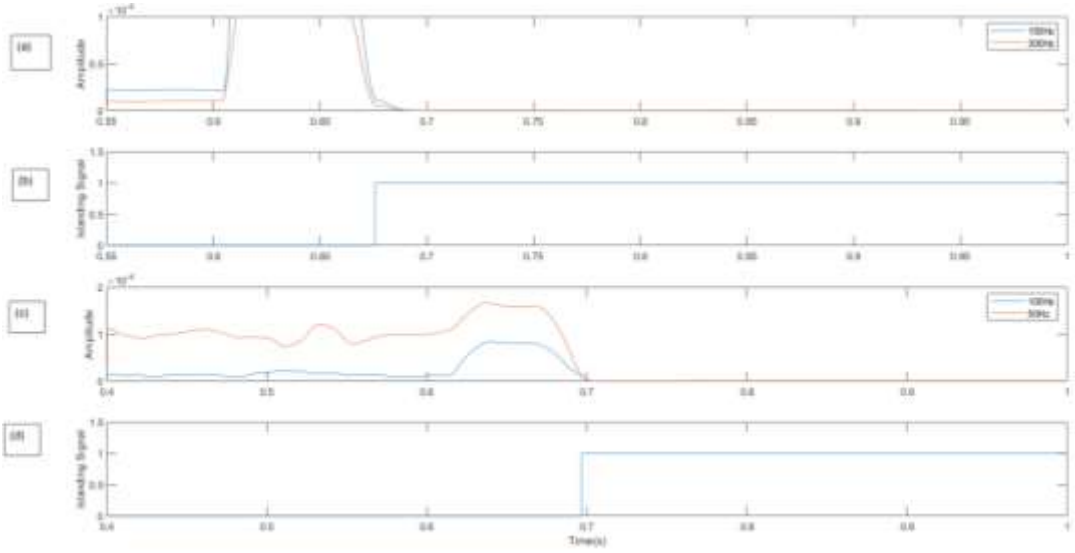

Figure 6-6 Islanding detection with AC loads (a) AC loads in three phase connected dc microgrid (b) islanding detection three phase connected dc microgrid (c) AC loads in single phase connected dc microgrid (d)islanding detection in single phase connected dc microgrid

6.5 Behavior of the proposed algorithm under fault condition in the grid

In order to observe the effect of fault conditions for the proposed islanding detection method, faults are created at the AC grid side at 0.6 s and fault duration was changed in three different cases (case 1 : 0.01 s, case 2: 0.04 s and case 3: 0.06 s) for both single phase and three phase systems.

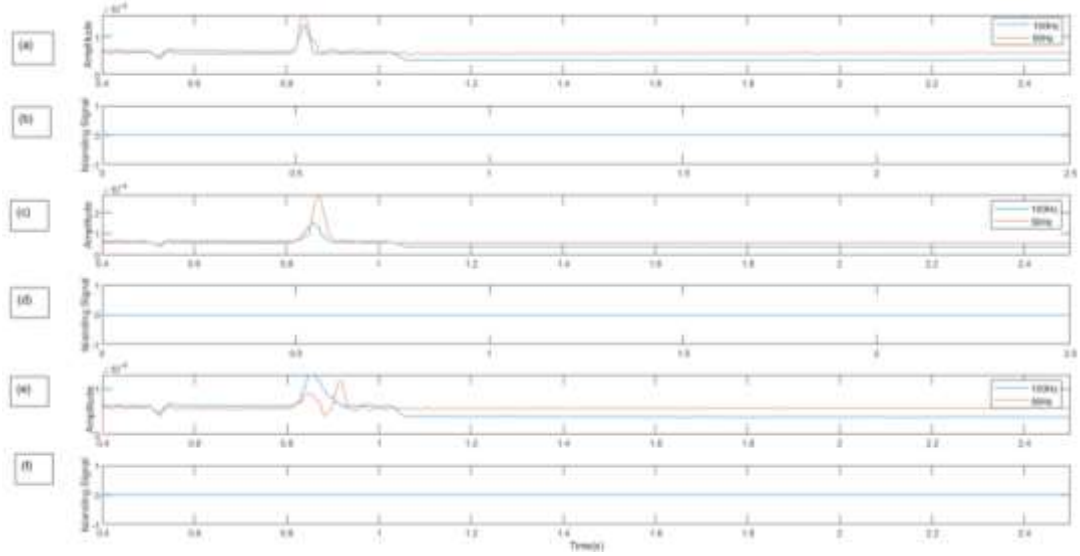

Figure 6-7 Behavior of detection algorithm in fault situation in AC side (single phase) (a)fault duration 0.01s(b)islanding detection (c)fault duration 0.04s (d)islanding detection (e) fault duration 0.06s (f)islanding detection

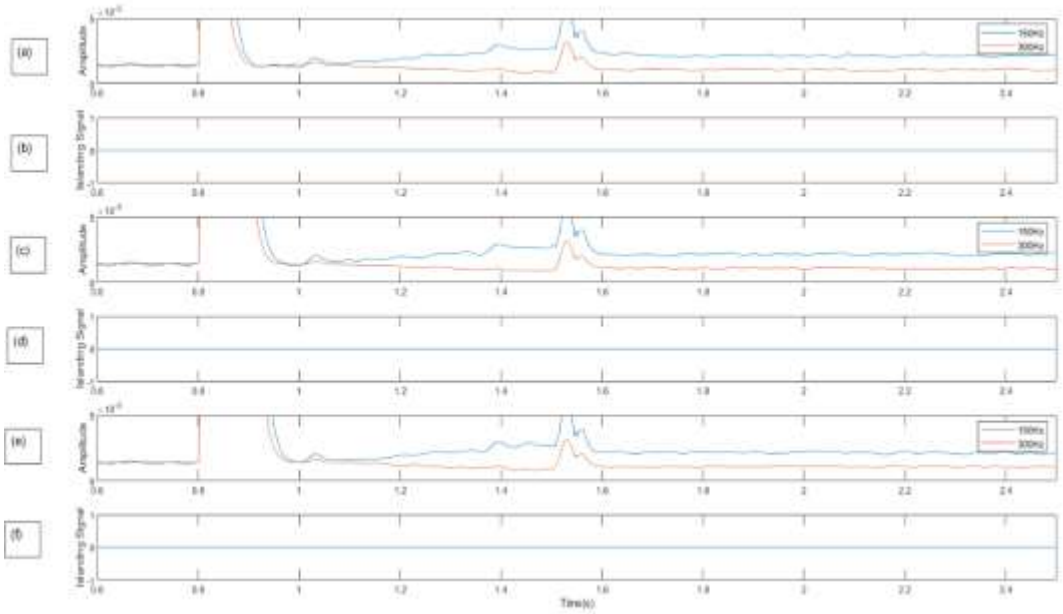

Figure 6-8 Behavior of detection algorithm in fault situation in AC side (three phase)) (a)fault duration 0.01s(b)islanding detection (c)fault duration 0.04s (d)islanding detection (e) fault duration 0.06s (f)islanding detection

The variation of dominant frequencies in the system show random variations while it is undergoing different fault situations are shown in Figure 6-7(a), (c), (e) for each case. As shown in Figure 6-7(b), (d), (f), the proposed islanding detection method accurately operates under the fault conditions, without any unwanted triggering of islanding. Similar accurate operation of the proposed method was observed for the DC microgrid connected to a three-phase system as illustrated in Figure 6-8.

6.6 Behavior of the proposed algorithm under faults in microgrid

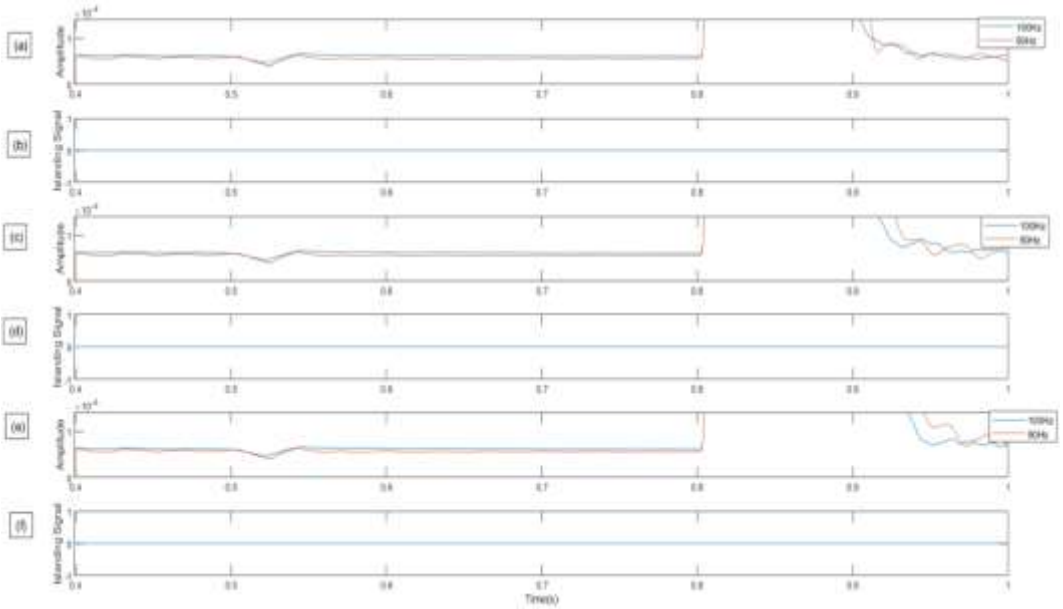

Figure 6-9 Behavior of detection algorithm in fault situation in DC side (single phase) (a)fault duration 0.01s(b) islanding detection (c)fault duration 0.04s(d)islanding detection (e) fault duration 0.06s9(f)islanding detection

To further analyze the effect of fault conditions, faults were created within the DC microgrid system. An earth fault was created at 0.6 s and fault duration was changed in three different cases (case 1: 0.01 s, case 2: 0.04 s and case 3: 0.06 s) for both single phase and three phase systems.

In the DC microgrid connected to the single-phase system, the variation of dominant frequencies shows random variations while it is undergoing different fault situations as shown in Figure 6-9(a), (c), (e) for each case. However, as shown in Figure 6-9 (b), (d), (f), the proposed islanding detection operates accurately without triggering an islanding.

Similar performance was observed for the DC microgrid connected to the three-phase system as illustrated by Figure 6-10.

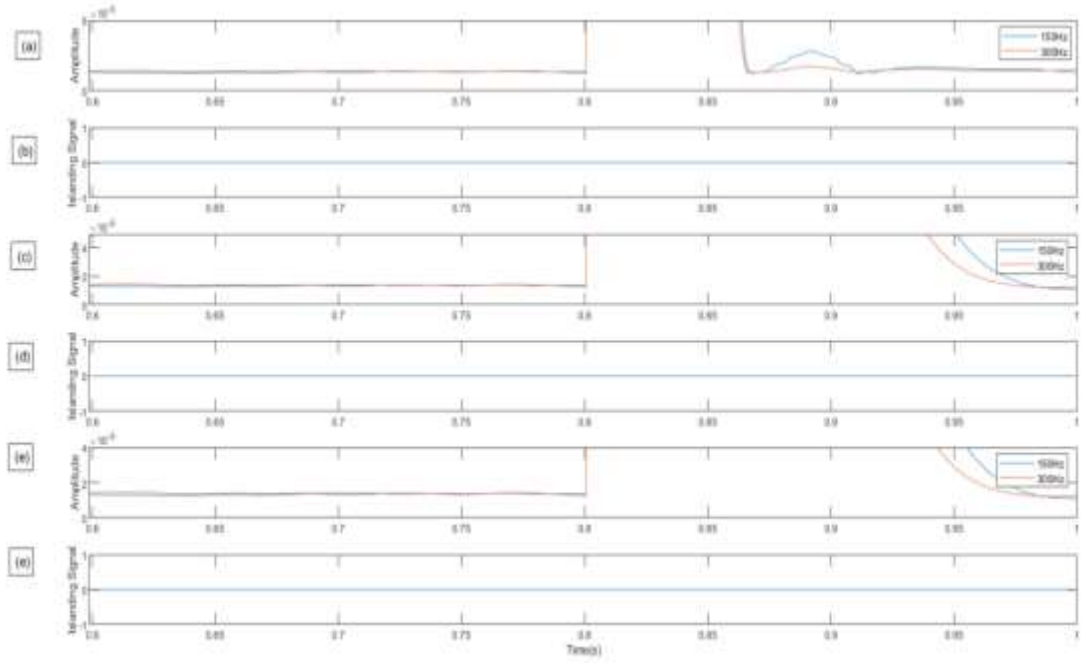

Figure 6-10 Behavior of detection algorithm in fault situation in DC side (three phase))(a)fault duration 0.01s(b) islanding detection (c)fault duration 0.04s(d)islanding detection (e) fault duration 0.06s9(f)islanding detection

6.7 Behavior of the proposed algorithm under variation of solar Irradiance

To evaluate the performance of the proposed islanding detection method under varying solar irradiance, system behavior was observed under varying irradiance levels of 1300 Wm^{-2} to 1500 Wm^{-2} at 1 s and 1500 Wm^{-2} to 1300 Wm^{-2} at 1.6 s. The 6-11 (a), (d) illustrates the variation of dominant frequency components for the DC microgrid connected to the single-phase system and Figure 6-11 (b), (e) show the change of solar irradiance levels. As shown in Figure 6-11 (c), (f) the proposed islanding detection method accurately operate without triggering for solar ramping conditions.

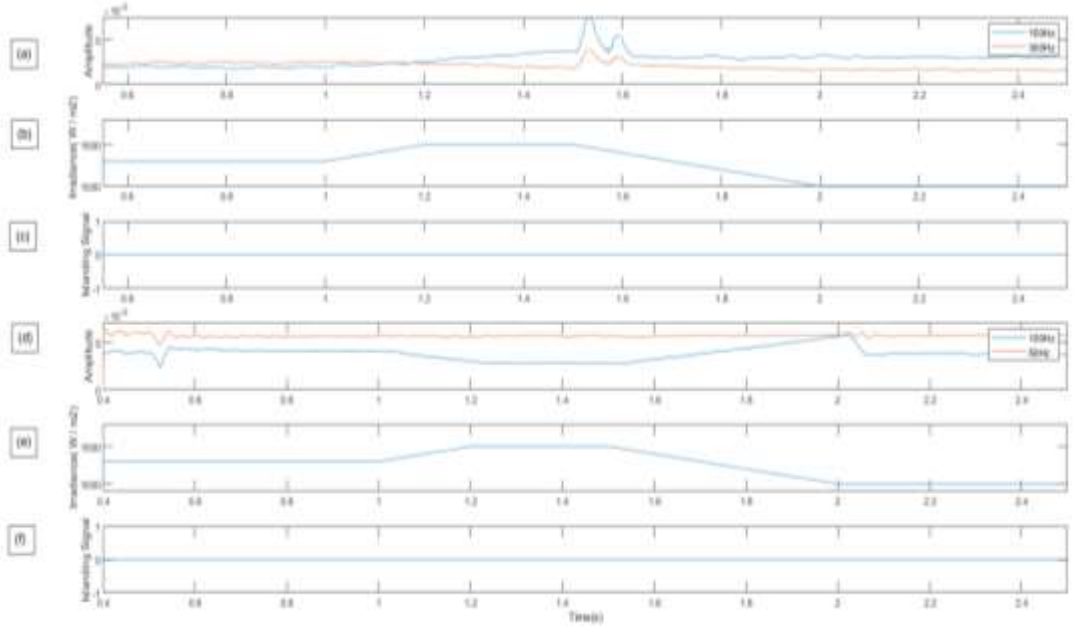

Figure 6-11 effect of the variation in solar irradiance for detecting the islanding status in DC microgrid connected to single phase system (a)Frequency variation(TP) (b)Irradiance(c)islanding detection (d)frequency variation(SP) (e)irradiance variation (f)islanding detection

Figure 6-12(c), (f) illustrates the islanding detection of DC microgrid for different solar irradiation levels (1300 Wm^{-2} and 1000Wm^{-2}) when connected to three phase system. Figure 6-12 (a), (d) shows the variation of the dominant frequency components. The detection time for solar irradiation with 1300 Wm^{-2} is 0.06 s and with 1000 Wm^{-2} solar irradiation it is 0.07 s.

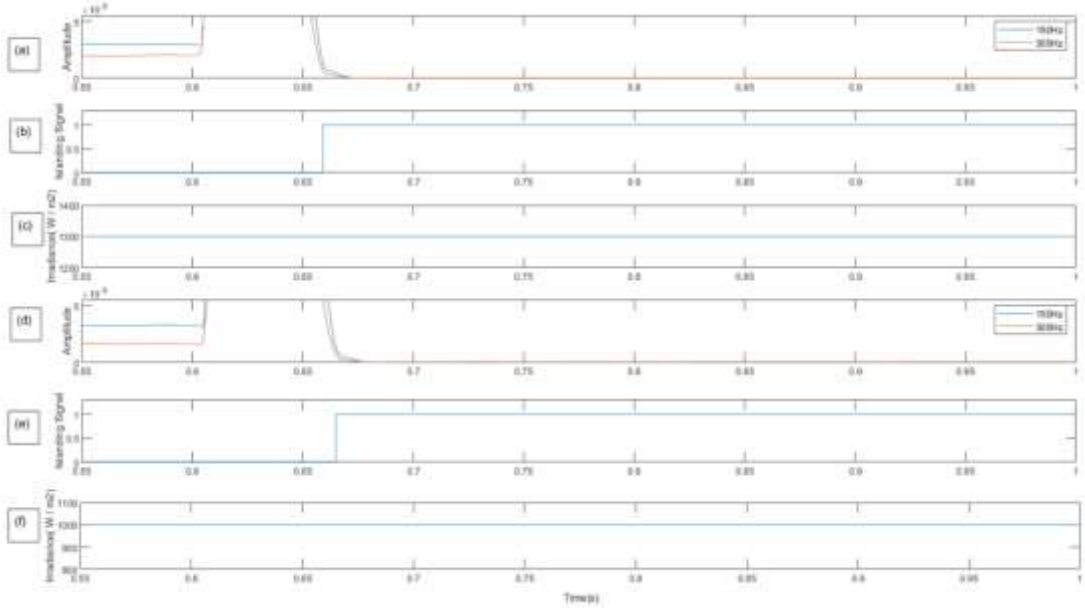

Figure 6-12 Islanding detection in different irradiance levels (three phase)

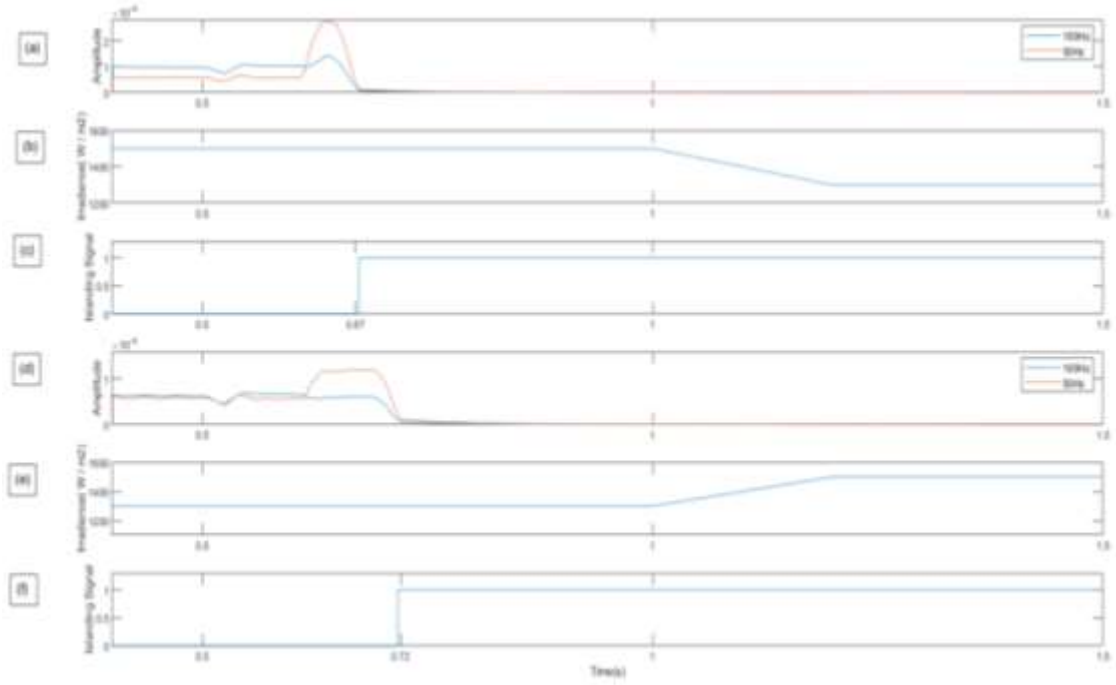

Figure 6-13 Islanding detection in different irradiance levels (single phase)

Figure 6-13(c), (f) illustrates the islanding detection of DC microgrid connected to the single-phase system under different solar irradiation levels (1500 Wm^{-2} and 1300Wm^{-2}). Figure 6-13 (a), (d) shows the variation of the dominant frequency components . The detection time for solar irradiation with 1500 Wm^{-2} is 0.07 s and with 1300 Wm^{-2} solar irradiation, it is 0.12 s .

Therefore, the response time of detecting islanding with the proposed methods do not depend on the solar irradiance levels.

6.8 Behavior of the proposed algorithm with grid parameters (voltage and frequency)

Typically, the voltage at the point of common coupling (PCC) of the DC microgrid to the grid is maintained at a rated value with a tolerance (±10%) and the frequency is maintained at a rated value with a tolerance (±1)[50]. To observe the performance of the proposed islanding detection algorithm, system parameters were varied within their limits.

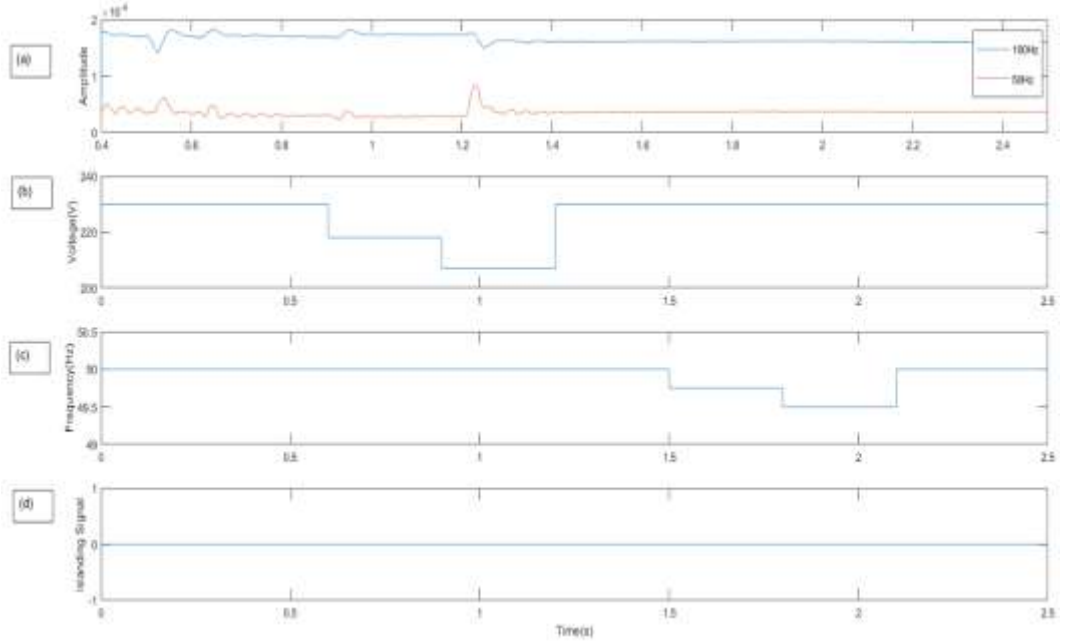

Figure 6-14 Behaviors of the proposed algorithm in different conditions in primary grid(single phase)

The 6-14 (a) illustrates the variation of dominant frequency components for the DC microgrid connected to the single-phase system. Figure 6-14 (b) shows the variation of voltage having a change between the time period of 0.5 s- 1.5 s whereas the variation of frequency is changed between 1.5 s - 2.5 s as illustrated in Figure 6-14 (c).

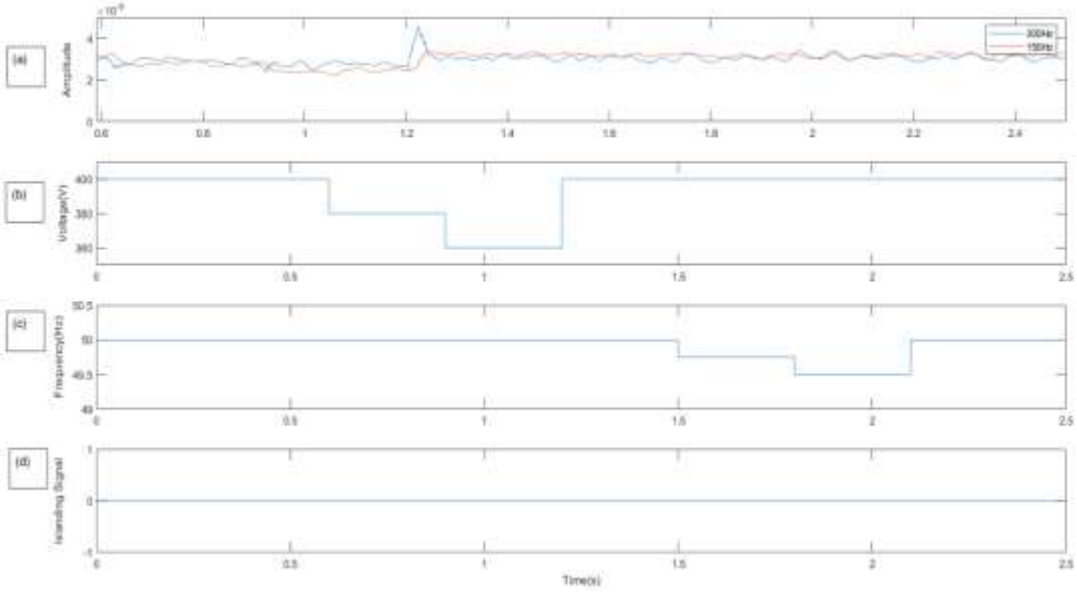

Figure 6-15 Behavior of the proposed islanding detection method in different primary conditions (three phase)

The 6-15 (a) illustrates the variation of dominant frequency components for the DC microgrid connected to the three-phase system. Figure 6-15 (b) shows the variation of voltage having a change between the time duration of 0.5 s- 1.5 s whereas the variation of frequency between 1.5 s-2.5 s illustrated in Figure 6-15 (c).

Above analysis indicates that the grid side parameters do not affect the islanding detection with the proposed system.

6.9 Islanding detection with different islanding instances

To evaluate the dependence of instance of islanding is initiated, the performance of the proposed islanding detection method was observed under islanding created in steps of 0.05 s differences in time.

Figure 6-16 (a),(c),(e) illustrates the variation of dominant frequency components for DC microgrid connected to single phase AC system. Figure 6-16 (b), (d), (f) shows the islanding instances along with the islanding detection signal for three cases where the instances time is changed with a step of 0.05 s.

Similarly, Figure 6-17 (a),(c),(e) illustrates the variation of dominant frequency components for three phase system. Figure 6-17 (b), (d), (f) shows the islanding instances along with the islanding detection signal for three cases where the instances time is changed with a step of 0.05 s.

Even though the instance time is changed, the detection time remains at constant values for both DC microgrid connected to single phase AC and three phase AC system. Therefore, it can be said that irrespective of the instance when islanded, the proposed method detects the islanding event and the detection time does not depend on the islanding instance.

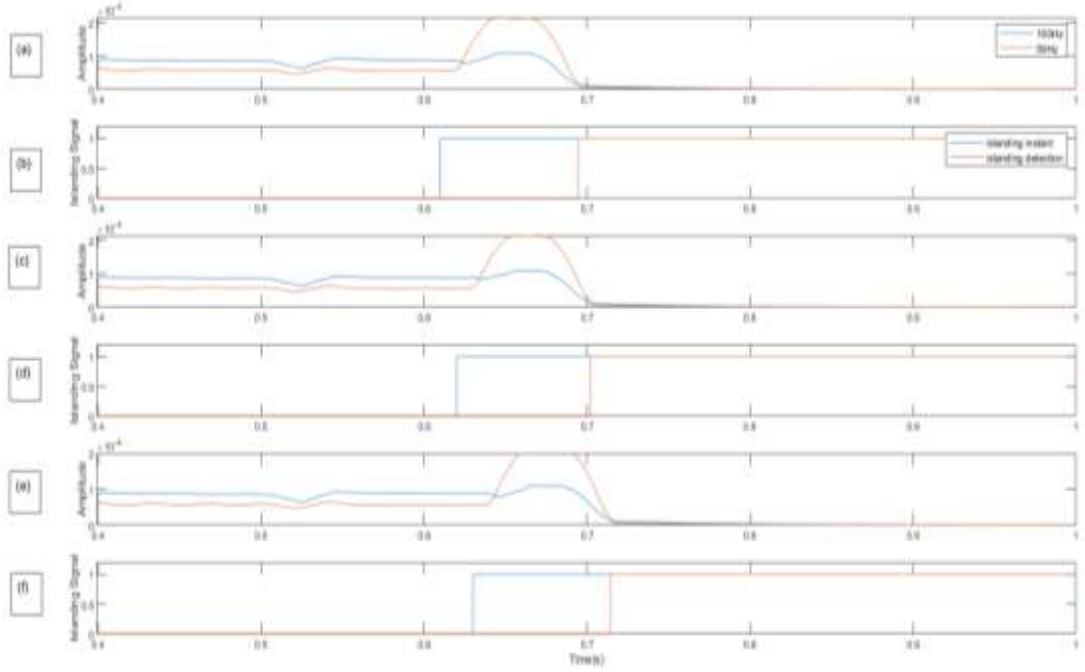

Figure 6-16 Effect of the islanding instant in as cycle of the AC voltage (single phase)

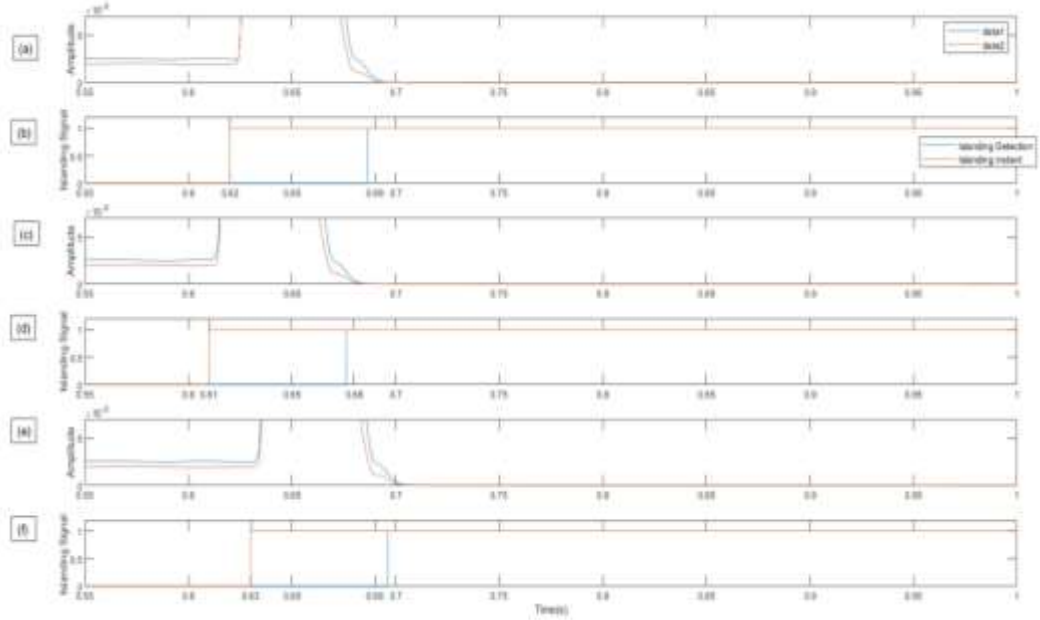

Figure 6-17 Effect of the islanding instant in as cycle of the AC voltage (three phase)

7. SENSITIVITY ANALYSIS

In this chapter, the reliability of the proposed islanding detection method was assessed under various cases, discussed in Chapter 6. Case studies with forty individual events (twenty events for each case) were considered for the two cases: DC microgrid connected to single phase AC system and DC microgrid connected to the three phase AC systems.

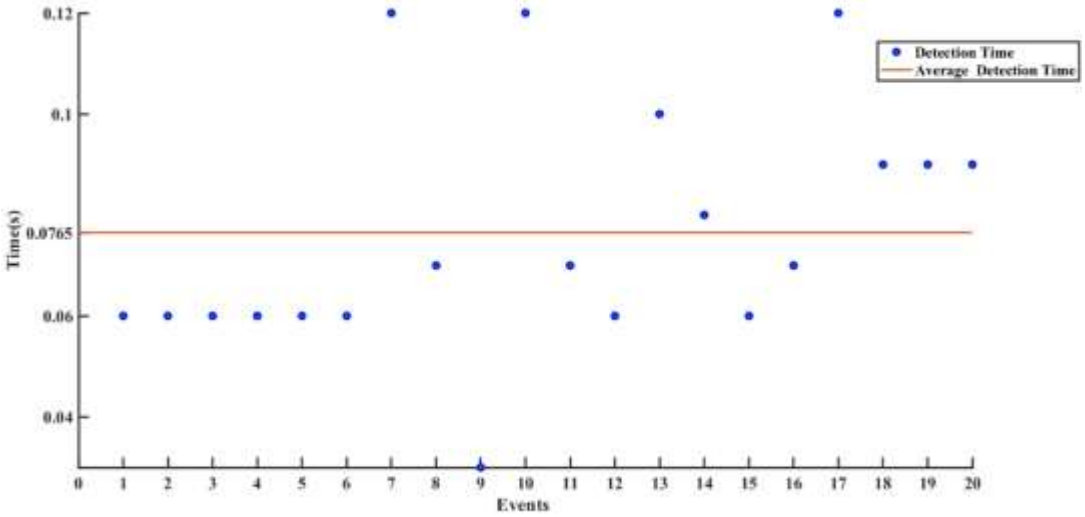

Figure 7-1 Islanding detection (single phase)

The detection time analysis for the twenty individual events for the case, DC microgrid connected to the single-phase system is shown in the Figure 7-1. It has minimum detection time of 0.025 s and maximum of 0.12 s. The average detection time for the single-phase grid interfaced configuration is 0.0765 s. Figure 7-2 illustrate the same analysis carried for DC microgrid connected to the three-phase system. It has minimum detection time of 0.05s and maximum detection time of 0.12s. The average value is 0.0865s. Hence, it can be stated that the average time taken to detect the islanding situation for DC microgrid connected to single-phase system is less than that for DC microgrid connected to the three-phase system. Behavior of the proposed islanding detection method in the both network configuration is illustrated in Figure 7-3. More importantly, the accuracy of the proposed islanding detection algorithm is 100% as shown in the Figure 7-4.

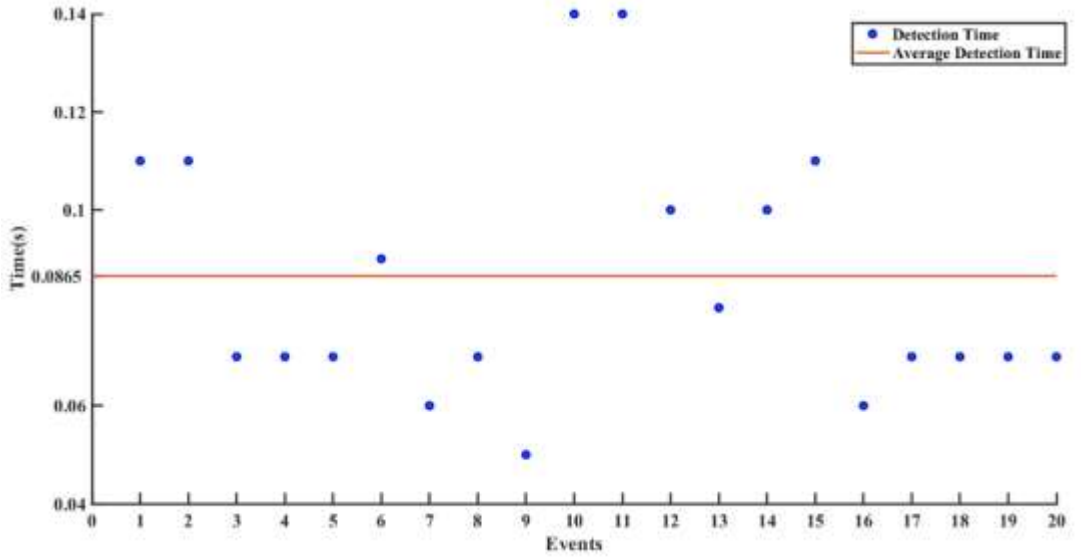

Figure 7-2 Islanding detection (Three Phase)

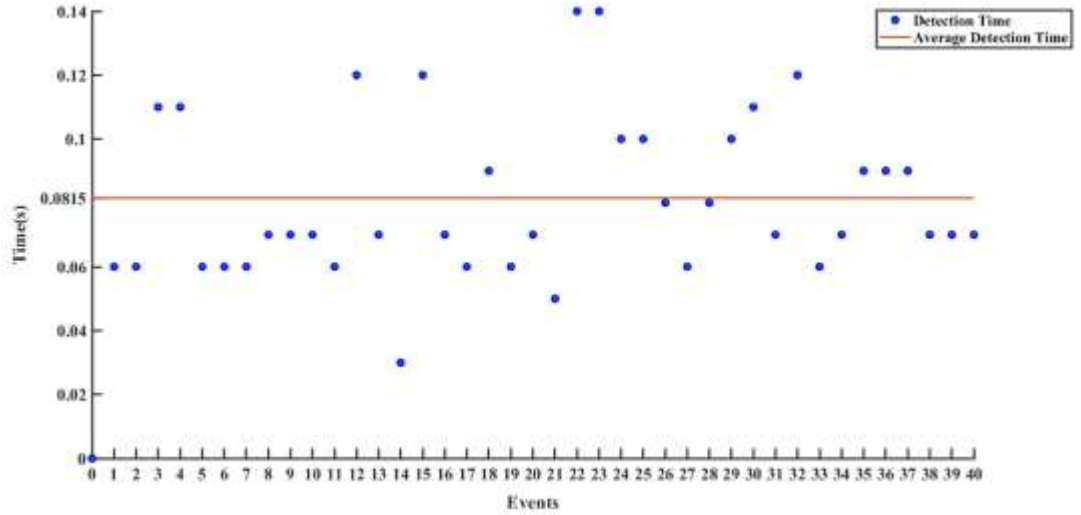

Figure 7-3 Islanding detection time analysis

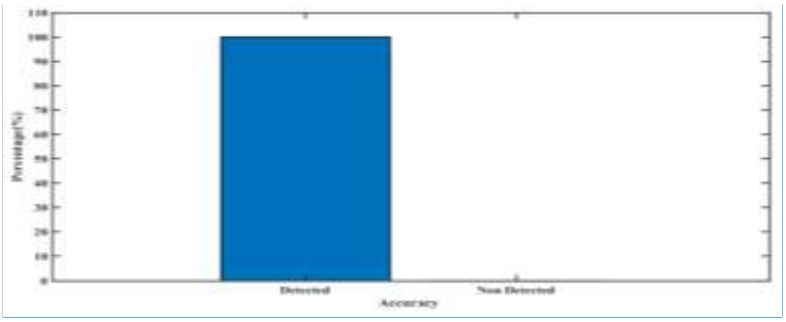

Figure 7-3 Islanding detection accuracy

8. CONCLUSIONS AND RECOMMENDATIONS

The main objective of this research was to design a reliable islanding detection method (IDM) for DC microgrids. As the first step, DC microgrid was modeled considering distribution generation (solar with MPPT), loads (AC and DC), battery Energy Storage Systems and power electronic interfaces. In order to observe the reliable operation of the proposed DC microgrid for both islanded and grid connected mode considering battery SOC, Energy Management System was introduced to select the control mode of the DC-DC converter.

This proposed method is a passive islanding method developed based on analyzing the frequency components in DC link voltage. Most of the passive islanding methods fail in the critical mode of operation, but the proposed islanding detection method accurately operate in any loading condition of the DC microgrid system (when generation and demand are balanced, generation exceeds demand and demands exceeds generation). Typically, active islanding techniques have low power quality, but this proposed algorithm does not affect the system power quality.

The proposed algorithm was tested under different case studies as illustrate in the chapter 6. The proposed algorithm presented a high accuracy level with fast detection time. The performance of the proposed islanding detection method was evaluated for all the possible system conditions including noise interfere, AC load integration, solar variation, etc. for both cases: DC microgrid connected to single phase system and three phase system. Results indicated the proposed islanding detection method is highly robust under all the tested conditions. However, the noise content of the measured voltage waveforms affects the detection of the islanding. Therefore, it can be concluded that proposed algorithm performs reliably if the SNR ratio is maintained above 30dB range for the measurement purposes.

It can also be concluded that the proposed algorithm is less complex compared to the other available detection techniques. Hence, this can be easily adapted to any DC microgrid configuration at lower cost. Finally, it can be concluded that the proposed islanding detection method for islanding detection in DC microgrids is accurate, fast, reliable, robust, simple and easily adaptable any system.

REFERENCES

[1] British Petroleum Company, “BP Statistical Review of World Energy Statistical Review of World,” 2019.

[2] G. Masson *et al.*, “A Snapshot of Global PV Markets - The Latest Survey Results on PV Markets and Policies from the IEA PVPS Programme in 2017,” in *2018 IEEE 7th World Conference on Photovoltaic Energy Conversion, WCPEC 2018 - A Joint Conference of 45th IEEE PVSC, 28th PVSEC and 34th EU PVSEC*, 2018, pp. 3825–3828, doi: 10.1109/PVSC.2018.8547794.

[3] IEA, “Global EV Outlook 2019 to electric mobility,” 2019.

[4] J. J. Justo, F. Mwasilu, J. Lee, and J. W. Jung, “AC-microgrids versus DC-microgrids with distributed energy resources: A review,” in *Renewable and Sustainable Energy Reviews*, 2013, vol. 24, no. August, pp. 387–405, doi: 10.1016/j.rser.2013.03.067.

[5] R. Bayindir, E. Hossain, E. Kabalci, and K. M. M. Billah, “Investigation on north American microgrid facility,” *Int. J. Renew. Energy Res.*, vol. 5, no. 2, pp. 558–574, 2015, doi: 10.20508/ijrer.90564.

[6] M. S. Bin Arif and M. A. Hasan, *Microgrid architecture, control, and operation*. Elsevier Ltd, 2018.

[7] S. J. Ranade, D. R. Sagi, R. Mulpuri, R. Surabhi, and J. Mitra, “Likelihood of islanding in distribution feeders with photovoltaic generation,” in *2007 IEEE Power Engineering Society General Meeting, PES*, 2007, vol. 88003, pp. 1–6, doi: 10.1109/PES.2007.386238.

[8] Q. Fu, A. Nasiri, A. Solanki, A. Bani-Ahmed, L. Weber, and V. Bhavaraju, “Microgrids: Architectures, Controls, Protection, and Demonstration,” *Electr. Power Components Syst.*, vol. 43, no. 12, pp. 1453–1465, 2015, doi: 10.1080/15325008.2015.1039098.

[9] F. Blaabjerg, R. Teodorescu, M. Liserre, and A. V. Timbus, “Overview of control and grid synchronization for distributed power generation systems,” *IEEE Trans. Ind. Electron.*, vol. 53, no. 5, pp. 1398–1409, 2006, doi:

10.1109/TIE.2006.881997.

[10] D. Kumar, F. Zare, and A. Ghosh, “DC Microgrid Technology: System Architectures, AC Grid Interfaces, Grounding Schemes, Power Quality, Communication Networks, Applications, and Standardizations Aspects,” *IEEE Access*, vol. 5, no. August, pp. 12230–12256, 2017, doi: 10.1109/ACCESS.2017.2705914.

[11] K. Patel and S. Singh, “an Overview of Dc-Microgrid Architecture With Renewable Energy Resources,” *Int. J. Adv. Eng. Res. Dev.*, vol. 3, no. 02, 2015, doi: 10.21090/ijaerd.e1076508.

[12] Z. Wang, Z. Chen, and X. Wang, “Research of the DC microgrid topology,” in *Proceedings of the 28th Chinese Control and Decision Conference, CCDC 2016*, 2016, pp. 2855–2859, doi: 10.1109/CCDC.2016.7531468.

[13] S. Whaite, B. Grainger, and A. Kwasinski, “Power Quality in DC Power Distribution Systems and Microgrids,” *Energies*, no. Dc, pp. 4378–4399, 2015, doi: 10.3390/en8054378.

[14] V. Kleftakis, D. Lagos, C. Papadimitriou, and N. D. Hatziargyriou, “Seamless Transition between Interconnected and Islanded Operation of DC Microgrids,” *IEEE Trans. Smart Grid*, vol. 10, no. 1, pp. 248–256, 2019, doi: 10.1109/TSG.2017.2737595.

[15] G. S. Seo, B. H. Cho, and K. C. Lee, “DC islanding detection algorithm using injection current perturbation technique for photovoltaic converters in DC distribution,” in *2012 IEEE Energy Conversion Congress and Exposition, ECCE 2012*, 2012, pp. 3722–3726, doi: 10.1109/ECCE.2012.6342473.

[16] M. N. Alam, S. Chakrabarti, and A. Ghosh, “Networked Microgrids: State-of-the-Art and Future Perspectives,” *IEEE Trans. Ind. Informatics*, vol. 15, no. 3, pp. 1238–1250, 2019, doi: 10.1109/TII.2018.2881540.

[17] A. Makkieh *et al.*, “Assessment of Passive Islanding Detection Methods for DC Microgrids,” in *The 15th IET International Conference on AC and DC Power Transmission*, 2019, pp. 1–6.

[18] F. Katiraei, S. Member, M. R. Iravani, and P. W. Lehn, “Micro-Grid Autonomous Operation During and Subsequent to Islanding Process,” *IEEE Trans. POWER Deliv.*, vol. 20, no. 1, pp. 248–257, 2005.

[19] C. N. Papadimitriou, V. A. Kleftakis, and N. D. Hatziargyriou, “A Novel Method for Islanding Detection in DC Networks,” *IEEE Trans. Sustain. Energy*, vol. 8, no. 1, pp. 441–448, 2017, doi: 10.1109/TSTE.2016.2604419.

[20] P. Rodríguez, R. Teodorescu, I. Candela, A. V. Timbus, M. Liserre, and F. Blaabjerg, “New positive-sequence voltage detector for grid synchronization of power converters under faulty grid conditions,” in *PESC Record - IEEE Annual Power Electronics Specialists Conference*, 2006, doi: 10.1109/PESC.2006.1712059.

[21] Y. V. P. Kumar and R. Bhimasingu, “Performance analysis of green microgrid architectures by comparing power quality indices,” in *2014 18th National Power Systems Conference, NPSC 2014*, 2015, doi: 10.1109/NPSC.2014.7103873.

[22] IEEE-SA-Standards-Board, “IEEE Recommended Practice for Utility Interface of Photovoltaic (PV) Systems,” 2000.

[23] P. Mahat, Z. Chen, and B. Bak-jensen, “Review of Islanding Detection Methods for Distributed Generation,” *DRPT2008*, no. April, pp. 2743–2748, 2008.

[24] R. Shariatinasab and M. Akbari, “New islanding detection technique for DG using discrete wavelet transform,” in *PECon2010 - 2010 IEEE International Conference on Power and Energy*, 2010, pp. 294–299, doi: 10.1109/PECON.2010.5697593.

[25] A. Timbus, A. Oudalov, and C. N. M. Ho, “Islanding detection in smart grids,” in *2010 IEEE Energy Conversion Congress and Exposition*, 2010, pp. 3631–3637, doi: 10.1109/ECCE.2010.5618306.

[26] W. Xu, G. Zhang, C. Li, W. Wang, G. Wang, and J. Kliber, “A power line signaling based technique for anti-islanding protection of distributed generators - Part I: Scheme and analysis,” *IEEE Trans. Power Deliv.*, vol. 22, no. 3, pp.

1758–1766, 2007, doi: 10.1109/TPWRD.2007.899618.

[27] C. Li, C. Cao, Y. Cao, Y. Kuang, L. Zeng, and B. Fang, “A review of islanding detection methods for microgrid,” *Renewable and Sustainable Energy Reviews*, vol. 35. Elsevier, pp. 211–220, 2014, doi: 10.1016/j.rser.2014.04.026.

[28] Q. Sun, J. M. Guerrero, T. Jing, J. C. Vasquez, and R. Yang, “An Islanding Detection Method by Using Frequency Positive Feedback Based on FLL for Single-Phase Microgrid,” *IEEE Trans. Smart Grid*, vol. 8, no. 4, pp. 1821–1830, 2017, doi: 10.1109/TSG.2015.2508813.

[29] T. S. Tran, D. T. Nguyen, and G. Fujita, “Islanding detection method based on injecting perturbation signal and rate of change of output power in DC grid-connected photovoltaic system,” *Energies*, vol. 11, no. 5, pp. 1–18, 2018, doi: 10.3390/en11051313.

[30] W. Y. Teoh and C. W. Tan, “An Overview of Islanding Detection Methods in Photovoltaic Systems,” *World Acad. Sci. Eng. Technol. Int. J. Electr. Comput. Eng.*, vol. 5, no. 10, pp. 1336–1344, 2011.

[31] G. Bayrak and M. Cebeci, “A Communication Based Islanding Detection Method for Photovoltaic Distributed Generation Systems,” *Int. J. Photoenergy*, no. July 2014, 2016, doi: 10.1155/2014/272497.

[32] IEEE Standard Association, “IEEE Std. 1547-2018. Standard for Interconnection and Interoperability of Distributed Energy Resources with Associated Electric Power Systems Interfaces,” 2018.

[33] IEEE-SA-Standards-Board, “IEEE Guide for Protective Relaying of Utility-Consumer Interconnections,” 2014.

[34] IEEE-SA-Standards-Board, “IEEE Recommended Practice for Protection and Coordination of Industrial and Commercial Power Systems,” 1986.

[35] A. M. I. Mohamad and Y. A. R. I. Mohamed, “Assessment and Performance Comparison of Positive Feedback Islanding Detection Methods in DC Distribution Systems,” *IEEE Trans. Power Electron.*, vol. 32, no. 8, pp. 6577–6594, 2017, doi: 10.1109/TPEL.2016.2618220.

[36] T. T. Son, G. Fujita, and N. D. Tuyen, “Islanding detection in DC network,” in *2017 52nd International Universities Power Engineering Conference, UPEC 2017*, 2017, vol. 2017-Janua, pp. 1–5, doi: 10.1109/UPEC.2017.8231909.

[37] S. Khichar, Y. Gopal, and M. Lalwani, “An Enhanced Control Strategy for the Stable Operation of Distributed Generation during Grid-connected and Islanded Mode,” *Int. J. Appl. Power Eng.*, vol. 7, no. 2, pp. 147–158, 2018, doi: 10.11591/ijape.v7.i2.pp147-158.

[38] B. Bahrani, S. Kenzelmann, and A. Rufer, “Multivariable-PI-based dq current control of voltage source converters with superior axis decoupling capability,” *IEEE Trans. Ind. Electron.*, vol. 58, no. 7, pp. 3016–3026, 2011, doi: 10.1109/TIE.2010.2070776.

[39] M. Ciobotaru, R. Teodorescu, and F. Blaabjerg, “Improved PLL structures for single-phase grid inverters,” in *Proc. Power Electronics and Intelligent Control for Energy Conservation Conference (PELINCEC)*, 2005, no. February, pp. 1–6.

[40] M. Ebrahimi and S. A. Khajehoddin, “A simple DQ current controller for single-phase grid-connected inverters,” in *Conference Proceedings - IEEE Applied Power Electronics Conference and Exposition - APEC*, 2015, vol. 2015-May, no. May, pp. 2840–2845, doi: 10.1109/APEC.2015.7104753.

[41] M. Ciobotaru, R. Teodorescu, and F. Blaabjerg, “A new single-phase PLL structure based on second order generalized integrator,” in *PESC Record - IEEE Annual Power Electronics Specialists Conference*, 2006, pp. 1–6, doi: 10.1109/PESC.2006.1711988.

[42] P. Das, “Maximum Power Tracking Based Open Circuit Voltage Method for PV System,” *Energy Procedia*, vol. 90, no. December 2015, pp. 2–13, 2016, doi: 10.1016/j.egypro.2016.11.165.

[43] K. Ishaque, Z. Salam, and G. Lauss, “The performance of perturb and observe and incremental conductance maximum power point tracking method under dynamic weather conditions,” *Appl. Energy*, vol. 119, pp. 228–236, 2014, doi: 10.1016/j.apenergy.2013.12.054.

[44] N. E. Zakzouk, A. K. Abdelsalam, A. A. Helal, and B. W. Williams, “High performance single-phase single-stage grid-tied PV current source inverter using cascaded harmonic compensators,” *Energies*, vol. 13, no. 2, 2020, doi: 10.3390/en13020380.

[45] M. Salem and Y. Atia, “Control scheme towards enhancing power quality and operational efficiency of single-phase two-stage grid-connected photovoltaic systems,” *J. Electr. Syst. Inf. Technol.*, vol. 2, no. 3, pp. 314–327, 2015, doi: 10.1016/j.jesit.2015.05.002.

[46] Y. Du and D. D.-C. Lu, “Harmonic Distortion Caused by Single-Phase Grid-Connected PV Inverter,” in *Power System Harmonics - Analysis, Effects and Mitigation Solutions for Power Quality Improvement*, no. Dc, 2018.

[47] Y. Du, D. D. C. Lu, G. James, and D. J. Cornforth, “Modeling and analysis of current harmonic distortion from grid connected PV inverters under different operating conditions,” *Sol. Energy*, vol. 94, no. September 2019, pp. 182–194, 2013, doi: 10.1016/j.solener.2013.05.010.

[48] Z. Quan, S. J. Shellhammer, W. Zhang, and A. H. Sayed, “Spectrum sensing by cognitive radios at very low SNR,” in *GLOBECOM - IEEE Global Telecommunications Conference*, 2009, pp. 1–6, doi: 10.1109/GLOCOM.2009.5426262.

[49] Y.-P. Lee, Y. S. Moon, N. Y. Ko, H.-T. Choi, L. Huang, and Y. Bae, “Measurement of DS-CDMA Propagation Distance in Underwater Acoustic Communication Considering Attenuation and Noise,” *Int. J. Fuzzy Log. Intell. Syst.*, vol. 15, no. 1, pp. 20–26, 2015, doi: 10.5391/ijfis.2015.15.1.20.

[50] L. Ekonomou, G. P. Fotis, V. Vita, and V. Mladenov, “Distributed Generation Islanding Effect on Distribution Networks and End User Loads Using the Master-Slave Islanding Method,” *J. Power Energy Eng.*, vol. 04, no. 10, pp. 1–24, 2016, doi: 10.4236/jpee.2016.410001.